Dissertation zur Erlangung des Doktorgrades
der Fakultät für Chemie und Pharmazie
der Ludwig-Maximilians-Universität München

Tumor necrosis factor (TNF) is a necroptosis-associated alarmin

Francesca Pinci

Aus

Mailand, Italien

2020

Table of contents

1. Introduction

1.1 The immune system

The physiological function of the immune system is the defense against pathogens. This important process consists of two lines of defense: an early one that is activated within minutes or hours from the beginning of the infection and a late more specialized one that intervenes within days. Two distinct branches of the immune system are responsible for the early and the late events that occur after infection: the innate and the adaptive immunity, respectively [1]. The innate branch is the evolutionary older type of immunity that is already present in invertebrate animals, and indeed operational in single celled eukaryotic and non-eukaryotic cells. It provides rapid sensing and elimination of infections. The adaptive immune system offers more finely refined mechanisms to recognize and defeat pathogens, but it needs more time to come into play. Innate and adaptive branches of immunity differ with regards to the sensing modalities they employ to identify the presence of pathogens. Cells of the innate immune system can recognize only a limited amount of microbial moieties, which are evolutionary conserved and are referred to as pathogen associated molecular patterns (PAMPs). Receptors responsible for the recognition of PAMPs are termed pathogen recognition receptors (PRRs) and are germ line-encoded [1]. Following pathogen recognition, cells of the innate immune system employ different strategies to directly kill pathogens or inhibit their growth or facilitate the activation of the adaptive immune system. Cells of the adaptive immune system, namely T and B lymphocytes, can recognize a plethora of moieties, termed antigens, via receptors produced by recombination of specific genetic loci [1]. Receptors produced by B cells are called antibodies and can be secreted, providing a humoral type of immunity by direct neutralization of the pathogen or the toxin and activation of different effector mechanisms (usually executed by cells of the innate immune system) for the elimination of the threat [2]. Unlike antibodies, T cell receptors (TCRs) are not secreted and recognize antigens presented by major histocompatibility complex (MHC) molecules on the surface of other cells, leading to direct cytotoxic effects (CD8+ T cells) or to modulatory effects on other immune cells (CD4+ T cells) [3,4]. Dendritic cells (DCs) play an important role in the activation of T cells and B cells, acting as professional antigen presenting cells: immature DCs constantly patrol the tissues and the blood stream and, in case of pathogen sensing (usually via PRRs), they mature and move to the lymph nodes, where they present antigens to naïve T cells and B cells [5]. In this sense, DCs link innate and adaptive immunity by facilitating the activation of adaptive immune cells after the detection of an infection by the innate immune system. As mentioned above, the adaptive immunity relies on effector mechanisms of the innate branch, such as phagocytosis of opsonized pathogens (see section 1.2) to fight infections. This crosstalk between innate and adaptive branches not only helps with the elimination of the threat, but also provides protection in case of a second challenge. In fact, by selecting antibodies and TCRs specific for the encountered pathogen and clonally expanding the respective lymphocytes, the adaptive immune system develops memory for pathogens that have already been in contact with the body. Of note, many mechanisms are

employed to prevent improper activation of the immune system, such as compartmentalization of PRRs to avoid detection to host structures similar to pathogen moieties or elimination of self-reactive T cells in the thymus during their maturation stage [1]. However, when such mechanisms do not properly function, abnormal immune reactions can be observed. In particular, inadequate innate immune responses give rise to autoinflammatory pathologies, while response to self-antigens by the adaptive immune system results in the development of autoimmune diseases [6].

1.2 The innate immune system: cells and effector mechanisms

The immune system provides the host with different levels of protection against infections. In particular, it is possible to distinguish between anatomical barriers, antimicrobial proteins, humoral components (such as the complement system), cell-mediated responses of the innate immune cells and adaptive immunity [1]. With the exception of adaptive immunity (briefly discussed in section 1.1), all other mentioned levels of protection are considered to be part of the innate immune response. Epithelial tissues constitute a physical barrier that not only prevents microbes from invading the organism, but also actively produce anti-microbial agents, such as defensins and cathelicidins [7]. When a pathogen overcomes the epithelial barriers, the humoral and cellular components of the innate system intervene. Among the humoral components, collectins, ficolins and pentraxins are proteins that recognize different elements of the surface of microbes, thereby opsonizing them and leading to the uptake and elimination by effector cells and/or the activation of the complement system [8]. The complement system can also be directly activated by structures on the pathogens or by antibody-opsonized microbes and consists of a proteolytic cascade that leads to the direct elimination of the microbe following the formation of a lytic complex on its surface; alternatively, pathogen opsonization with components of the complement system can induce its phagocytosis by neutrophils or macrophages recruited by protein fragments produced by the complement proteolytic cascade itself [9]. Despite of the anti-microbial role of anatomical barriers and humoral proteins, infection of target cells can occur. In this case, specialized cell effector functions and local responses of the tissue-resident innate immune cells take place, often induced by a PRR-mediated sensing of the pathogen. In addition, the release of soluble immune mediators, such as cytokines, from the infected tissue leads to further recruitment of immune cells from the circulation. Specialized innate immune cells include monocytes, macrophages, granulocytes (subdivided into neutrophils, basophils, eosinophils and mast cells), and innate lymphoid cells, which include NK (natural killer) cells [1]. Neutrophils and monocytes are attracted to the site of infection via interaction with selectins expressed by the endothelial cells in proximity to the infected tissue, a process called leucocyte rolling [1]. Penetration of the endothelial tissue relies on strong interactions between the integrins on the leucocytes and their ligands on the endothelial cells, the expression of which is increased after exposure with inflammatory cytokines produced in the infected tissue. The latter also produces chemokines, a subclass of cytokines which attract leukocytes expressing the correspondent chemokine receptor. The so-recruited cells and the tissue

resident macrophages engulf pathogens by phagocytosis or other forms of endocytosis to kill them [10]. Pathogens are then killed by different effector mechanisms in the endolysosomal compartment. Activated phagocytic cells produce reactive oxygen species (ROS) via the nicotinamide adenine dinucleotide phosphate (NADPH) oxidase enzyme and nitric oxide (NO) by the inducible nitric oxide synthase (iNOS) [11]. These highly reactive chemical species, together with the action of proteolytic enzymes present in the endolysosoms and the acidity of these organelles, are extremely effective in killing pathogens. Besides bacteria and viruses, the body can be challenged by parasites, usually eliminated by eosinophils and basophils after release of the toxic content of their cytoplasmic granules upon activation [1]. Cell-mediated responses include not only the direct killing of the infectious agent, but also induction of death of infected cells. This can happen either in a cell-autonomous way, in a sort of cell suicide, or in a mechanism of elimination that depends on cell to cell interaction between an infected cell and a killer cell. In the first case, suicide cell death can be induced in the forms of apoptosis, pyroptosis or necroptosis, the latter two leading to intracellular content release and secretion of immune mediators which further activate bystander immune cells, thereby amplifying the immune response [12]. In the second case, killing of infected cells can be mediated by NK cells. NK cells exert direct cytotoxic effects on infected or abnormal cells, recognized by two classes of receptors: activating and inhibitory receptors. Activating receptors include Fc receptors, which recognize the Fc domain of antibodies and mediate the elimination of antibody-opsonized microbes, while inhibitory receptors recognize MHC class I molecules expressed on the cell membrane. Since infected or abnormal cells (for example tumor cells) generally downregulate MHC I molecules, the interaction between inhibitory receptors of NK cells and MHC I falls under threshold levels and, as a results, NK cells are activated [1,13]. This process is particularly important to restrict growth of intracellular pathogens, such as viruses. Moreover, replication of intracellular pathogens can be hindered by a set of restriction factors, the expression of which is not only limited to specialized immune cells, but can also apply to tissue cells. For example, RNase L (Ribonuclease L) degrades RNA in the cytosol after activation by OAS (oligoadenylate synthase-like) proteins that sense the presence of dsRNA; SAMHD1 (SAM domain and HD domain-containing protein 1) hydrolyzes the deoxynucleoside triphosphates (dNTPs) necessary for viral replication; APOBEC3 (Apolipoprotein B mRNA Editing Catalytic Polypeptide-like 3) proteins mediate deamination of viral DNA, leading to G-to-A hypermutations and introduction of amino acid substitutions and premature STOP codons [14]. If the infection cannot be easily resolved, the production of excessive amounts of immune mediators induces systemic responses which involve different organs, such as the brain and the liver. As a result, changes in the behavior (e.g. lack of appetite), fever and production of acute phase proteins can also contribute to the elimination of the cause of infection [1].

1.3 Pathogen recognition by cells of the innate immune system

In order to activate the above mentioned effector mechanisms, cells of the innate immune system need to sense the presence of pathogens. This process is mediated by the recognition

of essential, evolutionary conserved microbial components termed pathogen associated molecular patterns or PAMPs through germ line-encoded pathogen recognition receptors or PRRs. PRRs can be divided into membrane-bound and cytosolic, with their subcellular localization being essential for ligand accessibility [15]. Membrane-bound PRRs are divided into C-type lectin receptors (CLRs) and Toll-like receptors (TLRs) and can be found both on the cell membrane and on membranes of the endosomal compartments. CLRs are a family of receptors implicated in anti-fungal immunity, that bind to carbohydrate-based PAMPs in a calcium-dependent manner, resulting in respiratory burst, phagocytosis and NF-kB (nuclear factor kappa-light-chain-enhancer of activated B cells) activation [16]. Toll like receptors are a family of conserved type I membrane glycoproteins, firstly characterized based on the similarity to Toll receptor in Drosophila (biology of TLRs is reviewed in [15,17]). On the extracellular or luminal side they contain leucine-reach repeats (LRRs) and a binding domain for the PAMP, while in the cytoplasmic region they have a Toll/Interleuchin-1 (TIR) domain, shared also by IL-1R family. In total, 10 and 12 functional TLRs have been described in human and mouse, respectively. TLR3, 7, 8 and 9 sit on the endolysosomal membrane (with TLR3 being also on the cell surface), where they sense the presence of nucleic acids of endocytosed microbes. In particular, TLR3 recognizes dsRNA, TLR7 and 8 ssRNA, while TLR9 binds to ssDNA with unmethylated cytosine-phosphate-guanosine (CpG) motives, usually not present in mammals. All other TLRs exert their function on the cell surface. TLR2 heterodimerizes with TLR1 and TLR6 for the recognition of triacylated and diacylated lipopeptides respectively; TLR5 can sense bacterial flagellin and TLR4, in association with MD2 (myeloid differentiation factor 2), binds to lipopolysaccharide (LPS), an essential component of the cell wall of gram-negative bacteria. The recognition of LPS by TLR4 and MD2 is preceded by binding of LPS to the membrane protein CD14 (cluster of differentiation 14), which subsequently passes LPS on the TLR4-MD2 complex [18]. TLR10 has been described as a negative regulator of TLR signaling, although its role has not been fully characterized [19]. To initiate downstream signaling, TLRs use different combinations of adaptor proteins. TLR2, 5, 7 and 9 recruit Myd88 (myeloid differentiation primary response gene 88) and, in case of TLR2, also the co-adaptor MAL/TIRAP (MyD88 adaptor like protein); TLR3 only recruits TRIF (TIR-domain containing adaptor protein inducing IFNβ), while TLR4 has the ability to signal via both MAL-MyD88 and TRAM (Trif related adaptor molecule)-TRIF adaptors. Clustering of TIR domains upon TLR activation provides a platform for MyD88 and IRAK4 (IL-1 receptor-activated protein kinase4) recruitment and oligomerization, in a complex called Myddosome [20,21]. In the next step, IRAK4 phosphorylates IRAK1, which in turn dissociates from the complex and activates the E3-ubiquitin ligase TRAF6 (tumor necrosis factor receptor associated factor 6). The auto-polyubiquitination of TRAF6 leads to the formation of ubiquitin chains that allow the recruitment of TAK1 (transforming growth factor b activated protein kinase 1) through its adaptors TAB2 and 3 (TAK1 binding protein 2 and 3) to drive NF-kB and MAPK (mitogen-activated protein kinase) pathways. To drive NF-kB activation, TAK1 needs to phosphorylate IKK (inhibitor of nuclear factor B (IkB) kinase complex), which then phosphorylates IkB, resulting into its degradation. IkB is usually bound to NF-kB subunits p65 and p50 to keep

them in the cytosol, but upon its degradation, these subunits expose their nuclear localization signal and translocate to the nucleus, where they mediate the transcription of many pro-inflammatory and immunomodulating genes [22]. At the same time, TAK1-mediated activation of MAPK pathway results in the nuclear translocation of the transcription factor AP-1, again promoting the transcription of pro-inflammatory and pro-survival genes [23]. As mentioned above, a second adaptor, TRIF, contributes to TLR3 and TLR4 signaling. Upon binding to the cytosolic tails of these receptors, TRIF recruits on one hand TRAF6 and RIPK1 (receptor-interacting serine/threonine protein kinase 1), leading to subsequent engagement of TAK1 and NF-kB activation, as described for MyD88 signaling, and, on the other hand, TRAF3, which results in the activation of TBK1 (TANK-binding kinase1) and IKKε [24,25]. This complex mediates the phosphorylation of IRF3 to initiate type I interferon signaling. In addition to this, TRIF can also recruit RIPK3, via interaction of their RHIM (RIP homotypic interaction motif) domains, a pathway that can lead to RIPK3-dependent NF-kB activation, but also, in particular cases, to an inflammatory type of cell death named necroptosis (see section 1.8.2).
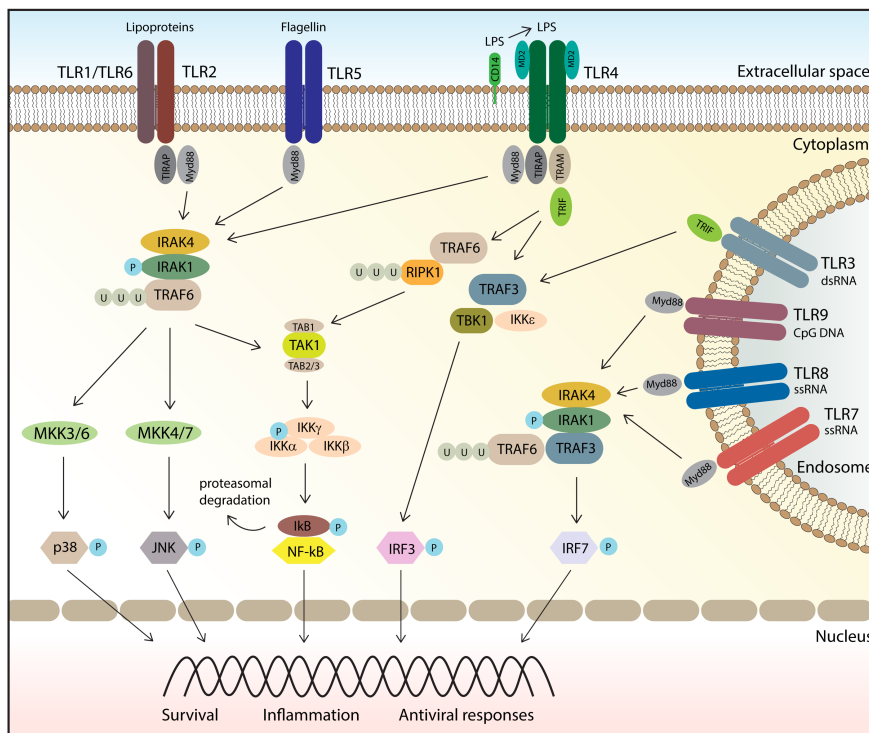
Fig. 1.1 Graphical representation of TLR receptors with their specific agonists and the respective signaling pathways. The activation of these immune receptors lead to cell survival, NF-kB-dependent inflammation and induction of antiviral responses. Details are explained in the text.

Cytosolic PRRs are further classified into RLRs (RIG-I like receptors), cGAS (cyclic GMP AMP synthase)-STING (stimulator of interferon genes) axis, NLRs (NOD like receptors) and AIM2 (Absent in melanoma 2). RIG-I (retinoic-acid inducible gene I), MDA5 (melanoma differentiation-associated protein 5), and LGP2 (laboratory of genetics and physiology 2) are RLRs that sense different forms of viral RNA and, through the common downstream adaptor MAVS (mitochondrial antiviral signaling protein), induce the activation of transcription factors as NF-kB and IRF3 (interferon regulatory factor 3), which contribute to the expression of inflammatory cytokines and the upregulation of type I interferons respectively, leading the

cell to an "antiviral state" that counteracts viral replication and, at the same time, alerts other cells of the immune system [26]. The cGAS-STING axis is involved in the response to cytosolic DNA: upon DNA binding, it generates cyclic GMP-AMP (cGAMP) which is sensed by STING, leading to a type I interferon response [27,28]. DNA can also be sensed by the AIM2 inflammasome, leading to pyroptotic cell death and release of the pro-inflammatory cytokine IL-1β [29,30]. NLRs can sense a great variety of ligands (i.e. flagellin, peptidoglycan, disturbances of the cell membrane integrity) and after activation lead to the formation of large signaling platforms such as the inflammasomes or the NOD signalosome, which contribute to different outcomes, like inflammatory cell death and NF-kB induction [31].

1.4 Cytokines of the innate immune system

Activation of NF-kB and IRFs by TLRs or other PRRs leads to *de novo* transcription of hundreds of genes that contribute to inflammation, immunomodulation, pathogen killing and antiviral response, with cytokines being among the most important target genes. Cytokines are a class of small proteins produced in response to microorganisms or other antigens, able to regulate immune and inflammatory reactions [1]. They can be produced by both cells of innate and adaptive immunity and they contribute to the modulation of inflammatory responses and the cross-talk between the two branches of the immune system. Biological functions of cytokines are usually pleiotropic and redundant, meaning that they can act on different types of cells and that the same biological outcome can be induced by different cytokines [1]. They bind to specific receptors with very high affinity (Kd = 10^{-7}-10^{-12}) and can exert their function in an autocrine, paracrine or systemic manner, depending on the amount and localization of the produced cytokine. Usually, their expression is limited in time and subjected to negative feedback regulation, in order to avoid an uncontrolled inflammatory response that could lead to deleterious effects for the host [1]. IL-1 family cytokines, IL-6, TNF (Tumor necrosis factor), IL-12, type I IFNs (type I interferons) and IL-10 are among the most important cytokines produced by cells of the innate immune system. The IL-1 family cytokines include, among the others, IL-1α, and IL-1β, which are produced as precursors and are cleaved during their maturation. While IL-1β is expressed mainly in monocytes and macrophages upon induction by a pro-inflammatory stimulus, IL-1α is constitutively expressed in many cell types, such as epithelial and mesenchymal cells [32]. Despite IL-1α can be processed by calcium dependent proteases such as calpain, its precursor maintains the biological functions [32]. Unlike IL-1α, IL-1β needs to be proteolytically matured to be biologically active, a process which occurs downstream of inflammasome activation in a caspase-1 dependent manner or, as more recently shown, in a caspase-8 dependent way [33]. Mature IL-1β is then secreted during inflammasome-induced pyroptosis or by other unconventional secretion mechanisms, which are not yet completely understood [32]. The biological functions of IL-1α and IL-1β, which include induction of pro-inflammatory gene expression, fever and production of acute-phase proteins by the liver, are exerted via binding to IL-1R family members, which signal through MyD88, as explained for TLRs. IL-6 is mainly produced by monocytes and macrophages (but also other cell types, such as endothelial and mesenchymal cells) downstream of TLRs

6

activation or after IL-1 and TNF stimulation. Its biologically active form is a homodimer that binds to the heterodimeric IL-6 receptor, composed by a signal transducing chain gp130, and an IL-6 binding chain IL-6R, which exists as membrane bound or soluble form. Upon binding to IL-6R, the IL-6/IL-6R complex induces homodimerization of gp130, thereby triggering the signaling cascade, namely JAK-STAT3 (Janus kinase/signal transducers and activators of transcription) and JAK-SHP-2 MAPK pathways [34,35]. IL-6 exerts its biological functions on different cell types, such as the hepatocytes, where it induces acute-phase proteins, T cells and B cells, facilitating their differentiation and antibody production, dermal fibroblast, to favor collagen production and fibrosis [35]. TNF is a cytokine mainly produced by macrophages, which not only exerts strong pro-inflammatory functions, but can also induce cell death in the forms of apoptosis and necroptosis (see section 1.8). IL-12 is produced mainly by macrophages and DCs and activates NK cells and T cells to produce IFN-γ and favors Th1 differentiation of naïve CD4 T cells [1]. Type I IFNs are a large family of cytokines that play an important role in mediating the immune responses during viral infections: they induce the synthesis of viral restriction factors such as OAS proteins (see section 1.2 and 1.3), promote the expression of MHC I molecules and the differentiation of CD4$^+$ T cells into Th1 [1]. Type I IFNs bind to their ubiquitous heterodimeric receptor, composed of IFNARI and IFNARII (Interferon α/β receptor I and II) chains, triggering the downstream pathway via JAK/STAT complex, which leads to phosphorylation of different STAT proteins (mainly STAT1 and STAT2 in different homo- or heterodimeric combinations) that translocate to the nucleus and act as transcription factors [36]. As mentioned above, cytokine production is a tightly regulated process and inhibitory mechanisms exist to limit the pro-inflammatory response in time and magnitude. The cytokine IL-10 acts to dampen the immune responses of macrophages and DCs by inhibiting the expression of pro-inflammatory cytokines, costimulatory and MHC II molecules. Mainly produced by macrophages, but also, in minor extent, by lymphocytes and DCs, it signals via IL-10R, which triggers the JAK/STAT3 pathway to modulate gene expression [1]. Among the transcribed genes, SOCS3 (Suppressor of cytokine signaling 3) inhibits PRR induced expression of many inflammatory genes [37].

1.5 Danger associated molecular patterns

As discussed above, a key feature of the immune response, is the ability to recognize self from non-self, in order to avoid an unspecific and dangerous response against host antigens. To do so, the immune system has evolved to recognize PAMPs with two important characteristics: their molecular structures are not shared by host molecules and/or their localization is unusual for a correspondent similar host molecule (for example nucleic acids recognition by endosomal TLRs or cytosolic DNA/RNA sensors). However, this theory (the "Stranger Theory") does not explain why strong immune responses are observed in sterile conditions, such as autoimmune and chronic diseases or trauma [38]. In 1994, a new theory, called "The danger theory" proposed that the immune system can react to danger signals released by the cells in particular pathological or stressful conditions, mounting a similar immune response to the one elicited during an infection [39]. In analogy with PAMPs, the host molecules responsible for

inflammation in sterile conditions have been later named DAMPs (Damage or Danger associated molecular patterns) [40]. Although the proper definition of danger signal is constantly under debate, increasing knowledge on sterile inflammation led to a classification of endogenous pro-inflammatory signals into more specific categories, namely DAMPs, alarmins and conditions able to induce effector-triggered immunity (ETI)[41,42]. DAMPs are endogenous molecules that have non-inflammatory functions in living cells but, under certain circumstances, exert PRR agonistic activity. Different causes can transform endogenous molecules into PRR ligands. First, they can be chemically modified from their natural form, thereby acquiring binding capacity for one particular PRR. One example is the recognition of oxidized lipoproteins by macrophages [43]. In addition, endogenous molecules act as DAMPs when they gain access to certain compartments that express PRRs and are usually devoid of such molecules. The immune system can therefore react to self-molecules as soon as they are mis-localized, making of the localization (and not anymore of the molecular structure) the main criteria to discriminate whether an immune reaction should be induced or not. One example is the sensing of mitochondrial DNA, released upon damage, by DNA-sensing pathways [44]. Moreover, the amount of a particular molecule present under certain conditions in a cellular compartment (or released extracellularly) can pass a threshold, after which it acquires PRR agonistic activity. Since the "Danger Theory" has been proposed, many molecules have been described to act as DAMPs, by their ability to induce inflammation *in vitro* and/or *in vivo* if purified and by reduction of the observed inflammation when they are selectively depleted [45]. One of the firstly discovered DAMP was the protein high mobility group box 1 (HMGB1) [46]. HMGB1 is a chromatin bound protein that stabilizes nucleosomes, but if released in the extracellular *milieu*, it can bind to TLR2 and 4 and to RAGE (Receptor for advanced glycation end products) to induce an immune response [46,47]. Other described DAMPs include mitochondrial DNA [44], ATP [48], HSPs (Heat shock proteins) [49], β-amyloid [50], cholesterol crystals [51], S100 proteins [52]. Furthermore, besides DAMPs, the concept of alarmin has been proposed: alarmins are considered to be endogenous, preformed molecules that are meant to exert inflammatory responses, but they are not inflammatory because they are sequestered in certain compartments that are breached upon damage [53]. A number of leader-less cytokines are considered to be part of this molecule category (e.g. IL-1α, IL-33). Moreover, perturbations of cells by mean of host molecules released under particular pathological conditions may lead to inflammation by triggering certain immune receptors without acting as direct ligands. For example, uric acid is a product of purine catabolism that can be released by injured cells and form crystals that damage bystander cells, which then activate the NLRP3 inflammasome because of cell membrane perturbation [54].

The exposure of danger signals to immune receptors usually occurs upon cellular stress or cell death: in particular, passive or programmed necrotic cell death (see section 1.8.2) can lead to massive cytosolic content release, exposing possible DAMPs or alarmins in the extracellular *milieu* and leading to inflammatory response to cell death [55,56]. The release of danger signals has already been linked to inflammation in various pathological conditions, such as autoimmune diseases, neurodegenerative diseases, atherosclerosis and even cancer [57].

However, the exact contribution of single DAMPs or alarmins to inflammation in pathological conditions is often hard to assess. On the one hand, this is due to the high complexity of the system under study and on the other hand, it is difficult to demonstrate direct causality between release of a specific molecule and a certain inflammatory effect. Nevertheless, the use of DAMPs or alarmins as potential biomarkers or even therapeutic targets has already been taken into consideration. Indeed, *in vivo* studies and clinical trials in this direction have been reported, such as the use of anti-HMGB1 antibodies in rodent models of arthritis [58] or HSP inhibitors in lung cancer patients [59].

1.6 TNF signaling

TNF is one of the master pro-inflammatory cytokines and is part of the tumor necrosis factor superfamily of ligands (TNFSL), which includes 19 members, among which there are Fas Ligand, lymphotoxin alpha and beta (LTα and LTβ) and CD40L [60]. All TNFSL are active as membrane-bound or secreted trimers by interaction with their respective receptors. The TNFSL and the corresponding TNF receptor superfamily (TNFRSF, 29 described members) are involved in immune responses as well as homeostatic and developmental processes in many organs [60–62]. For example, LT signaling is fundamental for the development of secondary lymphoid organs and contributes to immune regulation by influencing CD4$^+$ T cells differentiation and DCs homeostasis and by supporting type I interferon responses [63,64]. Moreover, a subgroup of TNFRSF members possess a death domain (DD) in their cytoplasmic tail that can engage a cell death program in the form of apoptosis or, in particular cases, necroptosis (see below and section 1.8.2). The binding of TNFSL to their receptors is often promiscuous, since more receptors can bind the same ligand, leading to a fine regulation of their biological effects [60]. TNF exerts its biological functions by activating TNFR1 or TNFR2 and is an NF-kB-induced gene mainly expressed by macrophages and monocytes, but also, even if at lower levels, by other cell types, such as T cells, B cells, NKs, neutrophils and fibroblasts [65,66]. TNF plays a critical role in the immune responses against pathogens, as demonstrated by the phenotype of TNF-deficient mice: although the deletion of TNF results in normal development and no morphological abnormalities, TNF-deficient mice show an impaired immune response when challenged with infectious agents and are unable to solve the infection [67,68]. Produced as a precursor type II transmembrane protein of 26kDa, TNF can be directly active at the cell membrane following cell-cell interaction, or it can be cleaved into its mature form by members of the ADAM superfamily, in particular by ADAM17 (see section 1.7), and act in an autocrine, paracrine or endocrine manner. While TNFR1 is expressed in all tissues and can be activated by both membrane TNF (mTNF) and soluble TNF (sTNF), TNFR2 is mainly present in immune cells, endothelial cells and neurons and its main ligand is mTNF [66,69]. The two receptors are type I transmembrane glycosylated proteins which share a similar extracellular domain, containing four cysteine rich domains that confer specificity for the ligand [66,70]. Nevertheless, they differ in the cytoplasmic domain, in that TNFR1 contains a death domain (DD), absent in TNFR2, which allows the recruitment of the TNFR1-associated DD (TRADD) [71]. Upon TNFR1 activation, a conformational change in its DD leads to the

recruitment of TRADD and RIPK1, which allows the formation of complex I, together with TNFR-associated factor (TRAF2) or 5, cellular inhibition of apoptosis protein (cIAP) 1 or 2 and linear ubiquitin chain assembly complex (LUBAC) [72–74]. The complex I is able to generate different and opposite outcomes, depending on the dominant signals that contributes to its regulation in the cell in that specific moment. In particular, the ubiquitination state of RIPK1 determines whether the cell activates NF-kB and pro-survival program or if it undertakes a cell death program, which can be in the form of apoptosis or necroptosis: when RIPK1 is highly poly-ubiquitinated by cIAPs and LUBAC, the ubiquitin chains form a platform for the further recruitment of the TAK1 and IKK complexes, responsible for downstream MAPK and NF-kB activation, which ultimately results in production of inflammatory cytokines and pro-survival factors [72,75–77]. Among the NF-kB-induced genes, cFLIP$_L$ (FLICE-like inhibitory protein long) plays an essential role in preventing apoptotic cell death: in fact, cFLIP$_L$ heterodimerizes with pro-caspase-8 in the complex IIa, formed upon release of TRADD from complex I and its interaction with FADD (Fas associated death domain), and prevents pro-caspase-8 self-cleavage, which would lead to caspase cascade activation and apoptosis [78,79]. Reduction of cFLIP$_L$ levels favors pro-caspase-8 dimerization and self-cleavage into its active form, which results in caspase cascade activation and apoptosis. On the other hand, deubiquitination of RIPK1 by cylindromatosis enzyme (CYLD) and cIAPs inhibition leads to the detachment of RIPK1 from complex I and the formation of complex IIb, which also comprises FADD (Fas associated death domain), RIPK3, cFLIP$_L$ and pro-caspase-8 [80,81]. As for complex IIa, cFLIP$_L$ levels determine whether pro-caspase8 is activated or not. Moreover, the presence of RIPK1 and RIPK3 in the complex potentially enables the execution of necroptotic cell death [82]. However, caspase-8 dimers or caspase-8-cFLIP$_L$ heterodimers cleave and inactivate RIPK1 and RIPK3, therefore inhibiting necroptosis. Only when caspase-8 levels are reduced or RIPK1 and 3 levels increased, RIPK1 remains active and phosphorylates RIPK3, which in turn phosphorylates itself and MLKL (mixed lineage kinase domain-like protein), the executioner of necroptotic cell death (see section 1.8.2). Contrarily to TNFR1, TNFR2 recruits the TNFR-associated factor (TRAF) 1 and 2 proteins but not TRADD [83]. TRAFs in turn bind cIAPs to promote cell survival and proliferation and NF-kB activation through complex I. In addition, since cytosolic TRAF2 and cIAPs are constantly engaged in the inhibition of the alternative NF-kB by mediating the ubiquitination of NIK (NF-κB inducing kinase), their recruitment to TNFR2 leads to depletion of TRAF2/cIAPs cytosolic pool and accumulation of active NIK, which phosphorylates the NF-kB precursor protein 100, thereby activating non-canonical NF-kB [84]. Interestingly, it has also been shown that mTNF can work as receptor, in a process called reverse or outside-to-inside signaling when engaged by its receptors or by anti-TNF antibodies. The cytoplasmic tail of TNF is phosphorylated in response to LPS and dephosphorylated by reverse signaling, a phenomenon that confers resistance to LPS [85,86]. In addition, it has been shown that the cytosolic tail of TNF contains a nuclear localization signal and, when released from the membrane by SPPL2a and b (signal peptide peptidase-like 2 a and b), the 10 kDa fragment can act as transcription factor to induce the expression of target genes, such as the E-selectin CD62E [86–89].
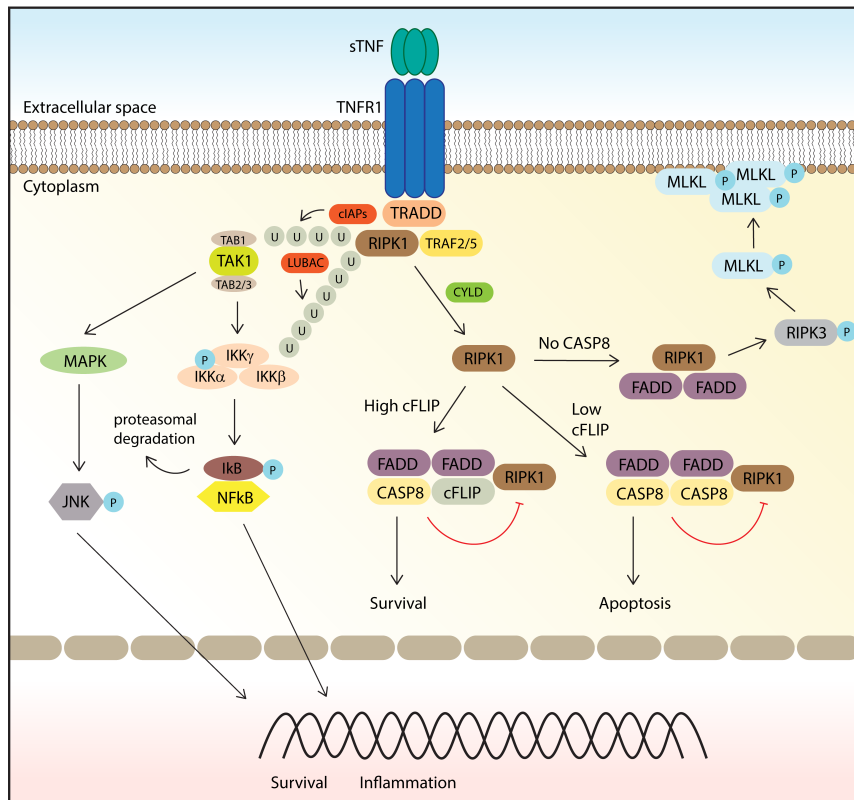
Fig. 1.2 Graphical representation of TNFR1-induced pathways and their different outcomes. Upon binding of sTNF, TNFR1 can induce NF-kB activation if RIPK1 is highly ubiquitinated, leading to cell survival and transcription of pro-inflammatory factors. If RIPK1 is de-ubiquitinated, it can form a complex with FADD and CASP8 in combination or not with the pro-surivival factor cFLIP$_L$. If no cFLIP$_L$ is present, CASP8 forms homodimers and activates the caspase cascade leading to apoptosis. If CASP8 is inhibited, downregulated or not present, RIPK1 phosphorylates RIPK3 which activates MLKL, leading to necroptosis. Details in the text.

TNF was firstly discovered as a serum molecule able to kill tumor cells, hence its name [90]. Later, its role as potent inflammatory inducer was described and implicated not only in the regulation of immune responses for the defense against pathogens, but also, upon dysregulated production, in the pathology of cardiovascular, neurological and pulmonary diseases, diabetes, cancer, obesity and inflammatory diseases, such as psoriasis, rheumatoid arthritis, inflammatory bowel disease and Crohn's disease [60]. As such, TNF and TNFRSF have been under intense study as targets for drug development. Anti-TNF drugs, such as the monoclonal antibody Infliximab, have been approved by the FDA for the treatment of the above mentioned diseases [60,91]. Although effective in regards to TNF-dependent inflammation, the use of these drugs has been associated with an increased risk of serious infection as side effect, given their strong immunosuppressive activity. Therefore, safer alternatives are still matter of research [91,92].

1.7 Function of ADAMs proteins

The ADAM (A Disintegrin and Metalloproteinase) proteins are a family of transmembrane and secreted proteins that mediate ectodomain cleavage of membrane anchored protein precursors into their soluble form, thereby contributing to signaling, proteolysis, cell migration and adhesion [93]. They are part, together with ADAMTS, BMPI/TLL, meprin and MMP genes, of the metzicins superfamily, characterized by the presence of a zinc protease domain [94]. ADAMs have been described in many species, from C. elegans to vertebrates, but are absent in plants. In humans, 21 ADAMs exist, of which only 13 have a protease activity. Among the proteolytically active ADAMs, ADAM20, 21 and 30 are testis-specific and mainly involved

in spermatogenesis, ADAM8 and 28 are mainly expressed in hematopoietic cells, while ADAM9, 10, 12, 15, 17,19 and 33 are broadly expressed in many tissues [95]. The proteolytically active ADAMs share a common multidomain structure: they are type I transmembrane proteins with a prodomain at their N-terminus, which binds and inhibits the catalytic site, preventing unspecific activation of the enzyme on the way from the endoplasmic reticulum (ER) to the Golgi apparatus, where the prodomain is cleaved by convertases such as furin (Fig. 1.3). In addition to that, the prodomain also plays a role as chaperon, by helping correct folding of the ADAM protein [96]. After the prodomain, comes the catalytic domain, the structure of which has been resolved by crystallography, with a catalytic center consisting of three histidine residues, one glutamic acid and one Zn^{2+} ion [97]. The catalytic domain is followed by a disintegrin domain, which mediates interaction with integrins, thereby supporting cell adhesion [96]. After the disintegrin domain, all ADAMs except ADAM10 and ADAM17 contain a cysteine rich domain and an EGF-like domain proximal to the cell membrane. Instead, ADAM17 and ADAM10 contain a membrane proximal domain (MPD), the conformation of which is crucial for their activity: an open, flexible conformation, potentially available for substrate recognition, and a close, rigid conformation, not accessible to substrates. These conformations only differ in two sulfide bonds and the switch between them is regulated by protein-disulfide isomerases [98]. Moreover, ADAM17 contains a unique sequence in its stalk region, called CANDIS (Conserved Adam seventeen Dynamic Interaction Sequence) that can interact with the cell membrane and is therefore involved in a conformational change that regulates the shedding activity [99]. A single transmembrane domain is then followed by a small cytosolic tail at the C-terminus of the ADAMs. ADAM proteins do not have a specific consensus sequence for cleavage in their substrates, which makes it very difficult to predict target proteins that can be shed by these enzymes. Nevertheless, a long list of substrates has been assembled with the help of proteomic approaches and *in vitro* cleavage assays [100]. ADAM17 and ADAM10 are the two members of the ADAMs family with the longest list of targets and the highest expression in immune cells [100,101] and are therefore involved more than others in the regulation of the immune response. One of the best known examples of shedding by ADAM proteins is the cleavage of TNF by ADAM17, which, for this reason, was originally named TACE (TNF converting enzyme) [102,103]. Other substrates of ADAM17 and ADAM10 with a role in the immune responses include cytokines, growth factors, adhesion molecules and receptors: for example, among common targets of ADAM17 and ADAM10 there are TGFα, CX3CL1, ICAM, IL6R, TNFR1 and CD40L. Since the proteolytic cleavage is irreversible and involves numerous proteins, this process must be tightly regulated at a post-translational level, to avoid unspecific cleavage. The regulatory mechanisms that control ADAMs activity are especially studied for ADAM17 and involve both the intracellular and the extracellular domain of the protein. As already mentioned, a first mechanism to avoid protein digestion on the way to the Golgi, is the inhibition of the catalytic domain by the prodomain of the enzyme. Moreover, the protein TIMP3 (tissue inhibitor of metalloproteinase 3) potently inhibits the catalytic domain by direct binding [104]. Regulation can also occur by phosphorylation of the cytoplasmic tail of the

enzyme, mainly by MAPK, p38 and PLK2 (Polo-like kinase 2), which is believed to activate the enzyme, even if the exact role of this phosphorylation events is still matter of debate [96,105,106]. At the cell membrane, ADAM17 can interact with integrins *in cis*, leading to inhibition of its activity via steric hindrance, or *in trans*, favoring cell-cell interaction and adhesion [96,107]. Furthermore, the localization of ADAM17 in lipid rafts has been demonstrated, implicating that the sequestration of its shedding activity in these membrane microdomains requires the co-localization of its substrates in this area [108]. A more recently discovered regulatory mechanism at the cell membrane is mediated by phosphatidylserine (PS) exposure: cell death or ADAM17 activators such as melittin, ionomycin or phorbol 12-myristate 13-acetate (PMA) provoke massive exposure of the negatively charged PS, which then binds positively charged amino acids in the flexible MPD of the enzyme, bringing the catalytic domain close to the cell membrane, where it can easily encounter the cleavage site of its substrates [109]. Finally, the iRhom proteins RHBDF1 and RHBDF2 are well known interactor partners of ADAM17 and have been discovered as essential mediators of the trafficking of the enzyme from the ER to the cell membrane [110,111]. In the last years additional regulatory effects have been attributed to iRhoms: phosphorylation of iRhom2 has been shown to induce its dissociation from ADAM17, promoting shedding activity [112]; moreover, the stability of ADAM17/iRhom2 complex on the cell surface strongly depends on FRMD8, an interactor partner of iRhom2 that prevents its degradation in the lysosome [113,114]. From the above mentioned mechanisms, it is clear how complex and intricate the regulation of shedding activity by ADAMs is and how intense study is still required to shed light on these processes.
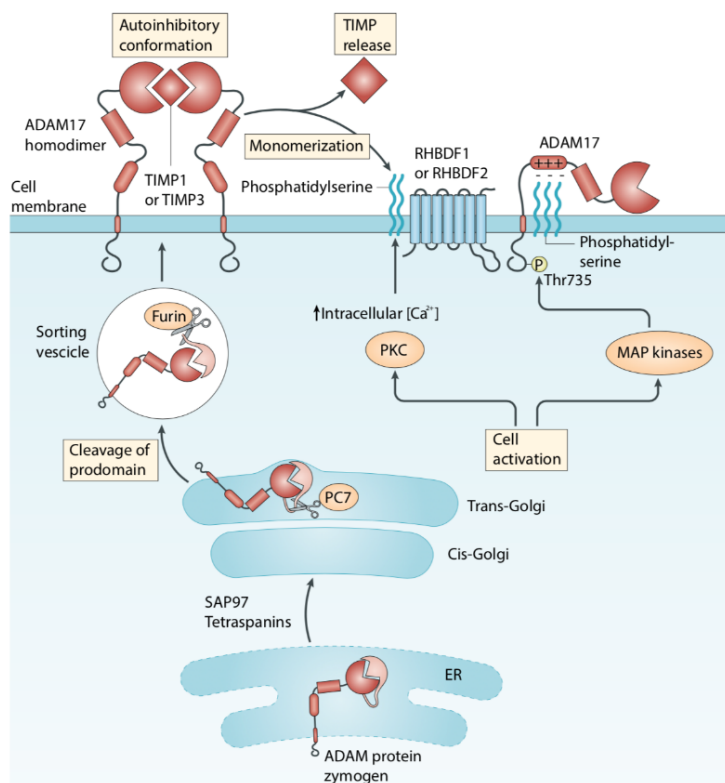
Fig. 1.3 Schematic representation of the regulatory steps that modulate ADAM17 activation. The pro-domain is cleaved by the proteases PC7 and Furin in the trans-Golgi or in the sorting vesicles before the enzyme reaches the cell membrane. Here, other regulatory mechanisms play a role in inhibiting or promoting the activity of ADAM17. Binding of TIMP proteins to the catalytic domain inhibit shedding, while phosphorylation or exposure of phosphatidylserine on the outer leaflet of the membrane are described to induce the shedding activity. The proteins RHBDF1 and RHBDF2 are essential adaptors of the enzyme.

1.8 Cell death mechanisms

Cell death is a biological process that plays an important role in multicellular organisms in maintaining tissue homeostasis, sculpting during embryogenesis, eliminating old or potentially harmful cells and developing the immune system [115]. For many years, cell death was considered to occur in two distinct forms: accidental cell death (uncontrolled and unwanted) and programmed cell death, also referred to as apoptosis. The concepts of programmed cell death and apoptosis were first formulated in 1960s-1970s and since then apoptosis has been considered, for many years, the only form of programmed cell death [116,117]. Only more recently, it started to become clear that programmed cell death can occur in many other ways and that different signaling pathways can actively induce diverse forms of cell death. At time, programmed cell death mechanisms can be subdivided into two categories: apoptosis itself and forms of regulated necrosis [118].
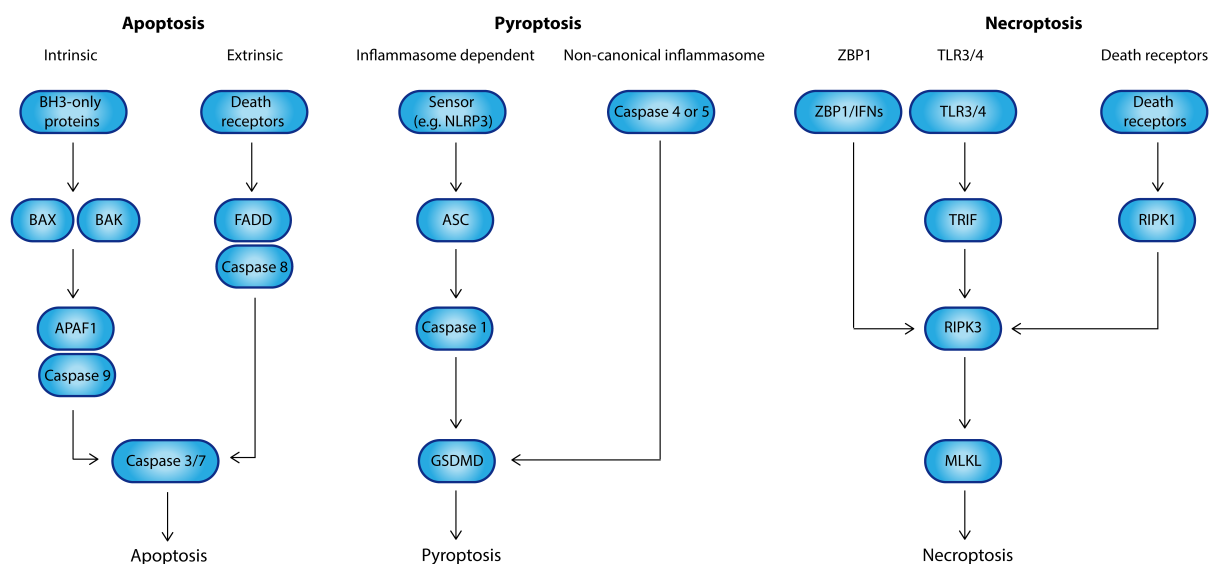
Fig. 1.4 Graphical scheme of the main cell death mechanisms.

1.8.1 Apoptosis

Apoptosis is morphologically characterized by cell shrinkage, chromatin condensation, nuclear fragmentation and formation of apoptotic bodies, which are then usually engulfed by phagocytes upon exposure of "eat me" signals such as phosphatidylserine exposure [119,120]. This type of cell death is considered to be non-inflammatory and immunologically silent, since no cell content is released in the extracellular environment [120]. Apoptosis can be subdivided into extrinsic and intrinsic on the base of the initial stimuli that lead to caspase activation: while extrinsic apoptosis is induced by external stimuli that activate death receptors, such as TNF/TNFR1 or FAS/FASL axes, intrinsic apoptosis initiation depends on factors released from the mitochondria upon a variety of cytotoxic stimuli, such as genotoxic stress or hypoxia [115]. The initiation of apoptosis depends on the downstream activation of a caspase cascade: the initiator caspases caspase-8 and caspase 9 are activated upon extrinsic and intrinsic apoptosis respectively, and lead to subsequent processing of executioner caspases (caspase-3,-6 and -

7), which initiate the events resulting in the cleavage of hundreds of target proteins and in the subsequent "cellular suicide" [115].

1.8.2 Forms of regulated necrosis

The term regulated necrosis describes programmed types of cell death which, although induced by different signaling pathways, share a necrotic-like morphology, characterized by membrane rupture, cell swelling and cytosolic content release. Unlike apoptosis, which is considered to be immunologically silent, forms of regulated necrosis can be inflammatory and potentially induce a potent immune response in the host [118]. Within the last two decades, different forms of regulated necrosis have been described, with a particular focus on pyroptosis and necroptosis.

Pyroptosis

Pyroptosis is a form of regulated cell death induced by inflammatory caspases, namely caspase-1, caspase-5 and caspase-4 [121]. Pyroptosis was initially described in macrophages infected with *Salmonella typhimurium* or *Shigella flexneri* and believed to be apoptosis [122,123]. Later, the term pyroptosis was proposed to describe this form of cell death to highlight its pro-inflammatory capacity [124]. Inflammatory caspases are activated by inflammasomes, macromolecular cytosolic complexes composed of sensor molecules, which recognize different PAMPs or DAMPs, inflammatory caspases and, in most of cases, the adaptor molecule ASC, which functions as a bridge between sensors and caspases [125]. Inflammasome sensors specifically respond to a variety of stimuli: AIM2 senses dsDNA [30,126], NLCR4 recognizes type III secretion proteins and flagellin through members of the NAIP family [127], human NLRP1 is activated by functional degradation [128] and NLRP3 senses disturbances of the cell membrane which cause K^+ efflux [129]. Engagement of the mentioned sensors by their ligands leads to caspase-1 recruitment and activation, which leads to cleavage of its substrates, among which gasdermin D (GSDMD) and IL-1 family members, such as IL-1β and IL-18. GSDMD is the executor molecule of pyroptosis, and its cleavage leads to release of its N-terminal domain, which oligomerizes to form pores in the cell membrane and ultimately kills the cell [130–133]. On the other hand, cleavage of IL-1 family leads to their maturation and their release in the extracellular environment, where they exert immunomodulatory functions (see section 1.4). The activation of caspase-4 and -5 (caspase-11 in mouse) is mediated by direct binding to intracellular LPS, in a process called non-canonical inflammasome activation [134]. Pyroptosis plays a role in the elimination of intracellular pathogens and in promoting immune responses upon infection, by release of IL-1β, IL-18 and other DAMPs. However, an improper activation of the inflammasome pathways is associated to autoinflammatory syndromes, such as the cryopyrin-associated periodic syndromes (CAPS) [135], and to the chronic inflammation observed in inflammatory diseases such as Alzheimer's disease or arteriosclerosis [51,136].

Necroptosis

Necroptosis is a caspase-independent form of regulated necrosis executed by the protein MLKL. It has firstly been described as a type of cell death which could be induced downstream of death receptors, alternatively to apoptosis, in absence of caspase-8 activity [137–141]. In addition, necroptosis can be induced downstream of other pathways, such as TLRs [142,143], interferon signaling [144,145], T cell receptor [146] and genotoxic stress-induced depletion of IAPs [147]. These pathways converge on the engagement of RIPK3, which, after autophosphorylation, phosphorylates MLKL at Thr 357 and Ser 358, leading to its oligomerization and recruitment to the cell membrane to execute cell death [148]. The most characterized pathways leading to necroptosis are TNF receptor signaling and TLR signaling. TNF dependent necroptosis depends on the formation, downstream of TNFR1, of complex IIb, which, in case of inhibited or absent caspase-8 activity, can evolve into the necrosome, composed of RIPK1, RIPK3, and MLKL (see section 1.6 for details on TNFR1 signaling). The presence of active caspase-8 instead leads to cleavage and degradation of both RIPK1 and RIPK3, preventing necroptosis. RIPK3 recruitment to complex IIb relies on the interaction between the RHIM domains present in both RIPK1 and RIPK3. The RHIM domain is present, in addition, in the adaptor molecule TRIF, which is recruited upon TLR4 and TLR3 activation (see section 1.3) and in the protein ZBP1 (Z-DNA-binding protein 1) [149,150]. For this reason, RIPK3 can be directly engaged upon TLR4 and TLR3 activation, and by ZBP1, leading in both cases to necroptosis in case of absent caspase-8 activity. Independently of the stimuli that initiate the necroptotic pathway, the formation of the necrosome is characterized by oligomerization of the involved proteins (RIPK3 alone or the combination of RIPK1 and RIPK3) via their RHIM domain in amyloid-like filamentous structures [151]. The oligomerization of RIPK3 is essential for its autophosphorylation and subsequent engagement of MLKL. Phosphorylation of MLKL in the necrosome results in a conformational change that unmasks the four-helix bundle (4HB) "killer" domain at the N-terminus of MLKL, which is usually inhibited by the pseudokinase domain of the protein. In line with this, N-terminal truncation of MLKL comprising the 4HB region but not the pseudokinase domain are able to induce necroptosis without further activation [152]. After the phosphorylation event and the exposure of the 4HB domain, MLKL oligomerizes and translocates to the cell membrane, where it exerts its cytolytic activity. Since MLKL has been discovered as the executor of necroptosis, research efforts have been focused on finding the mechanism by which this protein can induce membrane rupture and two main models have been developed. The first model implies that MLKL forms membrane ion channels to cause cell lysis [153,154]. However, evidences that MLKL can lyse *in vitro* produced lyposomes suggested a second model, where MLKL exerts direct lytic activity without downstream effectors [155,156]. Moreover, studies on the conformational change of MLKL after phosphorylation, identified the formation of tetramers which detach from the necrosome to be recruited to the cell membrane by binding to phosphatidylinositol phosphates [153,157,158]. These tetramers have been shown, in an independent study, to form octameric channels in the cell membrane and mutants that form tetramers but not octamers fail to induce necroptosis, implying again a direct cytolytic effect of MLKL [159].

A relevant question in necroptosis research is the identification of its physiological role. As highlighted above, necroptosis can only occur in absence of caspase-8 activity, since the presence of the latter would induce apoptosis or, combined with high levels of cFLIP$_L$, promote cell survival (see section 1.6). The importance of caspase-8 in preventing unwanted necroptosis is demonstrated by the fact that caspase-8 deficient mice die embryonically and that RIPK3 co-deletion protects mice from lethality [160–162]. Since necroptosis can be induced downstream of PRRs and TNFR1, it has been proposed that this type of cell death evolved as a defense against pathogens [163]. Indeed, pathogens exist that inhibit apoptotic cell death by inhibiting caspase-8 in order to prevent cell death and boost their spread. A study using vaccinia virus as infection model, showed that RIPK3 deficient mice are not able to control viral replication, have higher virus titer in many organs and finally succumb to infection [164]. Necroptosis induction in this model follows TNF production in response to the infection, but since vaccinia virus produces a natural caspase-8 inhibitor to prevent apoptosis (the protein B13R/Spi2), the necroptotic pathway is engaged instead. Other natural caspase-8 inhibitors include the protein vICA, encoded by murine and human CMV (cytomegalovirus) [165] and viral FLIP-like proteins, produced by herpesviruses and poxviruses [166,167]. The role of necroptosis as a "backup cell death" to control infections is also proved by the existence of viral RHIM domain inhibitors that prevent RIPK3 activation: murine CMV produces not only a caspase-8 inhibitor, but also an inhibitor of RIP activation (vIRA) to prevent necroptosis as consequence of caspase-8 inhibition [163]. A recent work has also described the existance of viral MLKL (vMLKL) encoded by poxviruses, which compete with celluar MLKL for RIPK3 binding, thereby inhibiting necroptosis induction [168].

Given its necrotic nature, necroptosis is believed to be inflammatory due to the potential release of DAMPs and alarmins (see also section 1.5) [53,55]. Moreover, necroptotic cells activate the NLRP3 inflammasome and hence pyroptosis in a secondary fashion, a phenomenon that leads to IL-1β release, which exacerbates the inflammatory effects [169,170]. Therefore, besides the positive role that necroptosis plays in pathogen clearance, this type of cell death has also been linked to the pathogenesis of inflammatory diseases. *In vivo* studies showed that mice lacking FADD in intestinal epithelial cells develop spontaneous colitis and ileitis, which are prevented by RIPK3 deficiency [171]. Another study showed that mice with FADD deficient keratinocytes develop RIPK3-dependent necroptosis and skin inflammation [172]. MLKL-dependent necroptosis was also proved to contribute to tissue inflammation in a mouse model of acute pancreatitis [173]. In addition, RIPK3 has been shown to play a role in the exacerbation of ischemia-reperfusion-induced injury and inflammation and in rejection of kidney and heart transplantations in mouse models [174–176]. Additionally to *in vivo* studies, evidences linked necroptosis to inflammation in some human diseases: epithelial cell death and chronic inflammation of the terminal ileum are hallmarks in patients with Crohn's disease, and RIPK3 overexpression was observed in samples from patients with the disease, suggesting necroptosis involvement [177]. Moreover, a study linked necroptosis of keratinocytes to cutaneous adverse drug reactions in a mouse model and in humans [178]. The contribution of necroptosis to hepatocyte death and liver inflammation has also been suggested in non-

alcoholic steatohepatitis, in alcohol-induced and drug-induced liver disease [156,179,180]. In addition, evidences for a role of necroptosis in neurodegenerative diseases have been reported in human samples and mouse models [181,182]. Taken together, these studies provide correlative evidences that necroptosis could be involved in inflammatory diseases, even if the statement of a causative association is difficult due to the complex pathogenesis of these diseases.

2. Aim of the work

As discussed above, necroptosis is believed to be involved in the pathogenesis and/or in the exacerbation of inflammatory diseases. The release of cellular content with potential DAMPs is often described as the cause of the inflammatory properties associated with this type of cell death. However, only few studies exist that try to identify the nature of potential DAMPs released by cells that die with a necrotic-like morphology [53]. *In vitro* studies have mainly used accidental necrosis as an experimental model, where cells are killed by freeze and thaw cycles or by heating [183–185]. The induction of pro-inflammatory responses has then been evaluated by the ability of necrotic cells to induce an immune response in supernatant transfer or co-culture experiments [53]. An obvious drawback of these experiments is that accidental necrosis does not necessarily lead to the secretion of the same inflammatory molecules that are released in the context of necroptosis. Moreover, many of these studies were able to identify an immunological outcome but not a specific DAMP responsible for the observed inflammatory phenotype. *In vivo* studies make use of genetic models where caspase-8 or FADD are deleted, in order to obtain a necroptotic-prone system. The advantage of these models is that necroptosis is induced by mean of genetic bases but, on the other hand, *in vivo* studies are often complicated to interpret, due to the multiple multidirectional relations that exist between tissue damage, DAMP release, necroptosis and cytokine production by immune cells, which can amplify the signals involved in both cell death and inflammation. This makes it difficult to establish a direct link between necroptosis (or necroptotic DAMPs) and the observed inflammatory phenotype [53,55]. In addition, the identification of specific necroptosis-associated DAMPs or alarmins *in vivo* is even a bigger challenge. Moreover, recent literature has described a direct role of RIPK3 in NF-kB activation, which introduces a necroptosis-independent role of RIPK3 in induction of inflammation [186–188]. This finding introduces another confounding variable in the investigation of necroptosis-dependent inflammation, since certain danger signals may be RIPK3 dependent but necroptosis independent.

Given the lack of studies that focus on the identification of necroptosis-specific DAMPs and that provide proves for the existence of a direct link between necroptosis and inflammation, with this work we aim to:

1. Develop an *in vitro* model to study the inflammatory capacity of necroptotic cells on bystander resting cells.
2. Dissect the immune pathways activated in resting cells upon supernatant transfer and co-culture experiments with necroptotic cells.
3. Identify necroptosis-associated DAMPs responsible for the activation of specific immune pathways in resting cells. The modality of production, release and action of the identified DAMPs is also a matter of this study.

3. Material and Methods

3.1 Material

The consumables for sterile and non-sterile laboratory work came from the following manufacturers: Bioplastics, Biorad, Biozym, Corning, Greiner, Labomedic, Neolab, Sarstedt and VWR.

3.1.1 Chemicals and reagents

Chemical/Reagent	Supplier
6X Loading Dye	Thermo Fisher Scientific
Acetic Acid	Roth
Agarose powder	Biozym
BD Pharm Lyse™	BD Biosciences
Bromphenolblue	Roth
BSA	Roth
$CaCl_2$	Roth
cOmplete™ Protease Inhibitor Cocktail	Roche
Deoxyribonucleic acid sodium salt from herring testes (HT-DNA)	Sigma-Aldrich
DMSO	Roth
DNA Ladder	Fermentas
DNA stain G	Serva
Doxycyclin Hyclate	Sigma-Aldrich
DTT	Roth
EDTA (0,5 M pH = 8 solution)	Life Technologies
EDTA powder	Roth
Ethanol	Roth
Gene Ruler 1kb or 100bp	Thermo Fisher Scientific
Glycerol	Roth
Glycin	Roth
HCl	Roth
Isopropanol	Roth
KCl	Roth
LB	Roth
LB agar	Roth
$MgCl_2$	Roth
Na_2HPO_4	Roth
NaCl	Roth
PageRuler™ Prestained Protein Ladder	Thermo Fisher Scientific
PhosSTOP Phosphatase Inhibitors	Roche
Pierce ECL WB substrate	Thermo Fisher Scientific
Ponceau S staining	Sigma-Aldrich

RNase A	Life Technologies
SDS	Roth
TRIS	Roth
Triton X 100	Roth
Trypsin EDTA	Gibco
Tween 20	Roth

3.1.2 Enzymes and enzyme buffers

Enzyme or buffer	Supplier
Fast digest restriction enzymes and buffers	Fermentas
NEB2 Buffer	NEB
Phusion Polymerase and buffer	Fermentas
Proteinase K	Roth
T4 DNA Ligase and buffer	Fermentas
T4 DNA polymerase	Enzymatics

3.1.3 Kits

Kit	Supplier
Amicon Ultra-15 Centrifugal Filter Unit, Ultracel, 10 KDa, 15 mL	EMD Millipore
BCA assay kit	Thermo Fisher Scientific
CD14 Microbeads	Miltenyi
CellTiter-Glo® Luminescent Cell Viability Assay	Promega
ELISA kits	BD Biosciences
Lineage Cell Depletion Kit	Miltenyi
Pierce LDH cytotoxicity assay kit	Thermo scientific
PureLink Maxi-Prep kit	Invitrogen
QIAquick gel extraction kit	Qiagen
QIAquick PCR purification kit	Qiagen

3.1.4 Buffers and solutions

Buffer/Solution	Components
10X PBS	800g NaCl 20g KCl, 142g Na_2HPO_4 add water to 10L, pH 7.4
10X TBS	240 g Tris base 880 g NaCl Dissolve in 900 mL distilled

	water Add water to 10 L, pH 7.6
10X Tris-Glycine buffer	290g Tris 1440g Glycine add water to volume 10 L
2X Laemmli Sample buffer	150 mM Tris-HCl pH 6.8 200 mM DTT 4% SDS >0.02% Bromophenol Blue 20% Glycerol add water to final volume 100 ml
50X TAE Buffer	242g Tris 57.1 ml Acetic acid 18.6g EDTA 2Na-2H2O add water to 1L
6X Laemmli Sample buffer	450 mM Tris-HCl pH 6.8 600 mM DDT 12% SDS >0.02% Bromophenol Blue 60% Glycerol Add water to 100mL
Direct Lysis Buffer	0,2 mg/ml Proteinase K 1 mM CaCl2 3 mM MgCl2 1 mM EDTA 1 % Triton X-100 10 mM Tris pH 7,5
HBS buffer	50 mM HEPES 280 mM NaCl 1.5 mM Na2HPO4 pH = 7 sterile filtered
LB agar	20 g LB 15 g Agar 1 L H2O Autoclaved before use
LB medium	20 g LB 1 l H2O Autoclaved before use
MACS buffer	2mM EDTA 2% FCS in PBS
Miniprep buffer N3	4,2 M Guanidinhydrochlorid

	0,9 M Kaliumacetat pH = 4,8
Miniprep buffer P1	50 mM Tris pH = 8,0 10 mM EDTA 100 µg/ml RNase A
Miniprep buffer P2	200 mM NaOH 1 % SDS
Miniprep buffer PE	10 mM Tris pH = 7,5 80 % ethanol
PBST (ELISA wash buffer)	1L 10X PBS 9L Water 5 ml Tween-20
TBST	1L 10X TBS 9L Water 5 ml Tween-20
Western Blot transfer buffer	200 ml 10X Tris-Glycine buffer 400 ml Ethanol 1400 ml water

3.1.5 Cell culture media and reagents

Reagent or medium	Supplier
ABT-737	Selleck Chemicals
B/B homodimerizer	Takara Bio
CLI095	Invivogen
DMEM with glutamine	gibco
Fetal cow serum (FCS)	gibco
FluoroBrite DMEM	gibco
GeneJuice	Merck
GSK'872	Aobious
HEPES	gibco
hIL-1β recombinant	Invivogen
hIL-3	PeptoTech
hM-CSF	PeptoTech
IVT4	Self-made
Lipofectamine 2000	Life Technologies
LPS (E. coli)	Invivogen
MCC950 (CRID3)	Invivogen
mFLT3L	PeptoTech
mIL-3	PeptoTech
mIL-6	PeptoTech
mSCF	PeptoTech
mTPO	PeptoTech

Penicillin/streptomycin	gibco
Puromycin	Roth
R848	Invivogen
Retronectin	Takara Bio
RPMI with glutamine	gibco
s63845	Selleck Chemicals
Sodium pyruvate	gibco
StemPro™-34 SFM (1x)	gibco
Z-VAD-FMK	Peptanova
β-estradiol	Sigma-Aldrich

3.1.6 Antibodies and FACS reagents

Antibodies	Supplier	Application	Dilution
Anti-rabbit IgG, HRP linked Antibody	Cell Signaling Technology	WB	1:3000
CaptureSelect™ Alexa Fluor™ 488 Anti-C-Tag Coniugate	Thermo Scientific	Live-cell imaging	1:480
CaptureSelect™ Biotin Anti-C-Tag Coniugate	Thermo Scientific	WB	1:800
hCASP8	Cell Signaling Technology	WB	1:1000
IkBα (L35A5)	Cell Signaling Technology	WB	1:1000
Lineage Cell Detection Cocktail-Biotin	Miltenyi	FACS	Manufacturer's instructions
MLKL	Thermo Scientific	WB	1:1000
Pacific Blue Annexin V	Biolegend	FACS	details in methods
Phospho-IkBα	Cell Signaling Technology	WB	1:1000
Phospho-NF-kB p65 (ser536)	Cell Signaling Technology	WB	1:1000
pMLKL (ser358)	Abcam	WB	1:800
Propidium iodide (PI)	eBioscience	Microscopy	1:250
hRIPK3	Cell Signaling Technology	WB	1:1000
TNF-α (D5G9) Rabbit mAb	Cell Signaling Technology	WB	1:1000
β-actin antibody with HRP	Santa Cruz Biotechnology	WB	1:2000

3.1.7 Primers

Name	Sequence	Used for
ADAM10_fwd	ACACTCTTTCCCTACACGACGCTCTTCCGATCTGTCCAGTGTAAATATGAGAGGTATC	Genotyping
ADAM10_rev	TGACTGGAGTTCAGACGTGTGCTCTTCCGATCTGTCAGCGTATTTCACAAATAGAC	Genotyping
ADAM17_fwd	ACACTCTTTCCCTACACGACGCTCTTCCGATCTGTAGGTGATGGCTGGATATTGAG	Genotyping
ADAM17_rev	TGACTGGAGTTCAGACGTGTGCTCTTCCGATCTTACACAGCCTCTTTCCAAACCAC	Genotyping
CASP4_fwd	ACACTCTTTCCCTACACGACGCTCTTCCGATCTGACGTCTTCTCTCTCGATCTTCT	Genotyping
CASP4_rev	TGACTGGAGTTCAGACGTGTGCTCTTCCGATCTTGGTGCACTGAAGGAAAGCAATG	Genotyping
CASP8_fwd	ACACTCTTTCCCTACACGACGCTCTTCCGATCTCAACATTCTCTTTTCCTGGAGTC	Genotyping
CASP8_rev	TGACTGGAGTTCAGACGTGTGCTCTTCCGATCTGTAGCCTTTGATGAACAAGCCAG	Genotyping
EGFP_rev BclI	GTGCTGATCATTACTTGTACAGCTCGTCCATG	Cloning
IL1R_fwd	ACACTCTTTCCCTACACGACGCTCTTCCGATCTGTGGAGTCAAAGATAGGCTCATC	Genotyping
IL1R_rev	TGACTGGAGTTCAGACGTGTGCTCTTCCGATCTGAGGTCGTCTTGGATTTGGTTTC	Genotyping
IL6_fwd	ACACTCTTTCCCTACACGACGCTCTTCCGATCTAAGCCTACCCACCTCCTTTCTCA	Genotyping
IL6_rev	TGACTGGAGTTCAGACGTGTGCTCTTCCGATCTCTCCCAGCTGTGCTGTCAGCTCA	Genotyping
LICsgRNA_rev	AACGGACTAGCCTTATTTTAACTTGCTATTTCTAGCTCTAAAAC	LIC cloning
LTA_fwd	ACACTCTTTCCCTACACGACGCTCTTCCGATCTCCATTCTCCTGCTGCCTCACCTG	Genotyping
LTA_rev	TGACTGGAGTTCAGACGTGTGCTCTTCCGATCTTCTGACTGCATCTTGTCCCCTTC	Genotyping
MAVS_fwd	ACACTCTTTCCCTACACGACGCTCTTCCGATCTGGCATTGTGTCTTCCAGGATCGA	Genotyping
MAVS_rev	TGACTGGAGTTCAGACGTGTGCTCTTCCGATCTTACAGGGAGAGAGAAAAGGAGAG	Genotyping
mCherry_fwd fusion	GTACAAGGGGGGAGGCGGAAGTAGCACTGAAAGCATGATCCG	Cloning
mCherry_fwd NheI	GATCGCTAGCATGGTGAGCAAGGGCGAGGA	Cloning
mCherry_fwd XhoI	ATGCCTCGAGATGGTGAGCAAGGGCGAGGA	Cloning
mCherry_rev BamHI	GTCAGGATCCTCACTTGTACAGCTCGTCCATG	Cloning
mCherry_rev fusion	CAGTGCTACTTCCGCCTCCCCCCCTTGTACAGCTCGTCCATGCC	Cloning
mCherry_rev NotI	GATTGCGGCCGCTCACTTGTACAGCTCGTCCATG	Cloning
MLKL BglII rev	GTATAGATCTTCACTTGTCATCGTCGTCCTTGTAGTCCTTAGAAAAGGTGGAGAGTT	Cloning
MLKL DE/AA mut fwd	ACGTGAACAGGAAGCTGAGTGCTGTCTGGAAGGCGCTCTCGCTGTTACTTCAGGT	Mutagenesis
MLKL DE/AA mut rev	ACCTGAAGTAACAGCGAGAGCGCCTTCCAGACAGCACTCAGCTTCCTGTTCACGT	Mutagenesis
MLKL TS/ED mut fwd	GTTGAGGAAAACACAGGAAGACATGAGTTTGGGAACTACGAG	Mutagenesis
MLKL TS/ED mut rev	CTCGTAGTTCCCAAACTCATGTCTTCCTGTGTTTTCCTCAAC	Mutagenesis
MLKL_1-154_FLAG_rev BamHI	ATAGGATCCTCACTTGTCATCGTCGTCCTTGTAGTCATCTCTTCTTAGCA	Cloning

MLKL_1-201_FLAG_rev BamHI	ATAGGATCCTCACTTGTCATCGTCGTCCTTGTAGTCAAGCTGCTCCTTCTTG	Cloning
MLKL_fwd	ACACTCTTTCCCTACACGACGCTCTTCCGATCTCAAAGACCCAGCTTGCCTCTTC	Genotyping
MLKL_fwd NheI	TGCATGCTAGCATGGAAAATTTGAAGCATATTATC	Cloning
MLKL_rev	TGACTGGAGTTCAGACGTGTGCTCTTCCGATCTAGGAGGCTAATGGGGAGATAGAA	Genotyping
mRIPK3_fwd SpeI	GACAAACTAGTATGTCTTCTGTCAAGTTATGGCCTAC	Cloning
MYD88_fwd	ACACTCTTTCCCTACACGACGCTCTTCCGATCTCGCACGTTCAAGAACAGAGACAG	Genotyping
MYD88_rev	TGACTGGAGTTCAGACGTGTGCTCTTCCGATCTTTTTGCTCGGGGCTCCAGATTGT	Genotyping
nBFP_fwd XhoI	AGTCTCGAGATGCCAGCAGCGAAGAA	Cloning
nBFP_rev BamHI	AGTAGGATCCTCAATTAAGTTTGTGCCC	Cloning
RIPK3_fwd	ACACTCTTTCCCTACACGACGCTCTTCCGATCTTCCTTTGCAGCTGGCAGATTTTG	Genotyping
RIPK3_rev	TGACTGGAGTTCAGACGTGTGCTCTTCCGATCTAAAGCTGAGGATCGGTCCAATCA	Genotyping
STING_fwd	ACACTCTTTCCCTACACGACGCTCTTCCGATCTTTCTACCTCCCCCTGTGTCATAC	Genotyping
STING_rev	TGACTGGAGTTCAGACGTGTGCTCTTCCGATCTGTCTGGCTGTCACTCACAGGTAC	Genotyping
TLR4_fwd	ACACTCTTTCCCTACACGACGCTCTTCCGATCTCCAGCCAGACCTTGAATACAAGT	Genotyping
TLR4_rev	TGACTGGAGTTCAGACGTGTGCTCTTCCGATCTCTGACCAATCTAGAGCACTTGGA	Genotyping
TNF_fwd	ACACTCTTTCCCTACACGACGCTCTTCCGATCTTCTTGCGTCTCCATTTCCCCTTG	Genotyping
TNF_fwd NheI	TGCATGCTAGCATGAGCACTGAAAGCATGATC	Cloning
TNF_fwd XhoI	AGTCTCGAGATGAGCACTGAAAGCATGATC	Cloning
TNF_rev	TGACTGGAGTTCAGACGTGTGCTCTTCCGATCTCTGGAAAGGACACCATGAGCACT	Genotyping
TNF_rev BamHI	GATGGATCCTCACAGGGCAATGATCCCAAAG	Cloning
TNFR1A_fwd	ACACTCTTTCCCTACACGACGCTCTTCCGATCTCACACTCACCCTTTCGGCATTTG	Genotyping
TNFR1A_rev	TGACTGGAGTTCAGACGTGTGCTCTTCCGATCTTCTCCTAGAGACTTCAGGGAATC	Genotyping
TRIF_fwd	ACACTCTTTCCCTACACGACGCTCTTCCGATCTTCTAGAGGCATTGAAGGCCGATG	Genotyping
TRIF_rev	TGACTGGAGTTCAGACGTGTGCTCTTCCGATCTTTTCGGGCCTCATCCTGAAGTTC	Genotyping

3.1.8 Plasmids

Plasmid	Usage
pCMV-Gag-Pol	Retrovirus generation
pCMV-VSVG	Lentivirus/Retrovirus generation
pEF-BOS_nBFP	Transfection experiments
pFUGW_C-Tag-TNF	Transfection experiments
pFUGW_mRIPK3 2x Fv T2A EGFP	Transduction of J774 and HSC
pLI_C-Tag-TNF	Transfection experiments
pLI_C-Tag-TNF mCherry	Transfection experiments
pLI_ev (empy vector)	Transfection experiments
pLI_mCherry	Transfection experiments
pLI_MLKL TS/ED	Transfection experiments
pLI_MLKL TS/ED and DE/AA	Transfection experiments
pLI_MLKL1-154	Transfection experiments

pLI_MLKL1-201	Transfection experiments and generation of stable MLKL 1-201 expressing cells
pLI_TNF	Transfection experiments
pMDLg/pRRE	Lentivirus generation
pMini_U6_gRNA_CMV_BFP_T2A_Cas9	KO generation
pMini_U6_gRNA_CMV_mCherry_T2A_Cas9	KO generation
pRP_ev (empty vector)	Transfection experiments
pRP_mCherry	Transfection experiments and generation of stable mCherry positive BLaER1
pRP_TNF	Transfection experiments
pRSV-REV	Lentivirus generation
pRZ_Cas9_BFP	KO generation

3.1.9 sgRNAs

sgRNAs oligos are comprised of the sequence 5'-GGAAAGGACGAAACACCG-3' followed by the specific target site listed below without PAM sequence, followed by 5'-GTTTTAGAGCTAGAAATAGCAAGTTAAAATAAGG-3'. The PAM sequence is highlighted in bold.

Target gene	Sequence of target site
ADAM10	TTTCAACCTACGAATGAAG**AGG**
ADAM17	GAGCAGAACATGATCCGGA**TGG**
CASP4	CTCATCCGAATATGGAGGC**TGG**
CASP8	GCTCAGGAACTTGAGGG**AGG**
IL1R	CAAGCAATATCCTATTACC**CGG**
IL6	TGTGGGGCGGCTACATCTT**TGG**
LTA	ACGTTCAGGTGGTGTCATG**GGG**
MAVS	ACTTCATTGCGGCACTGAG**GGG**
MLKL	GAGCTCTCGCTGTTACTTC**AGG**
MYD88	CTGCAGGAGGTCCCGGCGC**GGG**
RIPK3	TTCTGGGGCCAAGTAGCCC**AGG**
STING	GCGGGCCGACCGCATTTGGG**AGG**
TLR4	GATAAAGTTCATAGGGTTC**AGG**
TNF	TGCAGCAGGCAGAAGAGCG**TGG**
TNFR1	GCAGTCCGTATCCTGCCCC**GGG**
TRIF	GGCCCGCTTGTACCACCTGC**TGG**

3.1.10 Laboratory equipment

Machine	Supplier
Absorbance readers	TECAN/ Epoch
AKTA Basic	GE Healthcare
Amicon Ultra-15, 10kDa	Merck
Biomek FX Robot	Beckman Coulter
Chemidoc imaging system	Biorad

Fusion Fx device	Vilber
Gene Pulser Xcell	Biorad
Microscopes	Leica
Nanodrop	Peqlab
Optima XPN-80 Ultracentrifuge	Beckman Coulter
PCR cycler	Biorad
Sony sorter SH800Z	Sony
Spinning disk microscope	Nikon
Superose 6 10/300 GL column	GE Healthcare
Thermoshaker	Eppendorf

3.2 Cell culture methods

3.2.1 Cell lines

BLaER1: a subclone of a human B cell-lymphoma cell line expressing the transdifferentiation construct CEBPα-ER-GFP.

THP1 (ATCC® TIB-202™): monocytic cell line obtained from a human leukemia patient.

HEK 293T (ATCC®CRL-3216™): human embryonal kidney cells stably expressing SV40 Large T antigen.

J774 (ATCC®TIB-67™): mouse macrophage cell line from ascites.

3.2.2 Cell culture conditions

All cells were cultivated at 37°C, 5% CO_2. FCS was heat-inactivated at 55°C for 1 h and filtered before use. BLaER1 and THP1 cells were cultured in RPMI 1640 medium supplemented with 10% FCS, 1% sodium pyruvate, 100 U/mL penicillin-strepomycin (all Gibco). For transdifferentiation into macrophages, 0.7 x 10^5 BLaER1 cells were plated in 96 wells in 100 ul of differentiation medium containing 10 ng/mL IL-3, 10 ng/mL M-CSF (both Peprotech) and 100 nM β-estradiol (Sigma-Aldrich). After 5 days, cells were stimulated according to the experimental needs in fresh regular RPMI medium. J774 macrophages and HEK293T cells were cultured in DMEM supplemented with 10% FCS, 1% sodium pyruvate, 100 U/mL penicillin-streptomycin. Splitting of all cell lines was performed every 3-4 days depending on cell confluence. Primary human monocytes were cultured in RPMI 1640 medium supplemented with 10% FCS, 1% sodium pyruvate, 100 U/mL penicillin-strepomycin. Differentiation into monocytes-derived macrophages was obtained with 7-8 days of culture in the presence of M-CSF (Peprotech) at the final concentration of 100 ng/mL. Fresh M-CSF was added to culture medium every 2-3 days during the differentiation period.

3.2.3 Isolation of PBMCs and primary monocytes

PBMCs were isolated from heparinized blood of informed consenting healthy volunteers. Samples were diluted in 0.9% NaCl solution to final volume of 100 ml. 13 ml of Ficoll solution was placed at the bottom of a 50 ml falcon tube, then 35 mL of diluted blood was gently

pipetted against the wall of the falcon, on top of the Ficoll layer. Cells were separated by centrifugation at 800 g for 15 minutes at room temperature (RT) with speed-up/break 9/1. The layer of white cells over Ficoll was then collected in separate falcon tubes, followed by dilution with 0.9% NaCl solution up to 50 mL and centrifugation at 450 g for 7-10 minutes. Supernatant was discarded and 10 ml of 1X BD Pharm lyse solution was added for 5 minutes to lyse erythrocytes. Cold PBS was next added up to 50 ml and cells were centrifuged at 450 g for 7 minutes at 4°C (speed-up/break 9/1). Supernatant was discarded and cells were resuspended in cold MACS Buffer (0.5% FSC, 2mM EDTA in PBS) for subsequent monocytes isolation using the CD14 positive selection method of MACS technology (Miltenyi). Purified monocytes were then plated as desired (0.8 x 10^5 cells/well in a 96 well plate or 1 x 10^6/well in a 24 well plate) and cultivated as described in section 3.2.2.

3.2.4 Isolation of hematopoietic stem cells from murine bone marrow

To isolate hematopoietic stem cells (HSC) from bone marrow cells, 8 weeks old WT C57BL/6 mice were euthanized by cervical dislocation. Femurs and tibias were taken, cleaned from tissue, washed in 70% ethanol for 1 minute and put in ice-cold PBS. Bone marrow was flushed with PBS from cut bones through a 70 um nylon strainer into a falcon tube. Cells were then centrifuged at 450 g for 10 minutes and the pellet was resuspended in 1X BD Pharm lyse solution for 2 minutes to lyse erythrocytes. After addition of cold PBS, cells were centrifuged a second time as above. Afterwards, cell pellet was resuspended in cold MACS Buffer to proceed to HSC isolation by negative selection with the Direct Lineage Depletion Kit (Miltenyi) using MACS technology. Isolated HSC were counted and seeded in 6-well plates at the concentration of 1 x 10^6 cells/mL in StemPro™-34 SFM (1X) media (gibco) supplemented with StemPro®-Nutrient Supplement, 100 U/mL penicillin-strepomycin and the following cytokines (all PeproTech): IL-3 (10 ng/mL), FLT3-L (10 ng/mL), SCF (100 ng/mL), TPO (20 ng/mL), IL-6 (20 ng/mL). The purity of isolated HSC was tested by flow cytometry by staining with the Lineage Cell Detection Cocktail-Biotin (Miltenyi) following manufacturer´s instructions.

3.3 Cell biology methods and stimulations

3.3.1 Stimulation of BLaER1 cells for necroptosis induction and supernatant transfer experiments

Unless otherwise stated, necroptosis prone CASP8$^{-/-}$ and necroptosis resistant CASP8$^{-/-}$ x RIPK3$^{-/mut}$ or CASP8$^{-/-}$ x MLKL$^{-/-}$ BLaER1 cells differentiated as described in section 3.2.2, were stimulated with LPS from *E.Coli* (Invivogen) at a final concentration of 2 ng/mL in 100 ul of a 96 well for the indicated periods of time. In case of supernatant transfer experiments, the supernatant from LPS-stimulated donor cells was collected after 18 h and centrifuged at 600 g for 5 minutes to eliminate remaining cells and cell debris. Supernatant was then used undiluted to stimulate recipient cells of the indicated genotypes for 24 h. For heat shock experiments, supernatant of donor cells was heated at 75°C for 10 minutes. If recipient cells were not in a TLR4$^{-/-}$ background, the TLR4 inhibitor CLI095 was added to the supernatant at a final concentration of 1 ug/mL to inhibit LPS-dependent NF-kB activation.

When needed, the NLRP3 inhibitor MCC950 (CRID3) was used at the final concentration of 5 uM. If supernatant samples were to be analyzed by western blot, cells were stimulated in 3% FCS containing medium and at least 15 wells of a 96-well plate were pooled for each sample.

3.3.2 Stimulation of immune receptors with specific agonists in BLaER1 cells

To prove specific deletion of different immune receptors, BLaER1 cells deficient for the respective immune pathways were stimulated with LPS (2 ng/mL) or the TLR7 and TLR8 agonist R848 (1 ug/mL) or transfected with 200 ng/well of IVT4 or HT-DNA in combination with 0.5 ul lipofectamine/well. For the transfection, two independent tubes were prepared with lipofectamine (or the needed nucleic acid in optimem (25 ul/well). After 5 minutes incubation, the two solutions were mixed and incubated for 20 minutes; lastly, 50 ul of the solution was added in each well of a 96-well plate. After 16 h, supernatant was collected for ELISA analysis.

3.3.3 Co-culture experiments

CASP8$^{-/-}$ and CASP8$^{-/-}$ x RIPK3$^{-/mut}$ donor and TLR4$^{-/-}$ recipient BLaER1 cells were plated in a 1:1 ratio in 96 well plates and differentiated as described in section 3.2.2. On the day of stimulation, cells were analyzed by flow cytometry for mCherry and GFP positivity (donor cells were GFP positive, recipient cells were GFP and mCherry positive) to monitor the percentage of donor and recipient cells after differentiation. Cells were then stimulated with 2 ng/mL LPS for 8h or 24h and further analyzed by LDH assay and ELISA.

3.3.4 Pyroptosis and apoptosis induction in BLaER1 cells

To induce pyroptosis, BLaER1 cells were primed with 2 ng/mL LPS for 3 h or 14 h, then nigericin was added at the concentrations of 6.5 uM, 3.25 uM and 1.62 uM for 2 h before supernatant harvesting. To induce apoptosis, BLaER1 cells were primed with 2 ng/mL LPS for 3h or 14h and then stimulated with the combination of the Bcl-2 inhibitor ABT-737 and the Mcl-1 inhibitor s63845 (both Selleck Chemicals) at the concentrations of 4 uM or 10 uM for 3 h or 6 h, respectively. Supernatant was then collected for Cell Titer Glo (CTG) assay and ELISA analysis.

3.3.5 Annexin V titration experiments

To study the effect of phosphatidylserine on ADAM17 activation upon necroptosis, CASP8$^{-/-}$ and CASP8$^{-/-}$ x RIPK3$^{-/mut}$ BLaER1 cells were incubated in Annexin V-containing medium at the concentrations of 0.32 ug/mL, 0.11 ug/mL or 0.03 ug/mL; cells were concomitantly stimulated with 2 ng/mL LPS for different periods of time to induce necroptosis. Successful binding of Annexin V to phosphatidylserine was tested by flow cytometry analysis of stimulated cells.

3.3.6 Necroptosis induction in primary monocytes-derived macrophages

Necroptosis was induced in primary macrophages with a combination of 0.2 ng/mL LPS and 20 uM Z-VAD-FMK (Peptanova) for 8 h. To inhibit necroptosis, the RIPK3 inhibitor GSK'872

(Aobious) was added to a final concentration of 3 uM. In case of western blot analysis, stimulation was performed in 3% FCS containing medium.

3.3.7 Stimulation of J774 and HSC with B/B homodimerizer

J774 transduced to express mRIPK3 2xFv T2A EGFP (see section 3.3.15) or left untransduced as control were seeded in 96 well plate at the concentration of 0.7×10^5 cells/well. The day after, cells were primed for 1 h with 2 ng/mL LPS and then stimulated for 15 h with B/B homodimerizer at given concentrations. Supernatant was then collected and analyzed by LDH assay to assess necroptotic cell death and by ELISA to measure secreted TNF. HSC were transduced or left untransduced as control. The day after transduction, 0.7×10^5 cells/well were plated in a 96 well plate and differentiated into macrophage-like cells in fully supplemented DMEM with addition of 100 ng/mL M-CSF for 5 days. Next, cells were stimulated for 15 h with B/B homodimerizer at indicated concentrations and medium was collected and analyzed by TNF ELISA and LDH assay.

3.3.8 Transfections

For western blot analysis, 0.65×10^6 293T cells were seeded in 6 well plates and transfected the day after as follows: 3 ug of DNA/well was diluted in 250 ul/well of Optimem medium (Gibco) and incubated at RT for 5 minutes. When 2 plasmids had to be transfected, 1.5 ug of each plasmid was used. In parallel, 6 ul of GeneJuice reagent (Merck) was diluted in 250 ul Optimem and incubated for 5 minutes. The two solutions were then mixed together and incubated at RT for further 20 minutes, after which 500 ul solution/well was added dropwise. For ELISA analysis, 293T cells were plated in 96 well plates at the concentration of 0.2×10^5 cells/well and transfected the day after with 200 ng DNA/well and 0.5ul GeneJuice/well in a total volume of 50 ul of Optimem. The same procedure as described above was used to prepare the transfection mixture.

3.3.9 Doxycycline stimulation and necroptosis induction in 293T cells

293T cells of the needed genotypes were transiently transfected as described in section 3.3.8. Cells plated in 96-well plates were treated with 1 ug/mL doxycycline 6 h after transfection to induce the expression of proteins encoded in pLI plasmid backbone, namely truncations or mutants of MLKL protein (MLKL 1-154 and MLKL 1-201, MLKL TS/ED, MLKL TS/ED_DE/AA), TNF or C-Tag-TNF. After 16 h, supernatant was collected for further analysis by LDH assay and ELISA. Cells transfected in 6-well plates for western blot analysis were incubated for 18 h after transfection. Afterwards, medium was replaced with fresh 3% FCS containing DMEM and cells were treated with 1 ug/mL doxycycline for 7 h before sample collection.

3.3.10 Enzyme-linked immunosorbent assay – ELISA

Absolute quantification of cytokines (human TNF, human IL-6, human IP-10, human IL-1β, murine TNF) in the supernatant of experimental samples was measured by ELISA kits (all OptEia, BD Bioscience) according to manufacturer's instructions. Briefly, high binding

plates were coated with the proper dilution of capture antibody in ELISA coating buffer overnight at 4°C. The next day, plates were washed 3 times with PBST and blocked with 10% FCS in PBS for 1 h at RT. Then, 50 ul of samples or standard were loaded on the plates and incubated 2 h at RT. If needed, samples were diluted in 10% FCS PBS to not exceed the highest point of the standard. After 5 more washings, a mix containing detection antibody and streptavidin-HRP was loaded for 1 h in the dark. Afterwards, plates were washed 5 more times and developed by addition of 50 ul of TMB solution (BD Bioscience). The reaction was stopped by addition of 2N sulfuric acid. Absorbance was read at 450 nm and 570nm by Gen5-Epoch microplate reader (BioTek).

3.3.11 Lactate dehydrogenase assay – LDH

The assay was performed according to manufacturer's instructions (Pierce LDH cytotoxicity assay kit - Thermo scientific). Briefly, a positive control with 100% cell death was generated by lysing untreated cells with 10x lysis buffer for 10 min at 37°C. Then, supernatant from samples and lysed control was centrifuged for 5 minutes at 450 g to remove cells and cell debris. Afterwards, 15 ul of supernatant was mixed 1:1 with LDH substrate in a flat-bottom 384 well plate and incubated in the dark at RT for 15-20 minutes. Absorbance was measured at 490 nm and 680 nm by Spark20M microplate reader (Tecan). Relative LDH release was calculated as follows: LDH release (%) = 100 x (measurement – unstimulated control)/ (direct lysis control –unstimulated control).

3.3.12 Cell titer Glo Assay

The assay was performed according to manufacturer´s instructions (Promega). Briefly, a positive control of 100% cell death was generated by lysing untreated cells with Triton-X for 2 min. Then, medium was removed from all samples and 75 ul of fresh medium was added to each well followed by 25 ul of cell titer glo reagent. After 5 min incubation, 40 ul of mixture was moved to a fresh white plate and luminescence was measured by Spark20M microplate reader (Tecan).

3.3.13 Size exclusion chromatography of supernatant from necroptotic cells and stimulation of recipient cells

To perform size exclusion chromatography experiments on supernatant of necroptotic cells, 0.7×10^5 THP1 monocytes, transduced to express the inducible MLKL 1-201 construct, were plated in 96 wells in 100 ul of culture medium with 100 ng/mL PMA (Sigma-Aldrich). After 8h incubation, differentiation medium was removed and cells were cultured in serum-free RPMI with or without 1 ug/mL doxycycline for 16 h. Then, supernatant from induced (necroptotic) and not induced cells (control), for a total of 40 mL of medium per condition, was collected and concentrated to 500 ul using Amicon Filters with 10 KDa cutoff. Flow-through was conserved for further analysis. The concentrated supernatant was loaded on a Superose 6 10/300 GL column (GE Healthcare). Isocratic run (1.2 column volume) was performed on an AKTA Basic instrument with a flowrate of 0.3 mL/min using degassed and filtered PBS as

running buffer. 500 ul fractions were collected in a plate and used for 14 h stimulation of TLR4^{-/-} BLaER1 recipient cells. The stimulation was performed by diluting the fraction 1:1 with RPMI medium and adjusting FSC content to 10% v/v.

3.3.14 Live-cell imaging

To analyze TNF shedding from HEK293T cells using C-Tag-TNF expressing vectors, live-cell imaging was performed as follows: 0.17×10^5 cells/well of the needed genotypes were plated in 96 well Ibidi plates with black walls in 200 ul FluoroBrite DMEM medium (Gibco) supplemented with 10% FCS, 100 U/mL penicillin-strepomycin, 1% sodium pyruvate and 10 mM HEPES (Gibco). The next day, cells were transfected with a total of 100 ng DNA (50ng pLI_C-Tag-TNF mCherry or pLI_C-Tag-TNF + 50ng pEF-BOS_nBFP) and 0.25 ul GeneJuice/well with the same procedure described in section 3.3.8. After 24 h, doxycycline was added to the wells at a final concentration of 1 ug/mL for 4 h. 20 minutes before imaging, CaptureSelect[TM] Alexa Fluor[TM] 488 Anti-C-Tag Coniugate (Thermo Scientific) was added to wells at a final dilution of 1:480. When needed, Propidium Iodide (eBioscience) was used at a final dilution of 1:250, while AnnexinV Alexa Fluor[TM] 647 (Biolegend) was used at a 1:125 dilution. Imaging was performed for 4h30 on a Leica DMi8 inverted microscope equipped with a HC PL APO 63x/1.20 W CORR CS2 objective, with a picture taken every 6 minutes. For high resolution images shown in Fig. 15A, the ti2 spinning disk microscope (Nikon) equipped with a Plan Apo λ 60x oil objective was used and images were captured with a 5 minutes interval. Cells were kept at 37°C and in 5% CO_2 for the entire duration of the imaging procedure. Images produced with the fluorescence inverted microscope were analyzed as follows. The contours of the individual cells were determined using a home-written Definiens XD 2.0 script. Segmentation of the nucleus was performed with the following procedure: as a first step, a 3D-Gaussian filter with a kernel size of 5x5x3 pixels was applied, then a second 3D-Gaussian filter was added, again with a kernel size of 5x5x3 pixels, and finally subtracted the latter image from the previous one. This procedure resulted in a background subtracted image. As a last step, we applied a global threshold and carried out segmentation using an algorithm implemented in the Definiens XD 2.0 software platform. The resulting segmented patterns of the nucleus were then used as seeds to detect the whole cells using the mCherry channel, in which the entire cytoplasm was visible. The individual cells were finally tracked over time based on pixel overlaps between the segmented patterns at the different times. This allowed extracting the mean fluorescence intensity over time per cell for the channels of interest. For the Annexin V and the PI stainings, an automated image analysis was not possible since their expression occurs only in dying cells at a very late stage during which the cells have the tendency to detach from the coverslip and move within the medium. Thus, for these stainings we manually identified the cells using *Image J* and tracked them visually. In addition, we also manually analyzed some of the cells were not accurately captured by the automated analysis. All the fluorescence time intensity trajectories were plotted and analyzed using Origin 7.0 (OriginLab).

3.3.15 Virus production and transduction of target cells

For the production of pseudotyped lentiviral particles, a third generation system was employed. 3.5×10^6 HEK293T cells were plated in 10 cm dishes and transfected the day after with 8 ug of transfer plasmid expressing the desired construct (in a pFUGW or pLI lentiviral backbone) and the following packaging plasmids: 12 ug of pMDLg/pRRE, 4 ug of pRSV-REV, and 8 ug of pCMV-VSVG. The DNA mixture was resuspended in 500 ul H_2O, mixed with 500 ul of 2X HBS buffer and 50 ul of 2.5M $CaCl_2$, and incubated at RT for 20 minutes. The mixture was then added dropwise to the cells and incubated for a minimum of 8 h to a maximum of 14 h. Afterwards a medium change was performed and plates were incubated for 48 h - 72 h. Subsequently, medium was collected, centrifuged at 1000 g for 10 minutes and filtered through a 0.45 um filter. If necessary, virus production was scaled up using multiple 10 cm dishes and virus containing medium was ultracentrifuged at 22800 rpm for 2 h and resuspended in fresh medium (concentration factor about 60x). Virus was used fresh or stored at -80°C until use. Retroviral particles were produced with the same procedure, but 20 ug of transfer plasmid (pRP backbone), 15 ug of pCMV-Gag-Pol and 6 ug of pCMV-VSVG packaging plasmid were used instead.

To transduce THP1, BLaER1 or HEK293T, 0.2×10^6 cells/well were seeded in a 6-well plate and 2ml of lentivirus produced as described above was added in each well and incubated for 24 h. THP1 or BLaER1 cells were then centrifuged at 450 g for 5 minutes and resuspended in fresh medium. A medium change was instead performed for HEK293T cells. 48h-72h after transduction, puromycin (Roth) was added to cell medium (2.5 ug/mL for THP1, 5ug/mL for 293T) and cells were kept under selection for 48 h - 72 h. After selection, THP1 cells were centrifuged as above and fresh medium without puromycin was added. A simple medium change was performed for HEK293T cells. BLaER1 were instead sorted for homogeneous mCherry expression and then were allowed to expand for one week before experiments. To transduce J774 macrophages, 2×10^6 cells were plated in a 10 cm dish and 50 ul of concentrated virus produced as described above was added to the media. After 24 h, cells were washed with PBS and fresh media was added. 5 days after infection, cells were sorted for homogeneous EGFP expression and allowed to expand before the experiments. To transduce HSC, a 24-well plate was first coated with retronectin (Takara Bio) diluted in PBS at the concentration of 50 ug/mL in PBS at RT for 2h, then the excess of retronectin was washed with PBS. 0.5×10^6 HSC isolated the day before were seeded on retronectin-coated wells and 200 ul of concentrated virus (see above in this section) was added on cells for 8 h. Finally, cells were washed with PBS twice and transferred to a new plate with fresh culture medium.

3.4 Cloning

3.4.1 Competent bacteria

DH5α chemically competent bacteria were generated according to the protocol described in the Promega Broschure "Subcloning Notebooks" (Promega).

3.4.2 Polymerase chain reaction

The DNA fragment of interest was amplified from cDNA of BLaER1 cells (cloning of TNF into pRP backbone and of MLKL 1-201 fragment into pLI backbone) or from plasmid DNA (all other plasmids). In case of amplification from cDNA, 10 ul of cDNA was used for a 50 ul PCR reaction, while plasmid DNA was used in the final amount of 10 ng/reaction. The Phusion polymerase (Thermo Scientific) was employed and a reaction mix was set following manufacturer's instructions. The optimal annealing temperature for primer pairs was assessed by the TM-calculator tool of *New England Biolabs*. PCR products were purified using the QIAquick PCR purification kit (Qiagen) following manufacturer's instructions. For the generation of the construct pLI_C-Tag-TNF mCherry and for mutagenesis of MLKL a fusion PCR was necessary, to create one DNA product starting from two partially overlapping sequences. To do so, the fragments of interest were separately amplified from previously cloned plasmids. After PCR purification, 50 ng of the longest product and the same molecular concentration of the second product were mixed in a PCR reaction without addition of primers. This mix underwent 10 cycles of amplification to allow the synthesis of the fused complete sequence. The obtained PCR product was diluted to 1 ng/μL and used for a second round of PCR (25 cycles) where forward and reverse primers annealing to the extremities of the full sequence were added.

3.4.3 Electrophoretic run on agarose gel

DNA fragments obtained by PCR or digested plasmids were analyzed via agarose gel electrophoresis. Agarose powder (Biozym) was suspended in 1x TAE and heated until completely dissolved. DNA stain G (Serva) was added in a 1:10000 dilution before pouring the gel into the electrophoresis chamber. 6X Loading Dye was added to the samples before loading on the gel. A size marker (Generuler 1kb or 100bp, Thermo Scientific) was used to estimate the weight of the fragments of interest. Gels were run at 100-120 V for 30-40 minutes before imaging with a Chemidoc system (Biorad). When necessary, PCR products or digested plasmids were cut from gel with a scalpel and purified using the QIAquick gel extraction kit (Qiagen) following manufacturer's instructions.

3.4.4 Restriction cloning

The desired DNA insert and plasmid backbone were digested with the required restriction enzymes (all FastDigest, Thermo Scientific) for 1 h at 37°C. DNA fragments were cloned into pLI and pFUGW backbone with NheI and BamHI or, when necessary, with enzymes generating compatible cohesive ends. For restriction cloning into pRP or pEF-BOS backbone, XhoI and BamHI were employed. DNA fragments were inserted into the respective vector with a ligation step using the T4 DNA Ligase (Thermo Fisher Scientific). 100 ng of vector were mixed with a 5-fold excess of insert and combined with 10x T4 Ligase Buffer and 1 ul of T4 Ligase. A final volume of 10 ul was adjusted by addition of water. This mixture was incubated at RT for at least 1 h.

3.4.5 Transformation in E. Coli

DH5α chemically competent *E. coli* were used for transformation. In particular, 50 µL of bacteria suspension were mixed with the ligation reaction and incubated on ice for 10 minutes. After a heat shock at 42°C for 70 seconds, bacteria were incubated 3 minutes on ice before addition of LB medium and incubation for 45 minutes at 32°C, shaking. Finally, bacteria were plated on LB-agar plates containing ampicillin and incubated at 32°C overnight.

3.4.6 Isolation of plasmid DNA from bacteria cultures

Some colonies present on LB-agar plates after transformation and overnight incubation were picked and let grow at 32°C overnight in LB medium with 100 ug/mL ampicillin, shaking. The day after, isolation of plasmid DNA was performed according to the protocol from QIAprep Spin Miniprep Kits (Qiagen) using homemade buffers and EconoSpin columns (Epoch Life Science). A control digestion with appropriate restriction enzymes was then performed to screen for positive clones. Correct sequence of the insert was confirmed by Sanger sequencing (performed by Eurofins). If the sequence was correct, a suspension culture of 300 mL of the positive clone was prepared and allowed to grow overnight to purify large amount of plasmid DNA using the PureLink Maxi-Prep kit (Invitrogen).

3.5 Western Blot procedure

3.5.1 Sample collection and Bicinchoninic acid assay (BCA)

For western blot experiments, supernatant samples were collected in tubes, centrifuged at 600 g for 5 minutes and moved to fresh tubes. Cells were collected by trypsinization (BLaER1) or simple PBS washing (HEK293T), moved to tubes and centrifuged at 450 g for 5 minutes. Supernatant was then removed and cell pellet was resuspended in 70-100 ul RIPA Buffer with protease inhibitors and, when necessary, phosphatase inhibitors (both Roche). Samples were stored at -80°C until use. In order to load an equal amount of sample on the SDS gel, protein concentration in cell lysates was measured by BCA assay (Thermo Fisher Scientific). Briefly, reagent A and B from the kit were mixed 1:50 and 200 ul of the solution was added to 5 ul of

sample or BSA standard. The reaction was incubated at 37°C for 20 minutes followed by absorbance measurement at 562 nm. A linear regression was applied on the standard curve and protein absorbance values from samples were interpolated to measure the protein concentration.

3.5.2 Methanol chloroform precipitation from supernatant

Supernatant samples were subjected to protein precipitation with methanol-chloroform before SDS-PAGE. 400-700 ul of supernatant were mixed with equal amount of methanol and 1/3 volume of chloroform, vortexed for a few seconds and centrifuged 16000 g for 2 minutes at RT. Then, the aqueous top layer was removed and 1 volume of methanol was added to the tubes. Afterwards, samples were vortexed and centrifuged as above and the supernatant was discarded. The protein pellet was allowed to dry before addition of 60-80ul 1X SDS laemmli buffer. Finally, samples were heated at 95°C and stored at -80°C until use.

3.5.3 Immunoblot

Samples in 1X SDS laemmli buffer, prepared as described above, were subjected to SDS-PAGE under denaturing conditions. After sample loading, gels were run at 100-120 V for 1.5 h. To enhance the separation of small proteins (TNF, C-Tag TNF), precast 12% Bis-Tris protein gels were used in combination with 1X MES Buffer (both Thermo Fisher Scientific), as suggested by the manufacturer. After separation, gels were subjected to western blot transfer. Proteins were transferred to nitrocellulose membrane (0.2um, GE Healthcare) in a wet system for 70 minutes at 4°C. Ponceau S staining (Sigma-Aldrich) was performed to control for transfer quality. After extensive washing in PBST, membranes were blocked with 5% Milk in PBST for 1 h at RT. Then, membranes were incubated overnight at 4°C in the required primary antibody. In case the anti-C-Tag antibody was used, the incubation time was prolonged up to 48 h. If a phosphorylation had to be detected, blocking and incubation in primary antibody was performed in 5% BSA in TBST. Membranes were then washed 3X with PBST (or TBST for detection of phosphorylated proteins) for 10 minutes before 1 h incubation at RT with the required HRP-conjugated secondary antibody diluted in 5% Milk PBST. After 3 more washing steps, membranes were developed using Pierce ECL WB substrate (Thermo Fisher Scientific) in a Fusion Fx device (Vilber). When necessary, the contrast of images was changed in a linear fashion.

3.6 RNA sequencing data analysis

RNA sequencing data of experiments previously performed by our laboratory were analyzed for the relative expression of ADAM proteins in BLaER1 macrophages stimulated with 200 ng/ml LPS or left unstimulated. Data are depicted as transcripts per million reads (TPM). Sample preparation was performed as described in [189].

3.7 Generation of KO cell lines by CRISPR-Cas9 technology

3.7.1 Generation of sgRNA expression plasmids by LIC cloning

When possible, plasmids expressing sgRNA targeting the gene of interest were chosen from our sgRNA library [190]. If the gRNA from the library targeted a late exon in the gene of interest or did not cover all the isoforms of the gene to delete or again was tested to be inactive or not efficient, a different gRNA was designed and cloned *de novo*. To do so, a ligation independent cloning (LIC) strategy was employed, as described in [190]. sgRNAs were chosen from the published Brunello library [191] or designed with the sgRNA finder chopchop [192]. For LIC cloning, 10 ul of expression vector (pMini_U6_gRNA_CMV_BFP_T2A_Cas9 or pMini_U6_gRNA_CMV_mCherry_T2A_Cas9) diluted to 200 ng/mL in H_2O were digested with ApaI and SpeI and purified from agarose gel. The overhangs were then generated exploiting the 3´-5´exonuclease activity of the T4 DNA polymerase in presence of dTTP in the following reaction:

10x NEB2 Buffer 10 ul
Vector (70ng/ul) 10ul
BSA (10mg/mL) 1 ul
dTTP (100mM) 1 ul
H_2O 74.66 ul
T4 DNA Polymerase (3 U/ul) 3.33 ul

The mixture was incubated for 5 minutes at 27°C, put on ice and inactivated for 20 minutes at 75°C. Afterwards, the vector was mixed with the universal reverse oligonucleotide LICsgRNA_rev (PAGE purified) as follows:

10x NEB2 Buffer 20 ul
Digested vector 10 ul
LICsgRNA_rev (100 uM) 0.5ul
H_2O 69.5ul

Subsequently, 2.5 ul of the generated mixture were mixed with 2.5 ul of the sgRNA of interest previously diluted with H_2O to a final concentration of 0.25 uM. This mix was incubated as follows:

70°C 1 min
65°C 1 min
60°C 30 sec
55°C 2.5 min (29 cycles, -1°C per cycle)
25°C ∞

Finally, the solution was used to transform competent *E.coli*. Colonies bearing the vector with the correct insert were used to generate big cultures for the isolation of plasmid DNA to use for further applications.

3.7.2 Electroporation of BLaER1 cells for KO generation

The day before electroporation, BLaER1 cells were seeded at a concentration of 0.2×10^6 cells/ml. The day after, 5×10^6 cells were suspended in 250 ul Optimem medium with 5 ug of the necessary plasmids for the expression of Cas9 and gene-targeting gRNA and incubated at RT for 10 minutes. Cells were then electroporated with a Gene Pulser Xcell Elektroporations-System (Biorad) in a 4 mm cuvette with an exponential decay protocol at 265 V, 975 µF und 700 Ω. Finally, cells were immediately seeded in a well of a 6 well plate with pre-warmed medium.

3.7.3 Transfection of HEK293T cells for KO generation

The day before transfection, 0.7×10^6 293T cells were plated in each well of a 6-well plate. The day after, a transfection with a total of 5 ug of required plasmids with a 1:2 DNA: GeneJuice ratio was performed, as described in more details in section 3.3.8. Cells were allowed to rest overnight before sorting.

3.7.4 Sorting of electroporated or transfected cells

24-48 h after electroporation or transfection respectively, BLaER1 cells or HEK293T cells were sorted for positivity to the fluorescent protein expressed in the Cas9 containing vector (usually BFP from pRZ_Cas9_BFP or from pMini_U6_gRNA_CMV_BFP_T2A_Cas9). 2-10% highest positive cells were sorted on a Sony sorter SH800Z into 15 mL tubes containing 3 mL of fresh medium.

3.7.5 Limiting dilution for the generation of monoclones

Sorted cells were plated in 96-well plates (U-Bottom for BLaER1 and F-Bottom for HEK293T) with a dilution of 4 cells/well, 2 cells/well or 1 cell/well for a total of 3 plates/dilution. Cells were allowed to grow for 3-4 weeks, then wells with clones were identified by absorbance at 600 nm and 96 clones were picked and transferred to a single 96-well plate by a Beckman Coulter Biomek FX Robot in case of BLaER1 cells or by hand picking for of HEK293T cells. A duplicate plate of the picked clones was created to allow genotyping.

3.7.6 Genotyping of monoclones

The duplicate plate created during the picking of monoclones was incubated in 30 ul of Direct Lysis Buffer with Proteinase K for 10 minutes at 65°C, then the reaction was inactivated at 95°C for 15 minutes. The lysate was next used for PCR amplification followed by Illumina sequencing of the region of interest targeted by the sgRNA employed for the KO generation. To do so, 2 subsequent PCR reactions were set. For the PCR1, specific primers containing overhangs as reported in section 3.1.8 were used in order to amplify the genomic region targeted by the sgRNA, for an amplicon size of about 250 bp. The PCR reaction was prepared in a total of 6 ul, with 5 ul of PCR mix and 1 ul of lysate, as follows:

PCR1

HF or GC buffer 1.2 ul
dNTPs (10mM) 0.12 ul
fwd primer (50uM) 0.06 ul
rev primer (50uM) 0.06 ul
phusion polymerase 0.06 ul
H2O 3.5 ul
Lysate 1 ul

The PCR reaction was then incubated as follows:

95°C 3 min
95°C 30 sec
62°C 30 sec
72°C 30 sec
18 cycles
72°C 3 min
12°C ∞

The so obtained PCR product was next used for a second level of PCR amplification using barcoded primers containing Illumina sequencing adaptors and binding to the overhangs introduced by PCR1. The PCR mix was prepared as follows:

HF or GC buffer 1.2 ul
dNTPs (10mM) 0.12 ul
primer mix (2.5uM) 1.2 ul
phusion polymerase 0.06 ul
H2O 3.92 ul
Lysate 1 ul

The same program used for PCR1 was employed for amplification. Afterwards, PCR reactions with a unique combination of barcode primers for the same genomic region were pooled, purified from agarose gel, precipitated and quantified. To precipitate nucleic acids, samples were mixed with 10% of their volume of 3M sodium acetate pH= 5.2. Subsequently, samples were diluted in 110% of their volume with isopropanol and the mixture was incubated for 30 minutes at -20°C, followed by a centrifugation step at 14 000 g for 15 min at 4°C. The DNA pellet was next washed with cold 70% (v/v) ethanol in H_2O and again centrifuged at 14000 g for 5 minutes at 4°C. The pellet was allowed to dry and resuspended in H_2O, then quantified at the Nanodrop, by measuring absorbance at 260 nm (1 A_{260} = 50 ug/ul dsDNA). The DNA sequencing was performed on an Illumina MiSeq Platform with 300 bp length single read sequencing with the v2 chemistry. Sequencing results were analyzed with the online available software "Outknocker" [193]. To do so, FastQ data were searched for the amplicon of interest and compared to the WT reference sequence. Clones with deletions or insertions leading to

frameshifts (out of frame mutations) were identified by the software as knock-out clones. When possible, clones with two differentially edited alleles with out of frame mutations were picked, expanded and used for further experiments. An exception was done for CASP8$^{-/-}$ x RIPK3$^{-/mut}$ cells, which bears one in frame mutation in the RIPK3 gene present in clone 2. This in-frame deletion led to residual expression of mutated protein (Fig. 2.1), which did not show biological activity, as demonstrated by cells being resistant to necroptosis induction in the same extent as clone 1, which bear two out of frame mutations and no residual RIPK3 expression (Fig.4.1 in results session). As such, these cells should be considered functional RIPK3 knock-out with a mutated allele, hence the nomenclature " $^{-/mut}$ " used for this gene. CASP8$^{-/-}$ x RIPK3$^{-/mut}$ were used to derive IL6 deficient CASP8$^{-/-}$ x RIPK3$^{-/mut}$ cells which appear in this work.
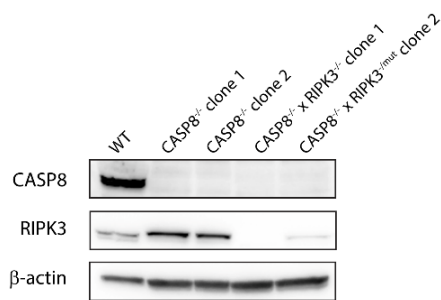

Fig. 2.1 BLaER1 clones of the indicated genotypes or WT parental cells were analyzed by western blot for the expression of CASP8 and RIPK3 proteins. β-actin was used as housekeeping gene.

3.8 Statistical analysis

If not otherwise states, data were searched for statistical significance using two-way ANOVA when the response was affected by two factors (e.g. genotype and stimulus) with Sidak's correction for multiple comparison. If only one factor influenced the results, a one-way ANOVA was employed. Paired t-test was used in case of microscopy data where two fluorescent signals were measured and compared for the same cell. * $p<0.05$, ** $p<0.01$, *** $p<0.001$. Data are represented as mean + SEM if at least three independent experiments were performed or as mean + SD if two independent experiments or one representative experiment is shown. All statistical analyses were performed using GraphPad Prism 8.2.1.
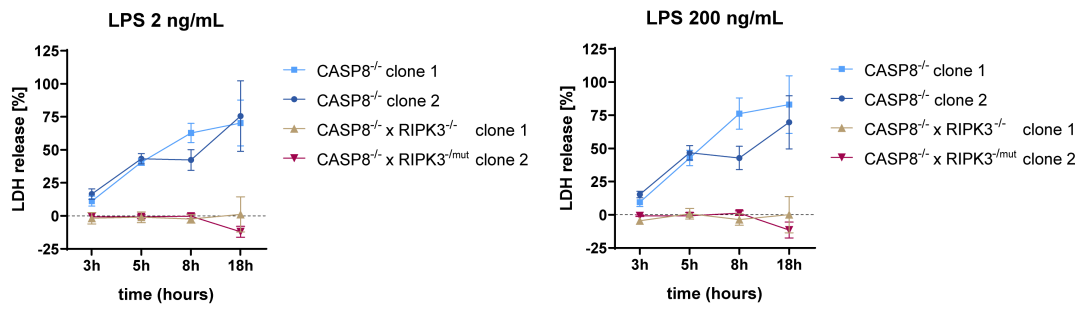
4. Results

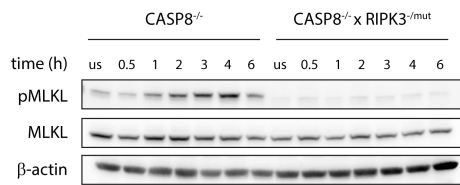## 4.1 Necroptotic cells induce a pro-inflammatory phenotype in resting cells

4.1.1 Development of an *in vitro* system to study the inflammatory properties of necroptosis

In order to prove the *in trans* pro-inflammatory capacity of necroptotic cells, we first aimed to develop a suitable *in vitro* model to measure markers of inflammation and immune activation in resting cells upon contact with potential DAMPs/alarmins released by necroptotic cells. Given the possible implication of different immune pathways in the induction of a pro-inflammatory phenotype, we made use of a B- cell line that can be transdifferentiated into macrophage-like cells to conduct our studies, namely BLaER1 macrophages. These cells are engineered to express the transcription factor C/EBPα coupled to the estrogen binding domain of the estrogen receptor, which, upon β-estradiol stimulation, mediates the translocation of C/EBPα to the nucleus where it efficiently induces transdifferentiation of B-cells into macrophages within 5-6 days of treatment in combination with M-CSF and IL-3 [194]. The so generated macrophage-like cells exhibit a typical macrophage transcriptional signature, behave similarly to primary macrophages and can be used to study macrophage biology [194]. If not otherwise stated, CASP4$^{-/-}$ BLaER1 cells were used as background for further genetic manipulation to prevent non-canonical inflammasome activation when cells are stimulated with LPS, a fact that could confound necroptosis-related phenotypes. To generate necroptosis-prone cells, CASP8 was deleted via CRISPR-Cas9 technology in BLaER1 cells. CASP8$^{-/-}$ x RIPK3$^{-/mut}$ cells were generated as control due to their inability to undergo necroptotic cell death. As expected, CASP8$^{-/-}$ cells readily underwent necroptosis when stimulated with LPS with increasing LDH release over time, while CASP8$^{-/-}$ x RIPK3$^{-/mut}$ cells survived LPS treatment for the entire duration of the experiment (Fig. 4.1A). Moreover, phosphorylation of MLKL could be induced by LPS treatment only in CASP8$^{-/-}$ cells, starting 1 h after LPS stimulation, with a peak after 4 h, while no pMLKL was induced in CASP8$^{-/-}$ x RIPK3$^{-/mut}$ cells (Fig. 4.1B). Having generated cells that die of necroptosis upon LPS treatment, we established an *in vitro* system to perform supernatant transfer and co-culture experiments between necroptotic or control donor cells (CASP8$^{-/-}$ and CASP8$^{-/-}$ x RIPK3$^{-/mut}$, respectively) and resting recipient cells (Fig. 4.1C). Of note, we made use of TLR4$^{-/-}$ recipient cells to make them insensitive to LPS contained in the supernatant of donor cells. As a readout for the ability of necroptotic cells to induce a pro-inflammatory phenotype in resting cells, we aimed at measuring IL-6 secretion by recipient cells in both supernatant transfer and co-culture settings. As such, to prevent IL-6 secretion by donor cells upon LPS stimulation, which would alter IL-6 measurements after supernatant transfer on recipient cells, we generated CASP8$^{-/-}$ x IL-6$^{-/-}$ and CASP8$^{-/-}$ x RIPK3$^{-/mut}$ x IL-6$^{-/-}$ cells. For additional control experiments, we also generated CASP8$^{-/-}$ x MLKL$^{-/-}$ x IL-6$^{-/-}$. All generated IL-6 deficient donor cells were able to undergo necroptosis as the parental cells, were NF-kB competent, as judged by IL-8 secretion, and did not produce IL-6 upon LPS stimulation (Fig. 4.1D).
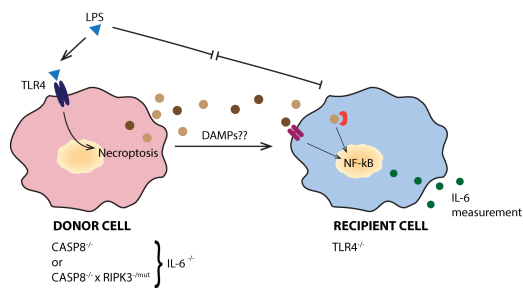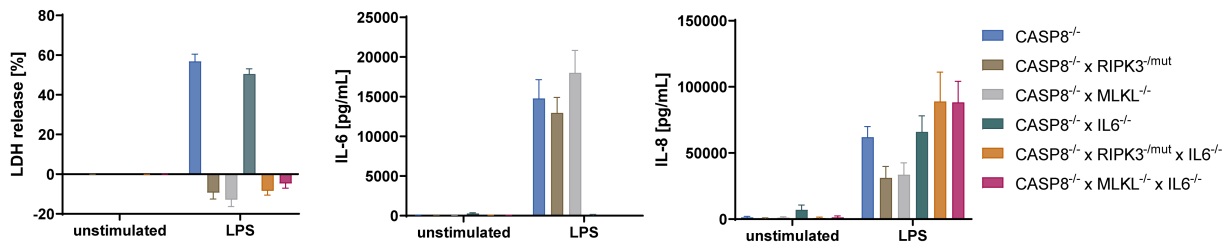
Fig. 4.1 (A) Two independent clones of CASP8$^{-/-}$ and CASP8$^{-/-}$ x RIPK3$^{-/mut}$ or CASP8$^{-/-}$ x RIPK3$^{-/-}$ BLaER1 macrophages were stimulated with 2 ng/mL or 200 ng/mL LPS for the indicated time points and necroptotic cell death was monitored by LDH release measurements. Mean + SEM of 3 independent experiments. **(B)** CASP8$^{-/-}$ and CASP8$^{-/-}$ x RIPK3$^{-/mut}$ BLaER1 macrophages were stimulated with 2 ng/mL LPS for the indicated time points and MLKL phosphorylation was detected in the cell lysates by immunoblot. us = unstimulated control. **(C)** Scheme of the *in vitro* model developed to perform supernatant transfer and co-culture experiments in BLaER1 macrophages. **(D)** IL6$^{-/-}$ cells were generated from CASP8$^{-/-}$, CASP8$^{-/-}$ x RIPK3$^{-/mut}$ and CASP8$^{-/-}$ x MLKL$^{-/-}$ and compared to parental clones for necroptosis induction, NF-kB activation and IL-6 production upon stimulation with 2 ng/mL LPS. Mean + SEM of 5 independent experiments.

4.1.2 Necroptosis induces *in trans* pro-inflammatory effects in resting cells via NF-kB activation

Taking advantage of the above-described system of donor and recipient cells, we performed supernatant transfer experiments from necroptotic and control cells (stimulated with LPS for 18 h or left unstimulated) to TLR4$^{-/-}$ resting cells and then measured IL-6 secretion (Fig. 4.2A). After 24 h, we could observe a significantly higher IL-6 production by recipient cells when stimulated with the supernatant of necroptotic cells compared to stimulation with supernatant from CASP8$^{-/-}$ x RIPK3$^{-/mut}$ control cells (Fig. 4.2B). To determine whether the difference in IL-6 induction observed in recipient cells corresponded to a difference in upstream NF-kB activation levels, we performed immunoblotting of NF-kB activation markers, namely phosphorylation of IkBα (pIkBα), p65 (pp65) and degradation of IkBα in a time course stimulation with supernatant of CASP8$^{-/-}$ necroptotic cells or CASP8$^{-/-}$ x RIPK3$^{-/mut}$ control cells. As expected, phosphorylation levels of both pIkBα and pp65 increased faster and were higher in recipient cells when stimulated with supernatant of necroptotic cells compared to supernatant of control cells. Moreover, IkBα degradation occurred earlier in necroptotic supernatant-induced cells, in line with a faster NF-kB activation under these conditions (Fig. 4.2C). To confirm that IL-6 production was induced by necroptosis-related DAMPs/alarmins, we repeated the experiment using CASP8$^{-/-}$ x MLKL$^{-/-}$ as control donor cells, since necroptosis-independent functions of RIPK3 have been described (see section 2). Again, we could observe abundant IL-6 production in recipient cells when stimulated with supernatant of CASP8$^{-/-}$ necroptotic cells but almost no IL-6 secretion when stimulated with supernatant of CASP8$^{-/-}$ x MLKL$^{-/-}$ control cells (Fig. 4.2D).

We next performed co-culture experiments in 1:1 ratio of donor:recipient cells. To be able to control that this ratio was unchanged after 5 days of differentiation, TLR4$^{-/-}$ cells stably expressing mCherry under the control of CMV promoter were used as recipient cells and FACS analysis was performed before the experiment to determine the percentage of donor cells (EGFP positive) and recipient cells (EGFP and mCherry double positive) for each combination (Fig. 4.2E). Similarly to what we observed in supernatant transfer experiments, co-culture of TLR4$^{-/-}$ resting cells with CASP8$^{-/-}$ necroptotic cells led to increased IL-6 production compared to co-culture with CASP8$^{-/-}$ x RIPK3$^{-/mut}$ control cells when LPS stimulation was performed. However, the difference was not as remarkable, with about a two-fold increase in IL-6 levels upon co-culture with necroptotic cells being observed. (Fig. 4.2E). Taken together, these experiments confirm that necroptosis can exert *in trans* pro-inflammatory functions through the release of one or more soluble factors that activate NF-kB pathway in resting cells.
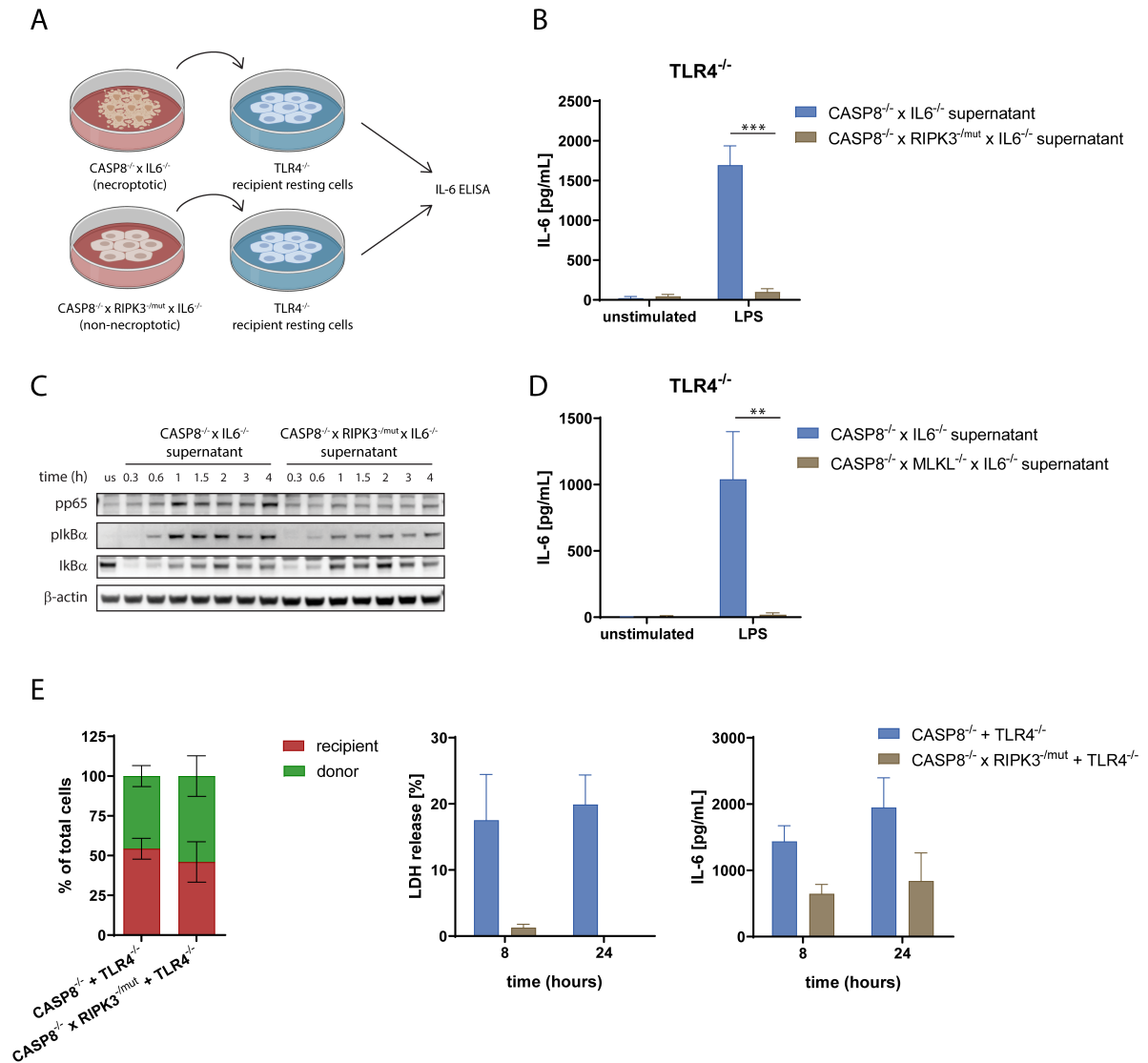
Fig. 4.2 (A) Scheme of supernatant transfer experimental procedure. **(B)** TLR4$^{-/-}$ recipient cells were stimulated for 24 h with supernatant from CASP8$^{-/-}$ x IL6$^{-/-}$ (necroptotic) or CASP8$^{-/-}$ x RIPK3$^{-/mut}$ x IL6$^{-/-}$ (control) cells previously induced with LPS for 18 h. Pro-inflammatory capacity of necroptotic and control supernatant was studied by ELISA measurement of IL-6 release by TLR4$^{-/-}$ recipient cells. Data depicted as mean + SEM of 4 independent experiments. **(C)** TLR4$^{-/-}$ recipient cells were stimulated as in (B) for the indicated time points. Immunoblot of pp65, pIkBα and IkBα was performed as markers of NF-kB activation. One representative of two independent experiments. us = unstimulated control. **(D)** CASP8$^{-/-}$ x IL6$^{-/-}$ and CASP8$^{-/-}$ x MLKL$^{-/-}$ x IL6$^{-/-}$ were stimulated with 2ng/mL LPS for 18 h and supernatant was applied to TLR4$^{-/-}$ recipient cells for 24 h, after which IL-6 release was measured by ELISA. Graph represents mean + SEM of three independent experiments. **(E)** CASP8$^{-/-}$ x IL6$^{-/-}$ or CASP8$^{-/-}$ x RIPK3$^{-/mut}$ x IL6$^{-/-}$ donor cells were co-seeded with TLR4$^{-/-}$ mCherry positive recipient cells in a 1:1 ratio and stimulated with 2 ng/mL LPS for 8 h or 24 h before LDH and IL-6 release measurements. The ratio of plated cells was tested by FACS analysis on unstimulated cells (the green part of the bars represents EGFP$^+$ donor cells, the red part represents EGFP$^+$ mCherry$^+$ recipient cells). Data represented as mean + SD of two independent experiments.

4.2 TNF is a necroptosis-associated DAMP

4.2.1 The DAMP/alarmin is a protein in the range of 20-70 kDa

Given the pro-inflammatory capacity of necroptotic cells observed in the previous experiments, we sought to investigate the nature of DAMP(s)/alarmin(s) responsible for NF-kB activation in resting cells. To explore the physiochemical nature of the pro-inflammatory mediator released upon death, we conducted a number of experiments, in which we subjected the supernatant to different treatments. Exposure of biological samples to heath shock is known to denature proteins and lead to their inactivation, while nucleic acids can refold and survive the treatment [195]. We therefore subjected the supernatant of necroptotic donor cells to heath shock to test whether it would prevent IL-6 secretion in recipient cells. As shown in Fig. 4.3A, the stimulation of recipient cells with heath shock-treated supernatant of necroptotic cells completely abolished IL-6 secretion, suggesting that the DAMP(s)/alarmin(s) leading to IL-6 production in our system is a protein or at least contains a protein, critical for its activity. To confirm this hypothesis, we performed size exclusion chromatography on the supernatant of necroptotic or control cells and stimulated recipient cells with the obtained fractions to determine their ability to evoke IL-6 secretion (Fig. 4.3B). A Superose 6 10/300 GL column was used to cover a wide range of molecular weight, from 5 to 5000 kDa. In order to be able to perform the experiment in FCS free conditions, we had to switch the model system, since BLaER1 monocytes do not tolerate low FCS conditions. As such, we utilized THP1 monocytes that we transduced with a doxycycline inducible N-terminal truncation of MLKL (amino acids 1-201) as donor cells. In these cells, doxycycline treatment induces the expression of the MLKL 1-201, which leads to necroptosis without any additional treatment (Fig. 4.3C) [152].
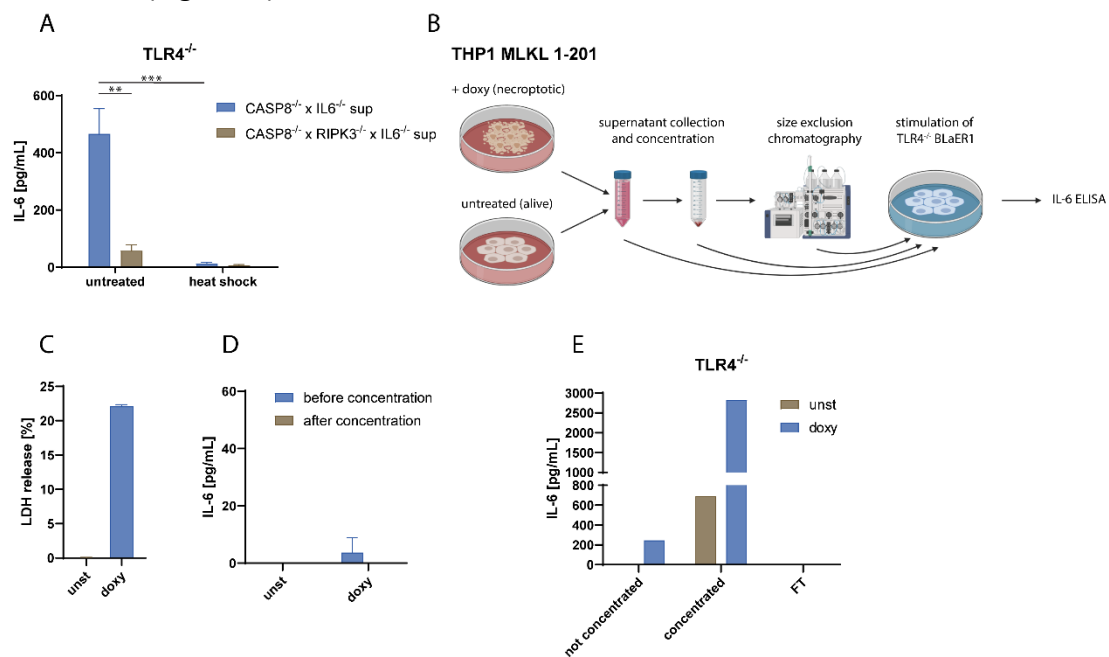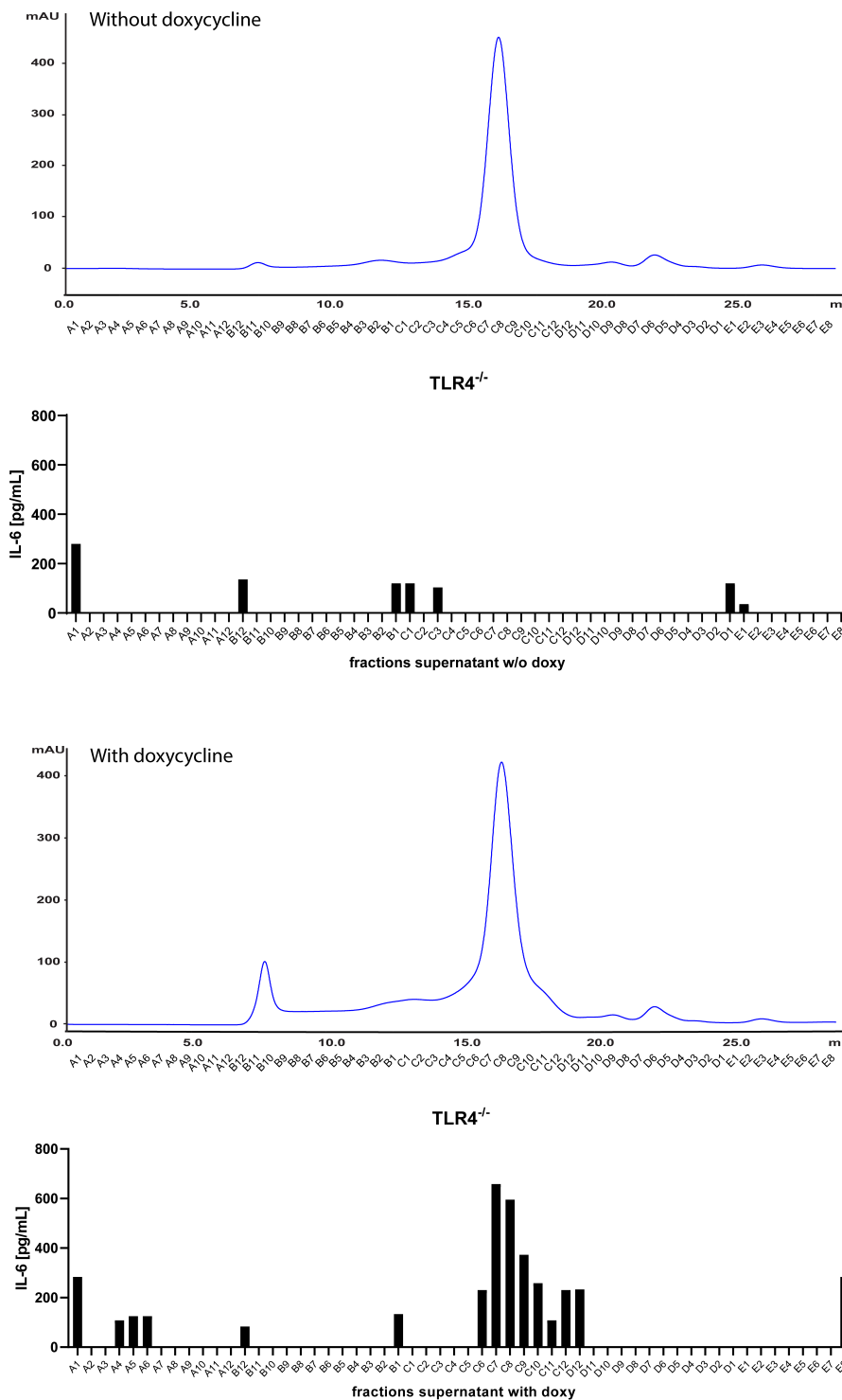
Fig. 4.3 (A) CASP8$^{-/-}$ x IL6$^{-/-}$ and CASP8$^{-/-}$ x RIPK3$^{-/mut}$ x IL6$^{-/-}$ cells were stimulated with 2 ng/mL LPS for 18 h. Supernatant was then subjected to heath shock at 75°C for 10 min or left untreated and used to stimulated TLR4$^{-/-}$ recipient cells. IL-6 secretion by TLR4$^{-/-}$ cells was measured by ELISA. Results are shown as mean + SEM of three independent experiments. Sup = supernatant. **(B)** Scheme of the procedure used for size exclusion chromatography on the supernatant of THP1 MLKL 1-201 cells. **(C)** THP1 MLKL 1-201 cells were differentiated with PMA for 8 h, then medium was removed and cells stimulated with 1 ug/mL doxycycline for 16 h or left untreated in FCS free RPMI medium. LDH release was measured for both conditions at the end of treatment. Mean + SD of technical duplicate. **(D)** Supernatant of cells stimulated as described in (C) was concentrated using an Amicon Filter with 10 KDa cutoff and IL-6 ELISA performed before and after concentration. Mean + SD of technical duplicate. **(E)** Supernatant and concentrated supernatant obtained as described in (C) and (D) or flow-through (FT) from Amicon Filter were used to stimulate TLR4$^{-/-}$ BLaER1 cells for 14 h. IL-6 produced by TLR4$^{-/-}$ cells was measured by ELISA. One representative of two independent experiments. **(F)** Concentrated supernatant from untreated or doxycycline-treated THP1 MLKL 1-201 cells prepared as described in (D) was subjected to size exclusion chromatography and obtained fractions were used to stimulate TLR4$^{-/-}$ BLaER1 recipient cells for 14 h. IL-6 secretion from TLR4$^{-/-}$ cells was then measured by ELISA. One representative of two independent experiments.

Importantly, PMA and doxycycline treated THP1 MLKL 1-201 cells did not secrete IL-6 that could interfere with IL-6 measurement after stimulation of recipient cells (Fig. 4.3D). However, stimulation of TLR4$^{-/-}$ BLaER1 recipient cells with the supernatant of THP1 MLKL 1-201 cells (Fig. 4.3E) led to IL-6 production in a necroptosis-dependent manner. As such, these data confirmed the validity of these cells as an alternative model system to study necroptosis-driven inflammation. Stimulation of recipient cells with the 80x concentrated necroptotic supernatant used to load the size exclusion column led to increased IL-6 secretion by recipient cells, as expected. However, a small, but measurable amount of IL-6 was also observed upon stimulation with concentrated supernatant from THP1 that were not treated with doxycycline. This could be due to the presence of another pro-inflammatory mediator that is also released by living cells or a due to a leakiness of the expression system. The stimulation of recipient cells with fractions obtained by size exclusion chromatography revealed a considerable IL-6 release, but only when supernatant from necroptotic THP1 cells were used. This activity was largely confined to fractions C6-D12 of the necroptotic supernatant, which corresponds to proteins in the range of about 20-70 kDa (Fig. 4.3F). Of note, the UV chromatogram of the supernatant from necroptotic cells was largely identical to the one of viable cells. This is so far expected, as proteins of the culture medium constitute the large proportion of proteins in these samples in this size range (Fig. 4.3F). Nevertheless, it is interesting to note that the supernatant from necroptotic cells generated an additional peak at 9 ml elution volume, which corresponds to a size bigger than 900 kDa, suggesting the presence of large complexes and aggregates derived from dead cells. Taken together, these data confirm the protein nature of the DAMP(s)/alarmin(s) and restrict the protein size to about 20-70 kDa.

4.2.2 IL-1β does not act as an alarmin in BLaER1 macrophages

Necroptosis is known to lead to secondary NLRP3 activation in myeloid cells, which is due to the loss of membrane integrity and consequent K$^+$ efflux [169,170]. We therefore asked whether IL-1β could act as DAMP in our system, leading to IL-1R engagement in recipient cells, downstream NF-kB activation and IL-6 release. To answer this question, we blocked NLRP3 in necroptotic cells by using MCC950, a specific NLRP3 inhibitor [196]. As expected, NLRP3 inhibition did not impact on necroptosis induction but it significantly reduced levels of IL-1β secreted by CASP8$^{-/-}$ necroptotic cells to the same levels of CASP$^{-/-}$ x RIPK3$^{-/mut}$ control cells (Fig. 4.4A). However, supernatant transfer experiments with MCC950-treated supernatant of necroptotic cells did not reduce IL-6 production by TLR4$^{-/-}$ recipient macrophages, suggesting that IL-1β does not play a role in our system (Fig. 4.4B). To confirm this finding, we knocked-out IL-1R in TLR4$^{-/-}$ BLaER1 cells and stimulated them with necroptotic supernatant or with recombinant IL-1β. We observed no differences in IL-6 secretion between TLR4$^{-/-}$ and TLR4$^{-/-}$ x IL-1R$^{-/-}$ cells upon stimulation with necroptotic supernatant and no response to recombinant IL-1β, implying a defective response of BLaER1 cells to IL-1β (Fig. 4.4C). In summary, these data show that IL-1β released by necroptotic cells does not act as alarmin in our system.
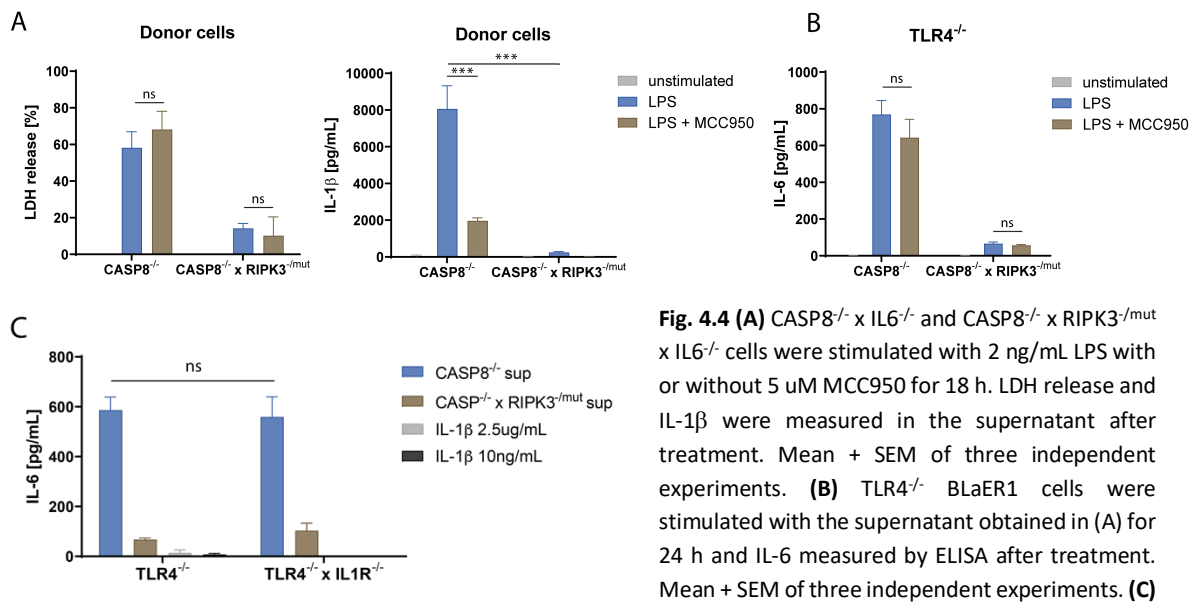
Fig. 4.4 (A) CASP8$^{-/-}$ x IL6$^{-/-}$ and CASP8$^{-/-}$ x RIPK3$^{-/mut}$ x IL6$^{-/-}$ cells were stimulated with 2 ng/mL LPS with or without 5 uM MCC950 for 18 h. LDH release and IL-1β were measured in the supernatant after treatment. Mean + SEM of three independent experiments. **(B)** TLR4$^{-/-}$ BLaER1 cells were stimulated with the supernatant obtained in (A) for 24 h and IL-6 measured by ELISA after treatment. Mean + SEM of three independent experiments. **(C)** TLR4$^{-/-}$ and TLR4$^{-/-}$ x IL1R$^{-/-}$ BLaER1 cells were stimulated with the supernatant of CASP8$^{-/-}$ x IL6$^{-/-}$ and CASP8$^{-/-}$ x RIPK3$^{-/mut}$ x IL6$^{-/-}$ cells (stimulated with 2ng/mL LPS for 18 h) or with indicated amount of recombinant IL-1β for 24 h. IL-6 release is shown as mean + SEM of three independent experiments.

4.2.3 IL-6 production in recipient cells is downstream of TNFR1 activation

To identify the pathway responsible for NF-kB activation and IL-6 secretion in recipient cells upon stimulation with necroptotic DAMP(s)/alarmin(s), we tested the response to supernatant of LPS-stimulated CASP8$^{-/-}$ BLaER1 macrophages in recipient cells deficient for specific innate immune adaptors or receptors. The rationale of this approach is that, in contrast to the large variety of molecules that can potentially behave as DAMP(s)/alarmin(s), only limited pathways lead to IL-6 secretion; therefore, identification of the receptors involved in the pro-inflammatory response could reduce the number of ligands to be investigated. As such, we tested MYD88$^{-/-}$ x TRIF$^{-/-}$ to check for a TLR dependency of observed IL-6 secretion, MAVS$^{-/-}$ x STING$^{-/-}$ to exclude the involvement of RLRs or cGAS and TNFR1$^{-/-}$ to address the role of TNF or LT-α in inducing a pro-inflammatory response in recipient cells. All clones were tested by stimulation with specific agonists to confirm that they are competent in all investigated immune pathways except the one that relies on the deleted receptor/adaptor (Fig. 4.5A). To exclude LPS-dependent effects on recipient cells, we made use of the TLR4 inhibitor CLI095, which we added on the supernatant of donor cells immediately before stimulation of recipient cells. The ability of CLI095 to completely inhibit LPS-dependent IL-6 secretion is shown in Fig. 4.5B. For technical reasons, recipient cells utilized in this experiment were produced in CASP4$^{-/-}$ (TLR4$^{-/-}$ and TNFR$^{-/-}$) or WT background (MAVS$^{-/-}$ x STING$^{-/-}$ and MYD88$^{-/-}$ x TRIF$^{-/-}$). Therefore, we conducted additional experiments, in which we compared WT to CASP4-deficient cells in their response to necroptotic supernatant. These experiments revealed that caspase-4 had not impact on this activity (Fig. 4.5C). To our surprise, when we compared the effects of necroptotic supernatant on the generated recipient KO clones, we observed that IL-6 secretion by TNFR1$^{-/-}$ recipient cells was

almost completely abolished, while deletion of different adaptors/receptors did not impact the response to necroptotic DAMPs (Fig. 4.5D). This experiment reveals that necroptotic supernatant induces an *in trans* pro-inflammatory response via TNFR1 in resting cells under investigated conditions.
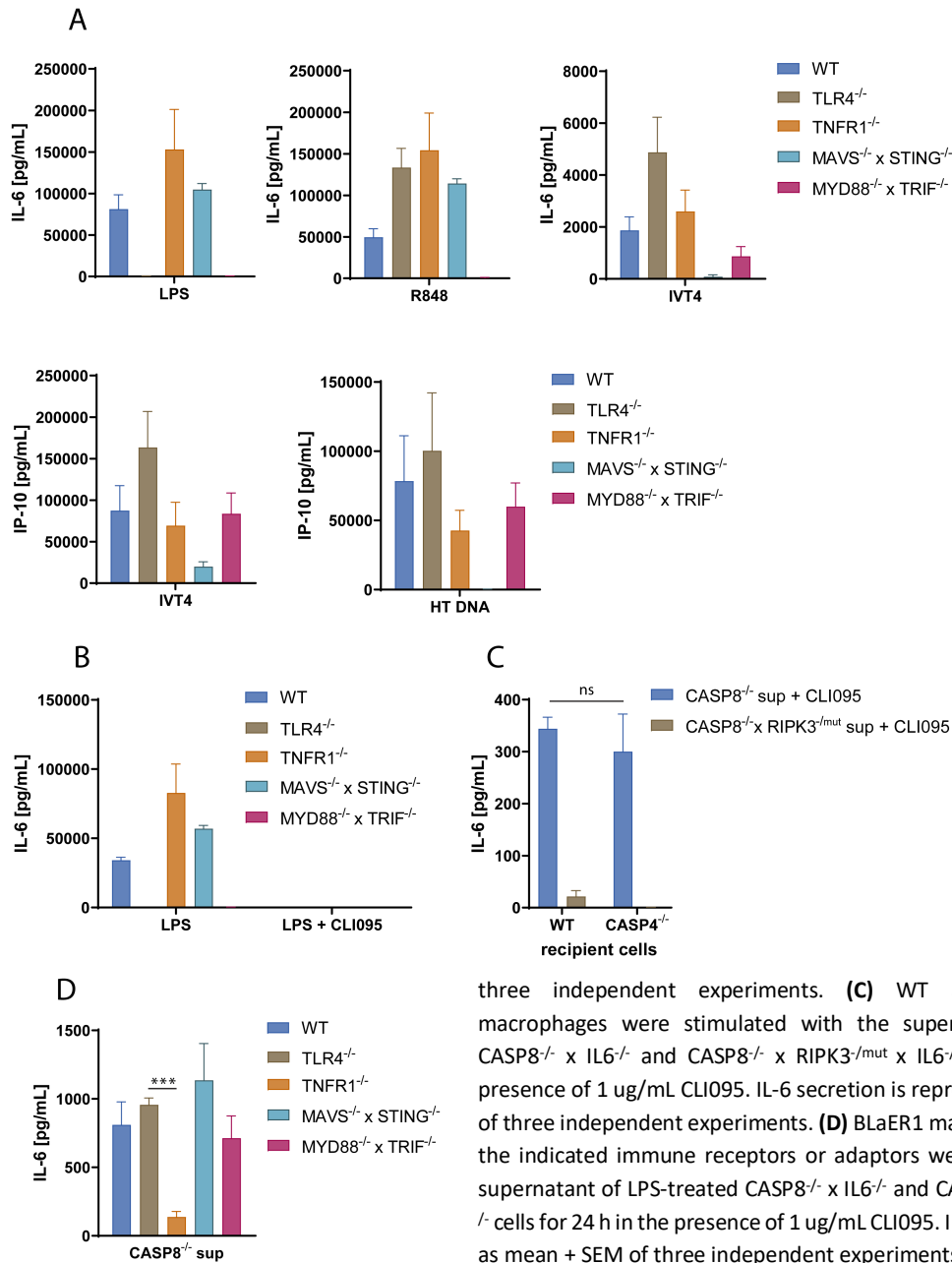
Fig. 4.5 (A) BLaER1 macrophages of the indicated genotypes were stimulated with LPS (2 ng/mL), R848 (1 ug/mL), or transfected with IVT4 or HT-DNA (200 ng/well + 0.5 uL lipofectamine/well) and cytokine secretion measured after 16 h. Results are shown as mean + SEM of three independent experiments. **(B)** BLaER1 macrophages of the indicated genotype were stimulated with LPS in presence or absence of the TLR4 inhibitor CLI095 (1 ug/mL). IL-6 secretion is shown as mean + SEM of three independent experiments. **(C)** WT and CASP4$^{-/-}$ BLaER1 macrophages were stimulated with the supernatant of LPS-treated CASP8$^{-/-}$ x IL6$^{-/-}$ and CASP8$^{-/-}$ x RIPK3$^{-/mut}$ x IL6$^{-/-}$ cells for 24 h in the presence of 1 ug/mL CLI095. IL-6 secretion is represented as mean + SEM of three independent experiments. **(D)** BLaER1 macrophages deficient for the indicated immune receptors or adaptors were stimulated with the supernatant of LPS-treated CASP8$^{-/-}$ x IL6$^{-/-}$ and CASP8$^{-/-}$ x RIPK3$^{-/mut}$ x IL6$^{-/-}$ cells for 24 h in the presence of 1 ug/mL CLI095. IL-6 secretion is depicted as mean + SEM of three independent experiments.

4.2.4 TNF but not LT-α acts as necroptosis-associated DAMP

In light of above observations, we next asked whether TNF or LT-α, which both signal via TNFR1, would be responsible for the observed pro-inflammatory activity. To do so, we generated TNF and LTA (LT-α) deficient CASP8$^{-/-}$ cells and compared their activity to unmodified cells. TNF or LT-α deficiency had no impact on necroptosis induction in donor cells upon LPS treatment. However, supernatant from TNF-deficient, but not LT-α deficient donor cells displayed a largely blunted IL-6 response in recipient cells (Fig. 4.6A and B). To address whether this TNF-dependent IL-6 inducing activity could be ascribed to higher TNF release in necroptotic cells, we directly measured TNF in the supernatant of these cells. Indeed, comparing the supernatant of CASP8$^{-/-}$ cells with CASP8$^{-/-}$ x RIPK3$^{-/mut}$ or CASP8$^{-/-}$ x MLKL$^{-/-}$ control cells upon LPS stimulation, we observed strongly increased TNF levels in cells succumbing to necroptosis (Fig. 4.6C and D).
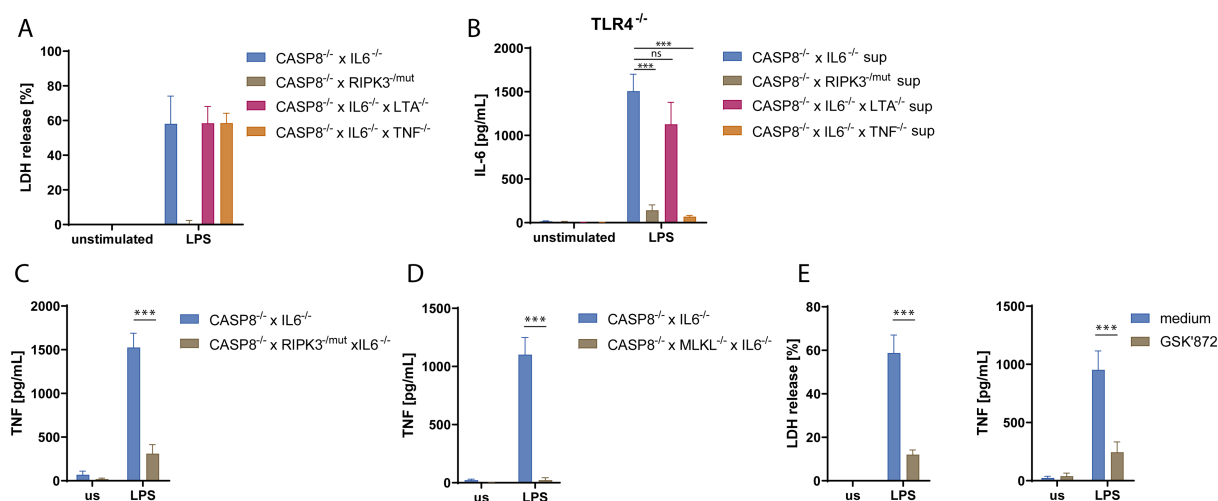

Fig. 4.6 (A) BLaER1 macrophages of the indicated genotypes were stimulated with 2 ng/mL LPS for 18 h. LDH release is depicted as mean + SEM of three independent experiments. **(B)** TLR4$^{-/-}$ BLaER1 macrophages were stimulated with the supernatant of LPS-treated cells shown in (A) for 24 h. IL-6 secretion is shown as mean + SEM of three independent experiments. **(C)** CASP8$^{-/-}$ x IL6$^{-/-}$ and CASP8$^{-/-}$ x RIPK3$^{-/mut}$ x IL6$^{-/-}$ cells were stimulated with 2 ng/mL LPS for 18 h or left unstimulated. TNF secretion is represented as mean + SEM of seven independent experiments. **(D)** CASP8$^{-/-}$ x IL6$^{-/-}$ and CASP8$^{-/-}$ x MLKL$^{-/-}$ x IL6$^{-/-}$ cells were stimulated as in (C). Data shown as mean + SEM of four independent experiments. **(E)** CASP8$^{-/-}$ x IL6$^{-/-}$ BLaER1 macrophages were stimulated with 2 ng/mL LPS or left unstimulated in presence or absence of the RIPK3 inhibitor GSK´872 for 18 h. LDH release and TNF secretion shown as mean + SEM of four independent experiments.

Similar results were obtained when we measured TNF production in CASP8$^{-/-}$ donor cells upon LPS stimulation in presence or absence of the RIPK3 inhibitor GSK´872: upon inhibition of RIPK3 by GSK´872, LPS-induced necroptosis was significantly lower, as well as TNF secretion, confirming that necroptotic cells produced more TNF compared to non-necroptotic cells (Fig. 4.6E). Altogether, these data show that the TNF but not LT-α is the necroptosis-associated alarmin that serves as ligand of TNFR1.

4.2.5 Shedding of TNF into its mature form by ADAM proteins is positively regulated in necroptotic cells

TNF is produced as a trimeric single-pass transmembrane protein that needs to be cleaved in order to generate the soluble cytokine (sTNF). This process, which is commonly referred to as shedding, is mainly carried out by members of the ADAM metalloproteases family, namely ADAM17 and ADAM10 (see section 1.6 and 1.7). However, because the membrane form of TNF is also biologically active, we asked whether the TNF measured in the supernatant of necroptotic cells is the sTNF or the membrane-bound proTNF. To answer this question, we analyzed proTNF and sTNF in both cell lysate and supernatant of necroptotic and control cells in a time course experiment by immunoblotting. Already starting from 3 h after LPS stimulation, we observed more abundant sTNF detectable in the supernatant of necroptotic cells compared to control cells, despite similar proTNF levels in cell lysates. This suggested that the TNF released by necroptotic cells is more efficiently cleaved from a comparable pool of proTNF in CASP8$^{-/-}$ compared to CASP8$^{-/-}$ x RIPK3$^{-/-}$ cells at early time points (Fig. 4.7A). Of note, when analyzing proTNF 8 h after LPS induction, we observed a strong difference in proTNF levels between CASP8$^{-/-}$ and CASP8$^{-/-}$ x RIPK3$^{-/-}$ cells, suggesting that, at later time points, a regulation on proTNF levels can also play a role in determining the pool of proTNF available for TNF maturation on the cell membrane (Fig. 4.7B). Indeed, subsequent analyses suggested that increased proTNF levels in necroptotic cells at later time points were likely attributable to post-transcriptional rather than transcriptional effects. As such, qPCR analyses did not show a discernable difference in TNF mRNA expression levels between these two conditions (data not shown). In the following, we decided to focus our research efforts on the early phase of necroptosis-induced TNF release rather than in the late phase of this process, since we speculate that the early phase is more relevant in an *in vivo* setting. This allowed us to study the maturation of proTNF into its mature form in the context of necroptotic cell death.

To understand which protease is responsible for active TNF shedding in BLaER1 necroptotic cells, we analyzed the expression of members of the ADAM family from RNA-seq data of untreated and LPS-stimulated WT BLaER1 cells available in the lab and found relatively high expression of ADAM9, ADAM10, ADAM15 and ADAM17 compared to all other ADAMs. Moreover, LPS treatment resulted in increased levels of ADAM10 and ADAM17 expression (Fig. 4.7C). Since the main metalloproteases described to cleave TNF are indeed ADAM17 and ADAM10, we sought to investigate whether these metalloproteases are involved in necroptosis-induced TNF shedding. To do so, we generated CASP8$^{-/-}$ x ADAM17$^{-/-}$ and CASP8$^{-/-}$ x ADAM10$^{-/-}$ cells and measured their ability to undergo necroptosis and induce TNF maturation. CASP8$^{-/-}$ x ADAM17$^{-/-}$ and CASP8$^{-/-}$ x ADAM10$^{-/-}$ cells were both necroptosis competent as the parental CASP8$^{-/-}$ cells as judged by LDH release, but only CASP8$^{-/-}$ x ADAM17$^{-/-}$ cells showed impaired TNF secretion.
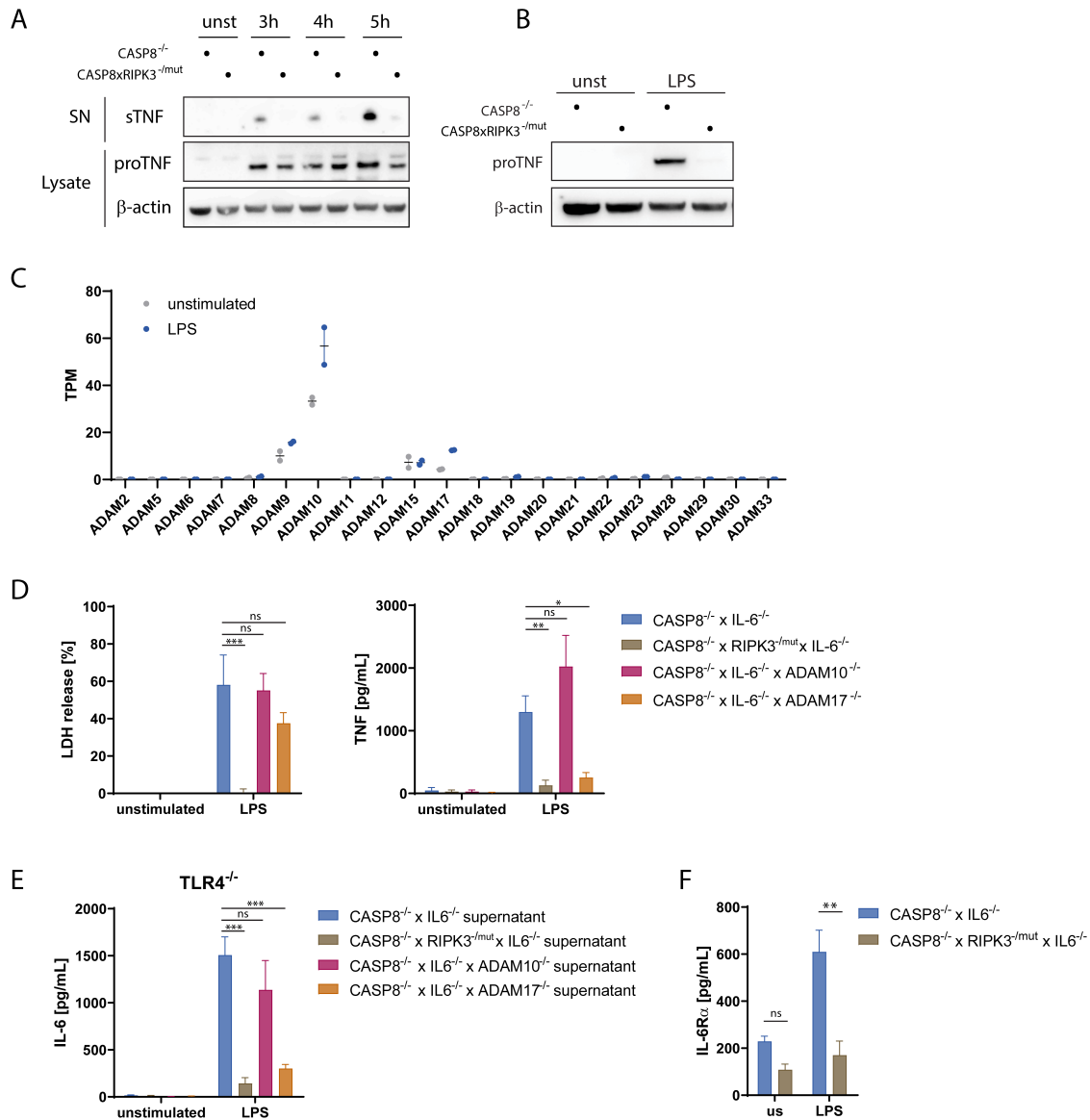
Fig. 4.7 (A) CASP8$^{-/-}$ x IL6$^{-/-}$ and CASP8$^{-/-}$ x RIPK3$^{-/mut}$ x IL6$^{-/-}$ cells were stimulated with 2 ng/mL LPS in 3% FCS containing medium for the indicated time points. Cell lysate and supernatant (SN) were subjected to SDS-PAGE and immunoblot and probed with TNF or β-actin specific antibodies. One representative clone/genotype shown of two independent experiments performed with 2 clones/genotype. **(B)** CASP8$^{-/-}$ x IL6$^{-/-}$ and CASP8$^{-/-}$ x RIPK3$^{-/mut}$ x IL6$^{-/-}$ cells were stimulated with 2 ng/mL LPS in 10% FCS containing medium for 8 h. Cell lysate was immunoblotted and probed with TNF or β-actin specific antibodies. One representative of two independent set of clones. **(C)** BLaER1 WT macrophages were stimulated with 200 ng/LPS for 2 h or 14 h or left unstimulated and cell lysate utilized for RNA-seq analysis. Data relative to ADAM proteins are shown as transcripts per kilobase million (TPM). **(D)** BLaER1 macrophages of the indicated genotypes were stimulated with 2 ng/mL LPS for 18 h. LDH release and TNF secretion is shown as mean + SEM of three independent experiments. Samples from CASP8$^{-/-}$ x IL6$^{-/-}$ and CASP8$^{-/-}$ x RIPK3$^{-/mut}$ x IL6$^{-/-}$ cells are the same used in Fig. 4.6D. **(E)** TLR4$^{-/-}$ BLaER1 macrophages were stimulated with the supernatant of cells of the indicated genotypes treated as in (D) for 24 h. IL-6 secretion is shown as mean + SEM of three independent experiments. Samples from stimulation with CASP8$^{-/-}$ x IL6$^{-/-}$ and CASP8$^{-/-}$ x RIPK3$^{-/mut}$ x IL6$^{-/-}$ cells supernatant are the same used in Fig. 4.6E. **(F)** CASP8$^{-/-}$ x IL6$^{-/-}$ and CASP8$^{-/-}$ x RIPK3$^{-/mut}$ x IL6$^{-/-}$ cells were stimulated with 2 ng/mL LPS for 18 h and IL-6Rα release measured by ELISA. Mean + SEM of three independent experiments.

These results implicated that ADAM17 is the primary sheddase involved in TNF maturation in BLaER1 necroptotic cells (Fig. 4.7D). In line with low TNF levels, the supernatant of necroptotic CASP8^{-/-} x ADAM17^{-/-} but not CASP8^{-/-} x ADAM10^{-/-} cells showed a reduced ability to induce IL-6 secretion in recipient cells in supernatant transfer experiments (Fig. 4.7E), confirming that ADAM17-shed TNF is the solely necroptosis-induced alarmin able to induce *in trans* inflammation in our system. To elucidate whether necroptosis specifically promotes TNF shedding or shedding activity of ADAM17 in general, we examined the levels of secreted IL-6Rα, another substrate of this metalloprotease [197]. Comparing cleaved IL6-Rα levels in the supernatant of CASP8^{-/-} necroptotic and CASP8^{-/-} x RIPK3[-/mut] BLaER1 cells, we detected increased shedding of IL-6Rα in CASP8^{-/-} cells, similar to TNF. This suggested that necroptosis positively regulates ADAMs-mediated shedding of its targets in general (Fig. 4.7F). In order to separate the contribution of ADAMs-mediated shedding from transcriptional or post-transcriptional regulatory events, we aimed at studying necroptosis-mediated TNF shedding in an NF-kB-independent context. To do so, we transiently transfected HEK293T cells with a plasmid leading to the expression of proTNF in combination with a doxycycline inducible construct for the expression of different N-terminal truncated MLKL proteins or mCherry, as control. The MLKL truncation 1-201 is able to induce necroptosis without further activation, as already mentioned (see section 4.2.1), while MLKL 1-154 loses this ability [152]. As expected, only cells transfected with MLKL 1-201 underwent considerable necroptosis, as judged by LDH release (Fig. 4.8A). Indeed, the combination of proTNF with MLKL1-201 led to significantly higher levels of TNF release compared to the co-expression of proTNF with MLKL 1-154 or mCherry (Fig. 4.8A). Moreover, when analyzing these conditions by immunoblot, we could confirm that despite similar levels of proTNF in the cell lysates, the amount of sTNF in the supernatant was considerably higher upon co-transfection with MLKL 1-201 compared to control conditions (Fig. 4.8B). Finally, to understand whether the observed TNF shedding was dependent on ADAM17^{-/-} and/or ADAM10^{-/-} in HEK293T cells, we generated ADAM17^{-/-}, ADAM10^{-/-} and ADAM17^{-/-} x ADAM10^{-/-} cells and repeated above-described co-transfection experiments. ADAM17^{-/-}, ADAM10^{-/-} and double deficient cells underwent necroptosis upon transfection with MLKL 1-201 with no significant difference. However, TNF shedding was partially impaired in both ADAM17^{-/-} and ADAM10^{-/-} cells, and strongly reduced upon deficiency of both ADAM17 and ADAM10 (Fig. 4.8C and D). Taken together, these data show that necroptosis promotes TNF maturation by inducing ADAM-dependent shedding of membrane proteins.
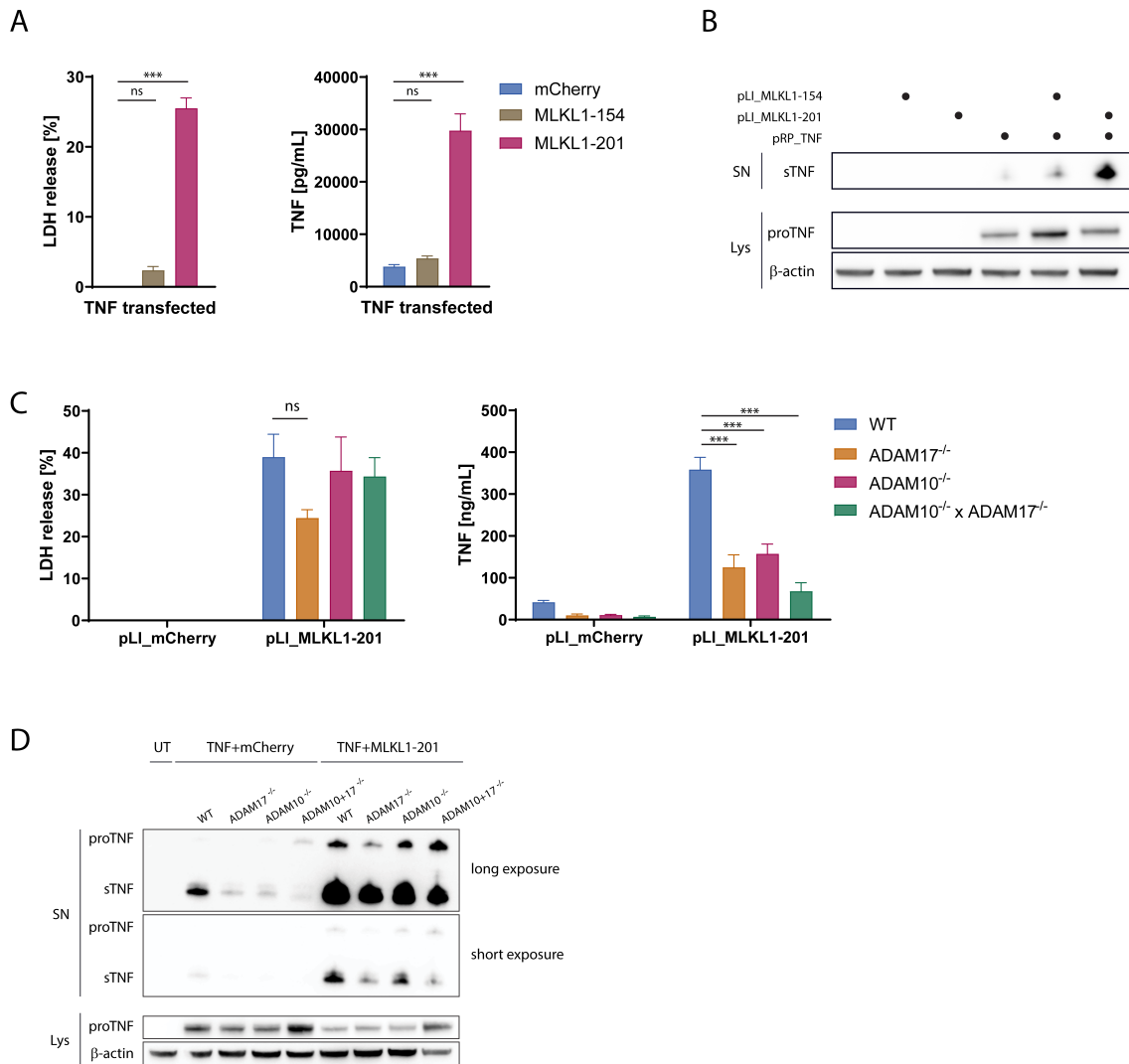
Fig. 4.8 (A) HEK293T cells were transfected with TNF and a doxycycline-inducible plasmid coding for two MLKL truncations (1-154 and 1-201) or mCherry as control. After 6 h, cells were treated with 1 ug/mL doxycycline for 16 h and supernatant was collected for LDH release and ELISA analysis (data represent mean + SEM of six independent experiments). **(B)** HEK293T were transfected with the indicated constructs or left untransfected. The day after, medium was removed and fresh 3% FCS containing medium with 1 ug/mL doxycycline was used to stimulate cells for 7 h. Supernatant and cell lysate from different samples were immunoblotted and analyzed with indicated antibodies. One representative of three independent experiments. **(C)** HEK293T cells of indicated genotypes were transfected with TNF and a doxycycline-inducible plasmid coding for MLKL 1-201 or mCherry as control. The day after, medium was removed and fresh 3% FCS containing medium with 1 ug/mL doxycycline was used to stimulate cells for 7 h. LDH release and TNF secretion are shown as mean + SEM of three independent experiments. **(D)** Supernatant and cell lysate from samples obtained as described in (C) were immunoblotted and analyzed with indicated antibodies. One representative of three independent experiments.

4.2.6 Necroptosis but not apoptosis or pyroptosis induces ADAM17-mediated TNF shedding in a phosphatidylserine exposure independent manner

We next asked whether other types of cell death could also promote TNF shedding by ADAM metalloproteases. This question is relevant to understand if TNF is a necroptosis-specific alarmin and to shed light on the possible mechanism of increased TNF shedding upon necroptosis: in fact, different types of cell death have distinct morphological and molecular features that could play a role in inducing TNF maturation. In particular, we studied the effects on TNF shedding upon induction of pyroptosis, which is another lytic type of cell death. At the same time, we also included stimuli to trigger intrinsic apoptosis, which is considered to be a non-lytic cell death.
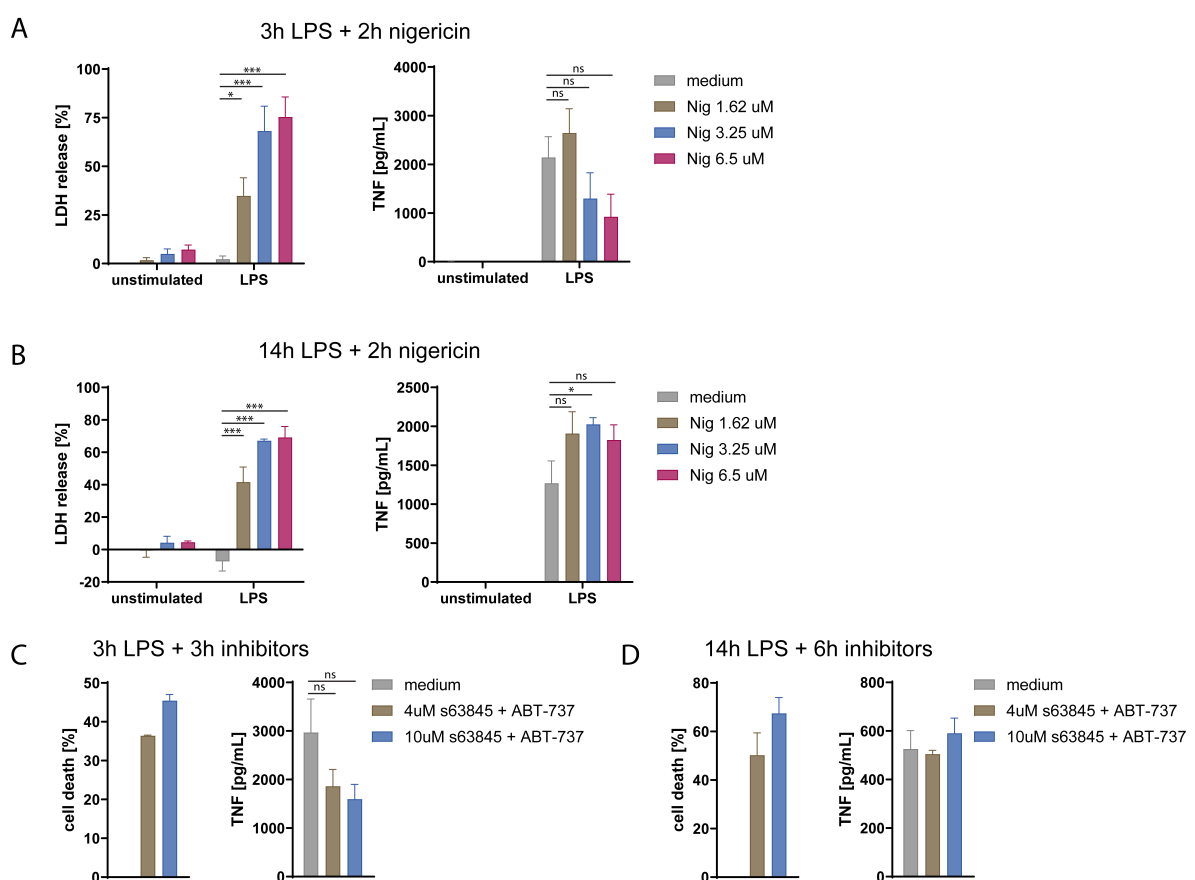
Fig. 4.9 (A, B) WT BLaER1 macrophages were primed with 2 ng/ml LPS or left unprimed for 3 h (A) or 14 h (B) then stimulated with indicated doses of nigericin for 2 h to induce pyroptosis. LDH release and TNF secretion are depicted as mean + SEM of three independent experiments. **(C, D)** WT BLaER1 macrophages were primed with 2 ng/ml LPS or left unprimed for 3 h (C) or 14 h (D) then stimulated with indicated doses of ABT-737 and S63845 for 3 h and 6 h respectively to induce apoptosis. CTG assay was used to assess cell death, TNF secretion was measured by ELISA. Mean + SEM of three independent experiments.

We induced pyroptosis in WT BLaER1 macrophages by 3 h or 14 h of LPS treatment (short and long priming, respectively) followed by 2 h of treatment with different concentrations of nigericin, an ionophore that leads to K^+ efflux and consequent NLRP3 inflammasome activation followed by pyroptotic cell death. For both priming conditions, increasing nigericin

concentrations led to increasing LDH release, indicative of pyroptotic cell death (Fig. 4.9A and B). TNF secretion upon short LPS priming resulted decreased upon nigericin treatment, implying that pyroptotic cell death had a negative impact on TNF secretion in these settings (Fig. 4.9A). Upon 14 h LPS priming, pyroptosis induction by nigericin showed only a limited positive effect on TNF shedding, not comparable to the 4-fold difference observed upon necroptosis induction (Fig. 4.9B). A similar experiment was performed to study TNF shedding upon apoptosis induction. Cells were primed 3 h or 14 h with LPS to induce transcription of TNF followed by additional treatment with a combination of MCL-1 and BCL-2 inhibitors (S63845 and ABT-737) at different concentrations and times to promote apoptosis. As shown by CTG assay, cell death was successfully induced upon treatment with the inhibitors (Fig. 4.9C and D). Similar to what observed upon pyroptosis induction, apoptosis had a negative impact on TNF shedding upon short LPS priming, with lower TNF secretion upon increasing concentrations of the inhibitors, while it had no effects upon long LPS priming (Fig. 4.9C and D).

Because phosphatidylserine exposure, a cell death associated event, has recently been described as an essential step to activate ADAM17-mediated shedding by leading the catalytic domain of the enzyme in close proximity with the cell membrane [109], we sought to investigate the role of phosphatidylserine exposure on necroptosis-induced activation of ADAM17. Since phosphatidylserine exposure is a common feature of necroptosis, apoptosis and pyroptosis [198], but only necroptosis was able to induce TNF shedding by ADAM17 in our hands, we did not expect an impact of this cell death-associated event in our system. Nevertheless, to test this hypothesis, we treated CASP8$^{-/-}$ and CASP8$^{-/-}$ x RIPK3$^{-/mut}$ cells with LPS over time in the presence of different concentrations of Annexin V, in order to compete for the binding of ADAM17 to exposed phosphatidylserine, thereby inhibiting TNF shedding. Annexin V specific binding to exposed phosphatidylserine on necroptotic cells was monitored by FACS analysis (Fig. 4.10A). LPS-treated CASP8$^{-/-}$ cells showed the appearance of Annexin V positive cells at all analyzed time points, with a percentage of positive cells dependent on the amount of Annexin V added to the medium. CASP8$^{-/-}$ x RIPK3$^{-/mut}$ cells were checked after 3 h or 16 h treatment and showed background levels of Annexin V positivity at 3 h, increasing at 16 h, most probably due to non-specific binding or uptake. Importantly, the addition of Annexin V did not impact on cell death induction, as shown by the LDH release assay (Fig. 4.10B). Moreover, no effect of Annexin V was visible on TNF secretion at any of the concentrations used, suggesting that ADAM17-mediated TNF shedding upon necroptosis is not inhibited by competition with phosphatidylserine binding of the enzyme (Fig. 4.10C). Taken together, these data indicate that ADAM17-mediated TNF shedding is a necroptosis-specific event that does not depend on phosphatidylserine exposure.
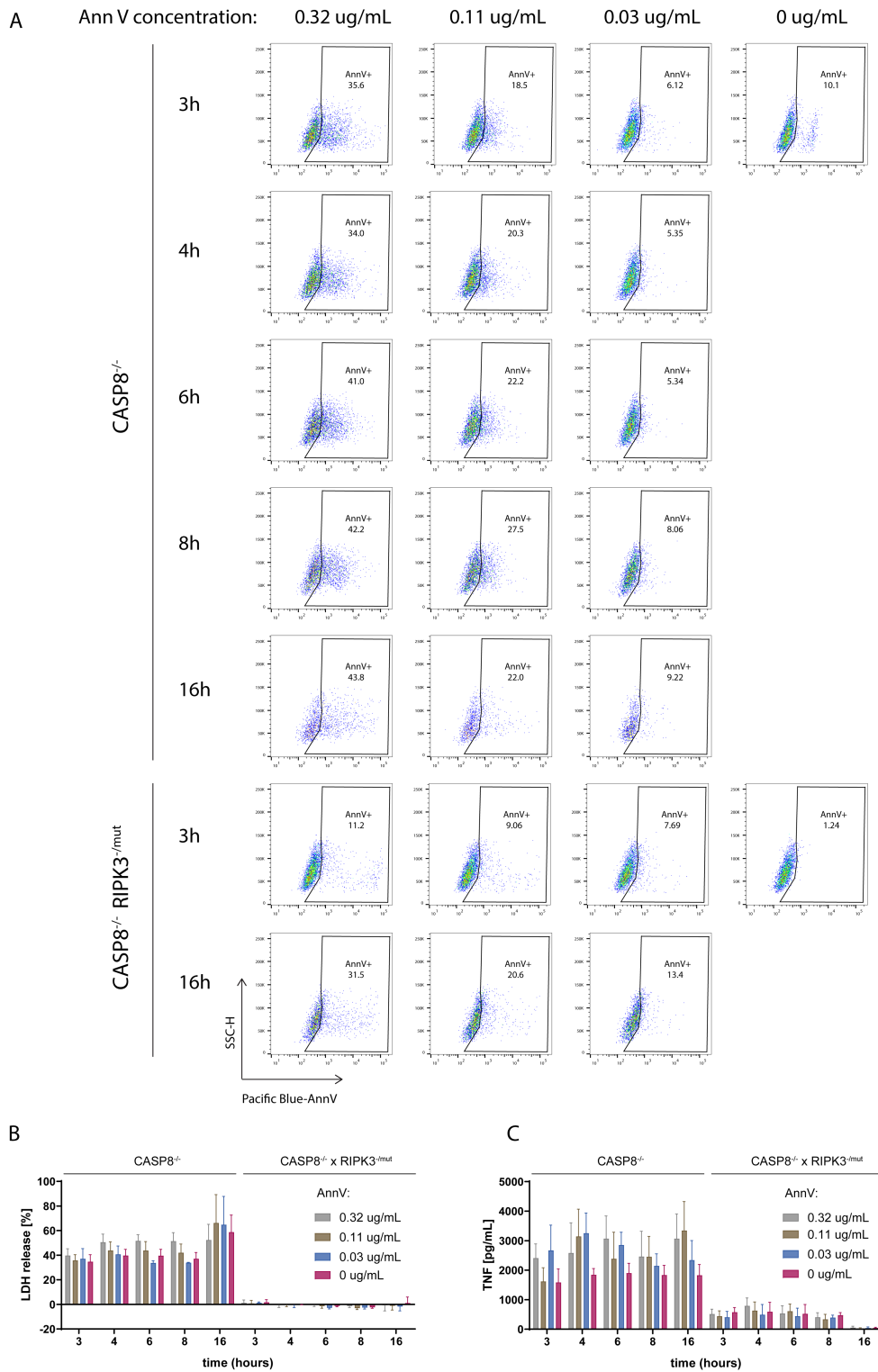
Fig. 4.10 (A) CASP8^{-/-} x IL6^{-/-} and CASP8^{-/-} x RIPK3[-/mut] x IL6^{-/-} cells were stimulated with 2 ng/mL LPS for the indicated time points in the presence of PacificBlue Annexin V at specified concentrations. Cells were then harvested and analyzed by flow cytometry for Annexin V positivity. **(B)** CASP8^{-/-} x IL6^{-/-} and CASP8^{-/-} x RIPK3[-/mut] x IL6^{-/-} cells were stimulated as described in (A). At the specified time points LDH release and TNF were measured. Mean + SEM of 4 independent experiments.

4.2.7 Necroptosis-associated membrane destabilization is necessary to enhance TNF shedding

To discern whether TNF shedding upon necroptosis requires the typical membrane perturbations of a necroptotic cell to occur or if it relies on MLKL-dependent but necroptosis-independent functions, we made use of a MLKL mutant (D107A/E111A) that does not kill the cell but is still able to be phosphorylated, to oligomerize and to get recruited to the cell membrane [158]. To study this mutant in HEK293T cells, we combined the above-mentioned amino acids substitutions with the phosphomimetic mutations (S357E/T358D) in the full-length MLKL, which make the protein constitutively active and able to induce necroptosis without further activation [148]. We therefore expressed the MLKL phosphomimetic mutant (S357E/T358D) or the MLKL construct with both regions mutated (S357E/T358D and D107A/E111A) and the MLKL 1-201 as control in HEK293T cells under a doxycycline inducible promoter. As shown by LDH release, the MLKL phosphomimetic construct could induce necroptosis in the same extent as the MLKL 1-201 truncation, while the introduction of D107A/E111A mutations impaired the ability of MLKL phosphomimetic construct to induce necroptosis (Fig. 4.11A). When co-transfecting the MLKL variants with TNF, we could observe enhanced TNF secretion upon expression of the MLKL 1-201 truncation or of the MLKL phosophomimetic version compared to an empty vector control, but not when we expressed the combination of phosphomimetic and D107A/E111A mutations (Fig. 4.11B). These results indicate that MLKL recruitment to the membrane alone is not sufficient to induce necroptosis associated TNF shedding. Instead, the membrane perturbating function of MLKL is required for this effect.
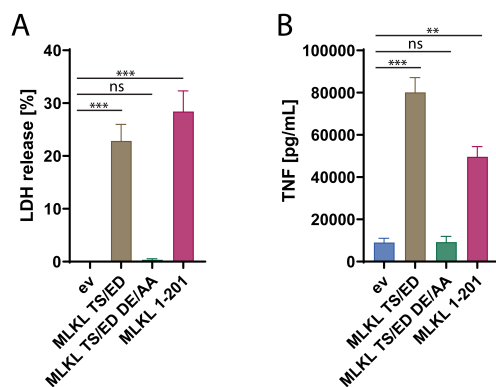
Fig. 4.11 (A,B) HEK293T cells were transfected with doxycycline-inducible plasmids for the expression of the phosphomimetic mutant of MLKL (TS/ED) in combination or not with the DE/AA mutation or of MLKL1-201 and an empty vector control (ev). After 6 h, cells were treated with 1 ug/mL doxycycline for 16 h and supernatant was collected for LDH release (A) and ELISA analysis (B). Data represent mean + SEM of three independent experiments.

4.2.8 Necroptosis promotes TNF secretion in primary human macrophages

In order to confirm our findings in primary cells, we isolated monocytes from PBMCs of different donors and differentiated the cells with hM-CSF for 7 days to obtain monocytes-derived macrophages. Cells were then stimulated with LPS alone or in combination with the caspase inhibitor Z-VAD, the RIPK3 inhibitor GSK´872 or both for 8 h (Fig. 4.12A). The stimulation with LPS and Z-VAD led to necroptotic cell death, while the addition of GSK´872 inhibited necroptosis by inhibiting RIPK3, as expected. We measured TNF secretion upon treatment with different combinations of inhibitors and found that necroptosis induction by LPS + Z-VAD strongly increased TNF release by macrophages compared to all other conditions. Interestingly, IL-6 secretion followed the opposite trend, with a negative impact of necroptosis on IL-6 levels in the supernatant of necroptotic cells, suggesting that one (or more) specific mechanism(s) regulates TNF secretion compared to other NF-kB-induced cytokines. Immunoblot on lysate and supernatant of 2 donors after 8h treatment revealed that TNF is matured by macrophages into its soluble form (Fig. 4.12B). However, as already observed in BLaER1 cells, it was not possible, at late time points, to dissect the specific contribution that increased proTNF levels observed in cell lysates and enhanced ADAMs-mediated shedding have on the total amount of matured TNF. In summary, our data show that necroptosis promotes TNF secretion in human primary macrophages.
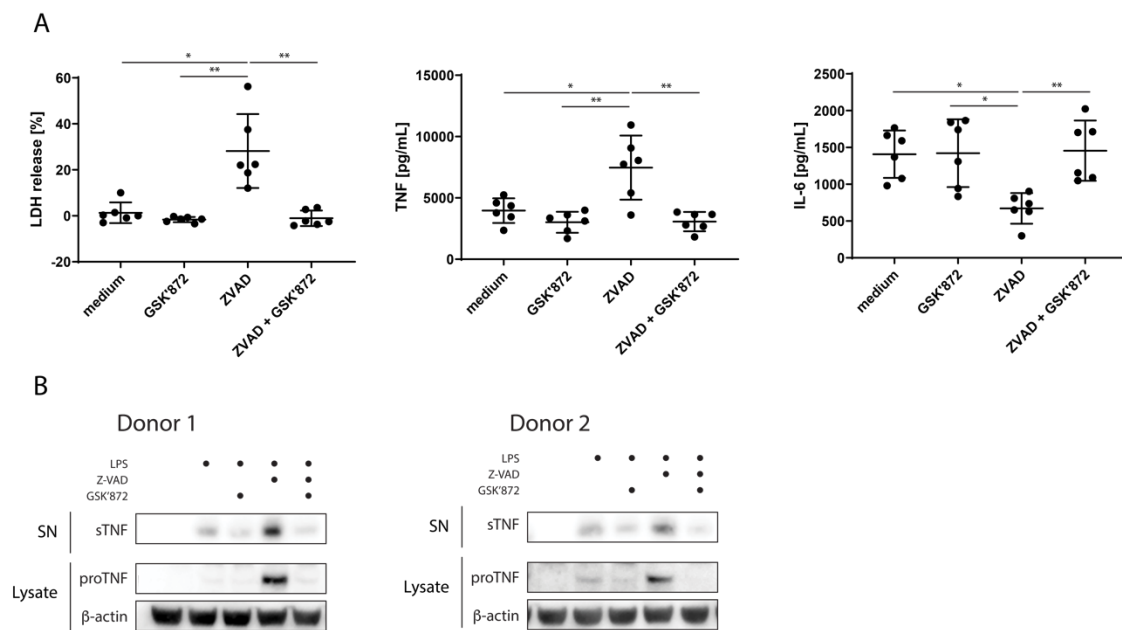
Fig. 4.12 (A) Primary monocytes derived from PBMCs of 6 different donors were differentiated into macrophages with 100 ng/mL MCSF for 7 days. Cells were then treated for 8 h with 0.2 ng/mL LPS alone or with the caspase inhibitor Z-VAD-FMK (20 uM), the RIPK3 inhibitor GSK'872 (3 uM) or the combination of both. LDH release and cytokine secretion were measured from collected supernatant. Dots represent individual donors, bars represent mean ± SEM. **(B)** Primary monocyte-derived macrophages from two donors were treated as in (A) in 3% FCS containing medium and subjected to immunoblot with indicated antibodies.

4.2.9 Preliminary *in vitro* experiments in murine cells for the development of an *in vivo* system to study inflammatory impact of necroptosis-mediated TNF shedding

A major problem in studying necroptosis-associated DAMPs is the lack of a proper *in vivo* model. Because of our finding that necroptosis contributes to inflammation by intrinsically promoting TNF release, we aimed to create the conditions for a future *in vivo* experiment to investigate the contribution of necroptosis-mediated TNF release in necroptosis-associated inflammation. To do so, we made use of a RIPK3-2xFv T2A EGFP construct that leads to RIPK3 activation upon addition of the B/B homodimerizer drug, which mediates the dimerization of two RIPK3 molecules by binding to the 2xFv dimerization domains fused to the protein [199]. In addition, the presence of EGFP after the T2A peptide facilitates the analysis and selection of successfully transduced cells. We first tested the system in the murine macrophage cell line J774. Transduced EGFP positive sorted cells and untransduced cells were primed with LPS for 1 h to induce TNF transcription and then treated with different concentrations of the B/B dimerizer for 14 h to induce RIPK3 activation and necroptosis. The treatment with B/B dimerizer induced LDH release only in transduced cells, in a dose dependent fashion, with no impact on untransduced cells (Fig. 4.13A). TNF secretion correlated with LDH release, with increased TNF production in transduced cells treated with the two higher doses of dimerizer, compared to low dose of the drug and to all conditions in untransduced cells (Fig. 4.13A), confirming that this approach can recapitulate necroptosis-induced TNF shedding observed in BLaER1 macrophages, HEK293T cells and primary human macrophages. We next aimed to test this system in murine hematopoietic stem cells (HSCs): this would allow the establishment of necroptosis-prone cells which can later be injected in lethally irradiated recipient mice for the generation of chimeric bone marrow with cells that can undergo necroptosis *in vivo* upon injection of the B/B dimerizer. As a preliminary *in vitro* experiment, we isolated HSCs from bone marrow of WT mice and transduced them with the RIPK3-2xFv T2A EGFP construct. The purity of isolated HSCs was assessed by FACS staining for a cocktail of lineage markers for which HSCs are negative (Fig. 4.13B). While all bone marrow cells resulted positive for the analyzed markers, with two distinct positive populations, HSCs appeared like a homogeneous population mostly negative for the lineage markers. Isolated HSCs were then transduced with the RIPK3-2xFv T2A EGFP construct and differentiated for 5 days with M-CSF to obtain HSC-derived macrophage like cells (Fig. 4.13C). On the day of experiment, 32.7% of cells resulted EGFP positive (Fig. 4.13D). Transduced and untransduced HSCs-derived macrophage-like cells were treated with two different concentrations of dimerizer or left untreated for 14 h, followed by LDH assay and TNF ELISA. As observed for J774 macrophages, the treatment with B/B homodimerizer specifically killed only transduced cells, with no LDH release detected in untransduced cells (Fig. 4.13E). Moreover, B/B homodimerizer-treated transduced cells secreted considerably more TNF compared to untransduced cells or transduced untreated cells, confirming the validity of this system to reproduce necroptosis-mediated TNF release in murine cells (Fig. 4.13F). Taken together, these preliminary experiments indicate the possibility to employ this system to successfully
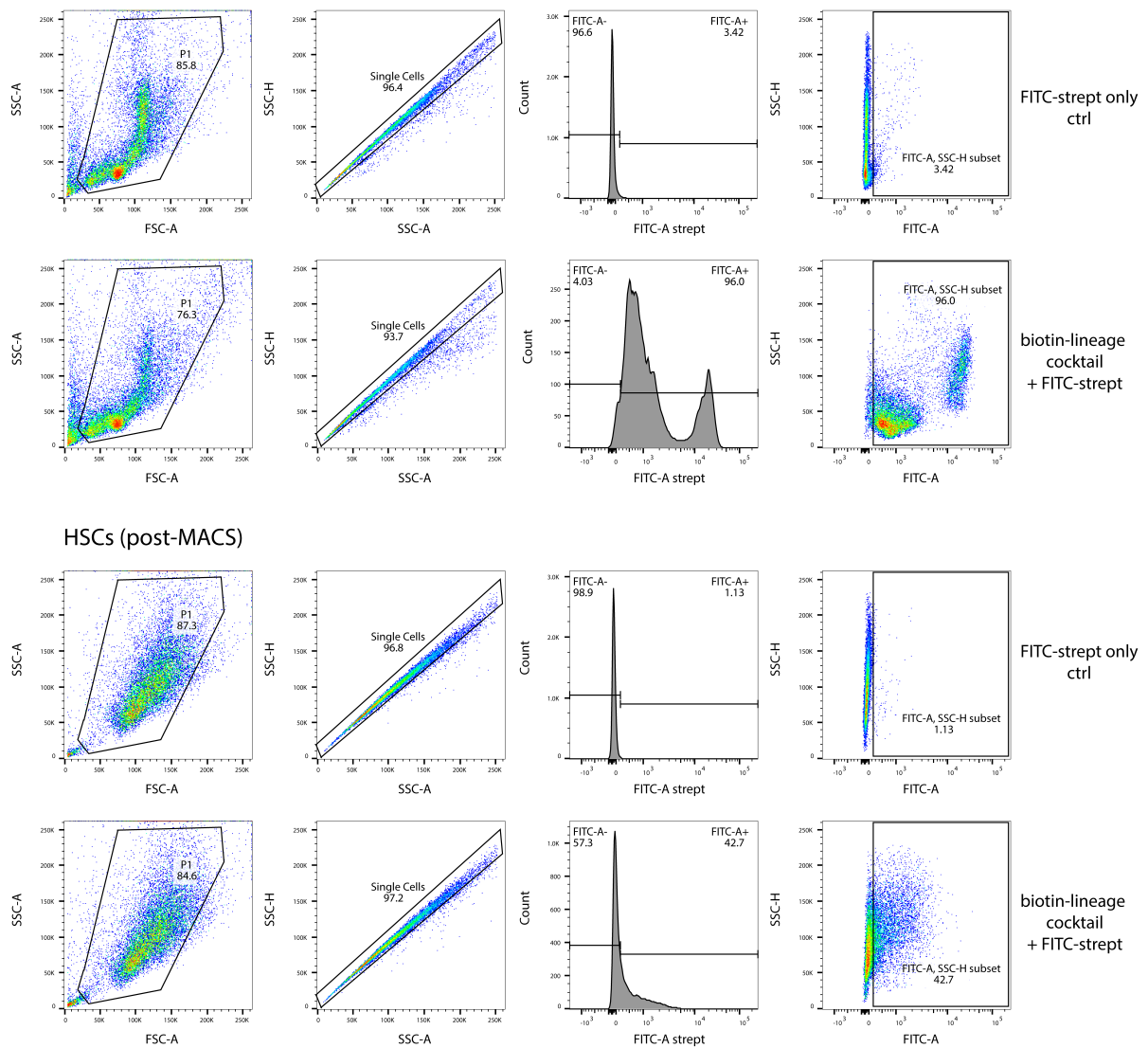
study the impact of necroptosis-mediated TNF shedding in the context of necroptosis-mediated inflammation *in vivo*.
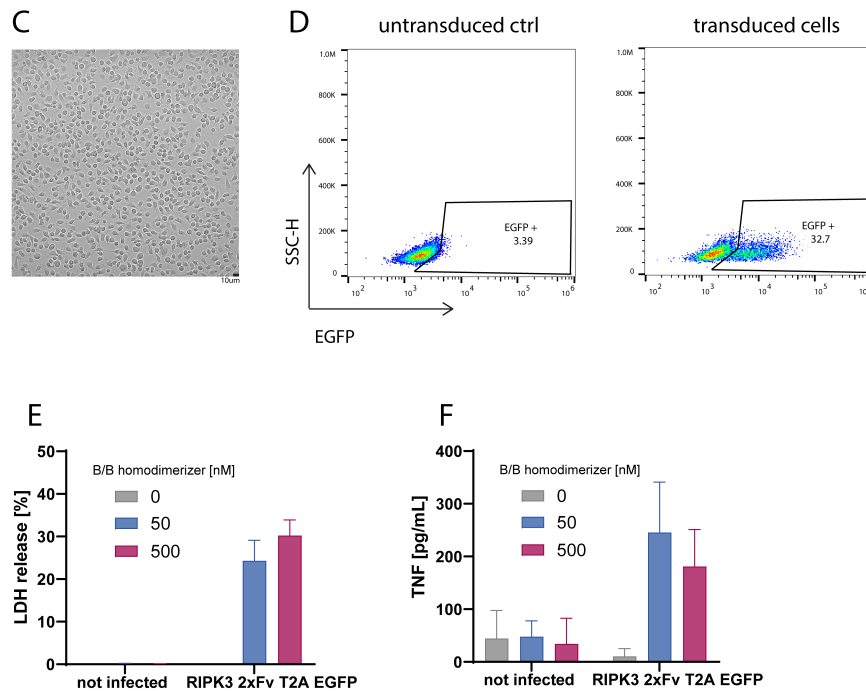
A
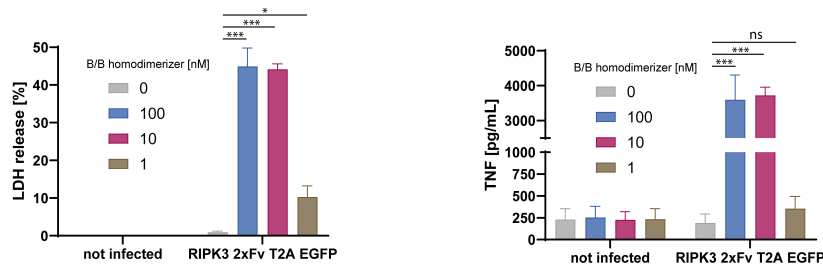
B

Bone Marrow (pre-MACS)

HSCs (post-MACS)

Fig. 4.13 (A) J774 WT and J774 RIPK3 2xFv T2A EGFP were primed with 2 ng/mL LPS for 1 h and then treated with B/B homodimerizer (AP20187) at indicated concentrations for 15 h before supernatant collection. LDH release and TNF secretion shown as mean + SEM of 3 independent experiments. **(B)** HSCs were isolated from bone marrow of WT mice. Successful isolation of HSCs was evaluated by flow cytometry for depletion of lineage positive cells. **(C, D)** HSCs were transduced with RIPK3-2xFv T2A EGFP and then differentiated for 5 days with 100 ng/mL M-CSF containing medium. A picture was taken to observe morphological characteristics of differentiated cells (C). On the day of experiment, cells were analyzed by flow cytometry for EGFP positivity (D). **(E,F)** HSCs transduced with RIPK3-2xFv T2A EGFP or left untransduced were stimulated for 14 h with B/B homodimerizer at indicated concentrations. LDH release (E) and TNF secretion (F) are shown as mean + SD of two independent experiments.

4.3 Generation of a reporter to study real time TNF shedding by necroptotic cells

4.3.1 C-Tag TNF is cleaved by ADAM metalloproteases similarly to WT TNF in necroptotic and non-necroptotic cells

So far, our data showed that necroptosis favors TNF maturation from the cell membrane by ADAM proteins, in particular ADAM17. However, end point experiments based on immunoblot and ELISA analysis could not help to understand dynamics, timing and mechanism by which necroptotic cells shed TNF. To answer these questions, we aimed at generating a reporter to monitor TNF shedding in real time by live-cell imaging. Since there is no antibody available that would only detect cleaved TNF, we modified the TNF sequence directly before the ADAM17 cleavage site (between A76 and V77), by adding a 4-amino acid-tag, called C-Tag. This tag can be detected by a specific nanobody only if it is exposed at the C-terminus of a protein, but not if present at the N-terminus or within the protein sequence (Fig. 4.14A). Since proTNF has its C-terminus in the extracellular region, its maturation by ADAM proteins leaves the C-Tag exposed extracellularly at the C-terminus of cleaved TNF and potentially available for detection by a fluorescently-labeled anti-C-Tag nanobody (Fig. 4.14B).

In addition, to be able to concomitantly detect proTNF levels by live-cell imaging, we fused mCherry to the cytosolic tail of C-Tag TNF and used this construct for microscopy experiments (Fig. 4.14B).
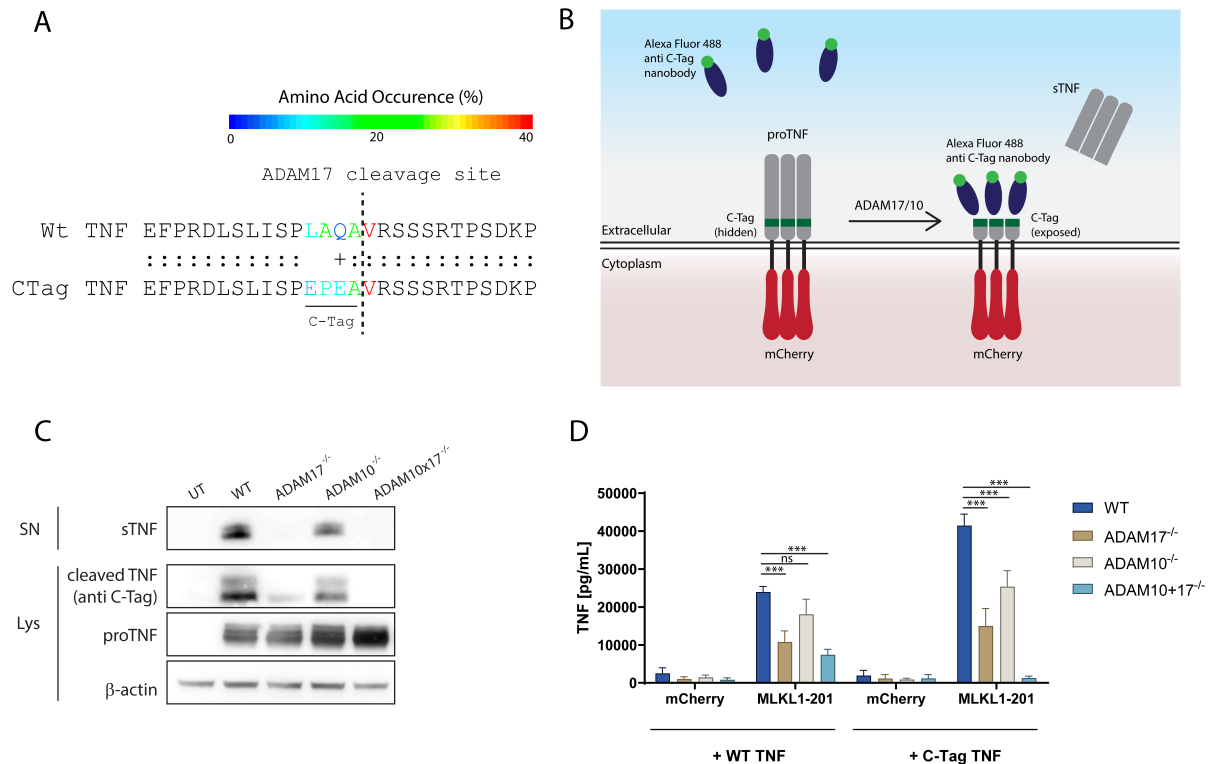

Fig. 4.14 (A) Comparison of WT TNF and C-Tag TNF sequence in the region of ADAM17 cleavage site. Colon represent identical amino acids. Colors represent amino acid occurrence (%) in the specific position of ADAM17 cleavage site sequence in its target proteins, according to [200] **(B)** Schematic overview of the detection of TNF shedding by live-cell imaging using the C-Tag TNF reporter. When proTNF is cleaved by ADAM proteins, the C-Tag is exposed and recognized by a specific nanobody added to the cell culture medium. To detect proTNF levels, mCherry was fused to the cytoplasmic tail of the protein. **(C)** HEK293T cells of the indicated genotypes were transiently transfected with C-Tag TNF. After 18 h supernatant was removed and replaced with 3% FCS containing medium with 1 ug/mL doxycycline. After 7h supernatant was collected and cells were lysed for immunoblot analysis. Samples were probed with the indicated antibodies. UT = untransfected control. One representative of two independent experiments. **(D)** Cells of the indicated genotype were transiently transfected with doxycycline-inducible WT TNF or C-Tag TNF constructs in combination with MLKL1-201 or mCherry expression plasmids. 6h after transfection, cells were stimulated with 1 ug/mL doxycycline and supernatant was collected to measure TNF secretion after 16 h. Data shown as mean + SEM of 3 independent experiments.

Even though the C-Tag sequence is compatible with amino acids typically found in the cleavage sites of ADAM17 substrates (Fig. 4.14A), we first wanted to test whether TNF cleavage by ADAM17 and ADAM10 is affected by the presence of the C-Tag. To do so, we transiently expressed C-Tag TNF in WT, ADAM10$^{-/-}$, ADAM17$^{-/-}$ and ADAM17$^{-/-}$ x ADAM10$^{-/-}$ cells HEK293T cells and performed western blot analysis of cell lysates and supernatants. As shown in Fig. 4.14C, we could readily detect cleaved TNF in the lysate of WT cells using the anti-C-Tag antibody in immunoblot. ADAM10$^{-/-}$ and, in particular, ADAM17$^{-/-}$ cells showed impaired TNF cleavage and a complete loss of TNF cleavage was seen in ADAM17$^{-/-}$ x ADAM10$^{-/-}$ cells. In addition, levels of matured TNF in the supernatant mirrored TNF levels detected

with the anti-C-Tag antibody in the cell lysates, confirming that the generated C-Tag-TNF can be cleaved in an ADAM17 and ADAM10 dependent manner as WT TNF. To study necroptosis associated TNF shedding for the C-Tag-TNF construct, we transiently transfected WT or ADAMs deficient HEK293T with WT TNF or C-Tag-TNF in combination with MLKL 1-201 or a control plasmid (mCherry). Subsequently we measured TNF secretion by ELISA. As shown in Fig. 4.14D, TNF secretion upon necroptosis was greatly increased for both WT and C-Tag TNF and was partially dependent on ADAM10 and ADAM17, whereas largely blunted in ADAM17$^{-/-}$ x ADAM10$^{-/-}$ cells. Of note, while residual TNF could be detected in the supernatant of ADAM17$^{-/-}$ x ADAM10$^{-/-}$ cells when expressing WT TNF, C-Tag TNF cleavage was completely abolished in ADAM17$^{-/-}$ x ADAM10$^{-/-}$ cells, indicating that the generated C-Tag TNF cleavage site is even more specific for ADAMs-mediated shedding than the WT TNF cleavage site itself. Taken together, these data demonstrate that shedding of the generated C-Tag-TNF reporter depends on ADAM17 and ADAM10 and is increased upon necroptosis induction, thereby resembling the conditions of WT TNF maturation.

4.3.2 TNF shedding in necroptotic cells is a relatively fast process that precedes actual cell death

The successful generation of a TNF shedding reporter, allowed us to perform live-cell imaging experiments to study the dynamics of TNF cleavage upon necroptosis. To do so, we made us of HEK293T stably transduced with MLKL 1-201 construct under doxycycline control and transiently transfected them with a doxycycline-inducible C-Tag-TNF expression plasmid. A plasmid for the expression of nuclear BFP (nBFP) was included to allow cell tracking over time. Cells were then doxycycline-treated to induce both C-Tag-TNF expression and necroptosis: with this inducible system, we can recapitulate the temporal coupling of LPS-induced TNF expression and induction of necroptosis, as studied in BLaER1 cells. 4h30min after doxycycline treatment, cells were subjected to live-cell imaging by spinning disk microscopy in the presence of Alexa488 anti-C-Tag nanobody in the supernatant. As shown in Fig. 4.15A, cells developed an intense, green fluorescent signal on the membrane, which preceded actual cell death, judged by typical morphological changes, such as increasing size and cell bursting. Analysis over time by widefield microscopy of multiple cells revealed a stable signal for mCherry TNF and a fast-rising signal for C-Tag TNF, until it reaches a plateau (Fig. 4.15C). Next, we aimed at comparing the dynamics of TNF shedding occurring in living and necroptotic cells by C-Tag positivity. To analyze whether the fluorescent signal observed before specifically raised from TNF shedding by ADAM proteins, we analyzed in parallel WT HEK293T cells and ADAM17$^{-/-}$ x ADAM10$^{-/-}$ HEK293T cells transduced with MLKL 1-201. The green fluorescent signal from cleaved TNF appeared faster and resulted in a remarkably higher signal in HEK293T MLKL1-201 cells compared to WT cells (Fig. 4.15B). Importantly, ADAM17$^{-/-}$ x ADAM10$^{-/-}$ necroptotic cells did not show a fluorescent signal associated with cleaved TNF, despite being necroptotic and displaying similar proTNF expression as WT HEK293T cells (mCherry signal). These results excluded that the C-tag nanobody non-specifically interacted with the membrane upon cell death (Fig. 4.15D).
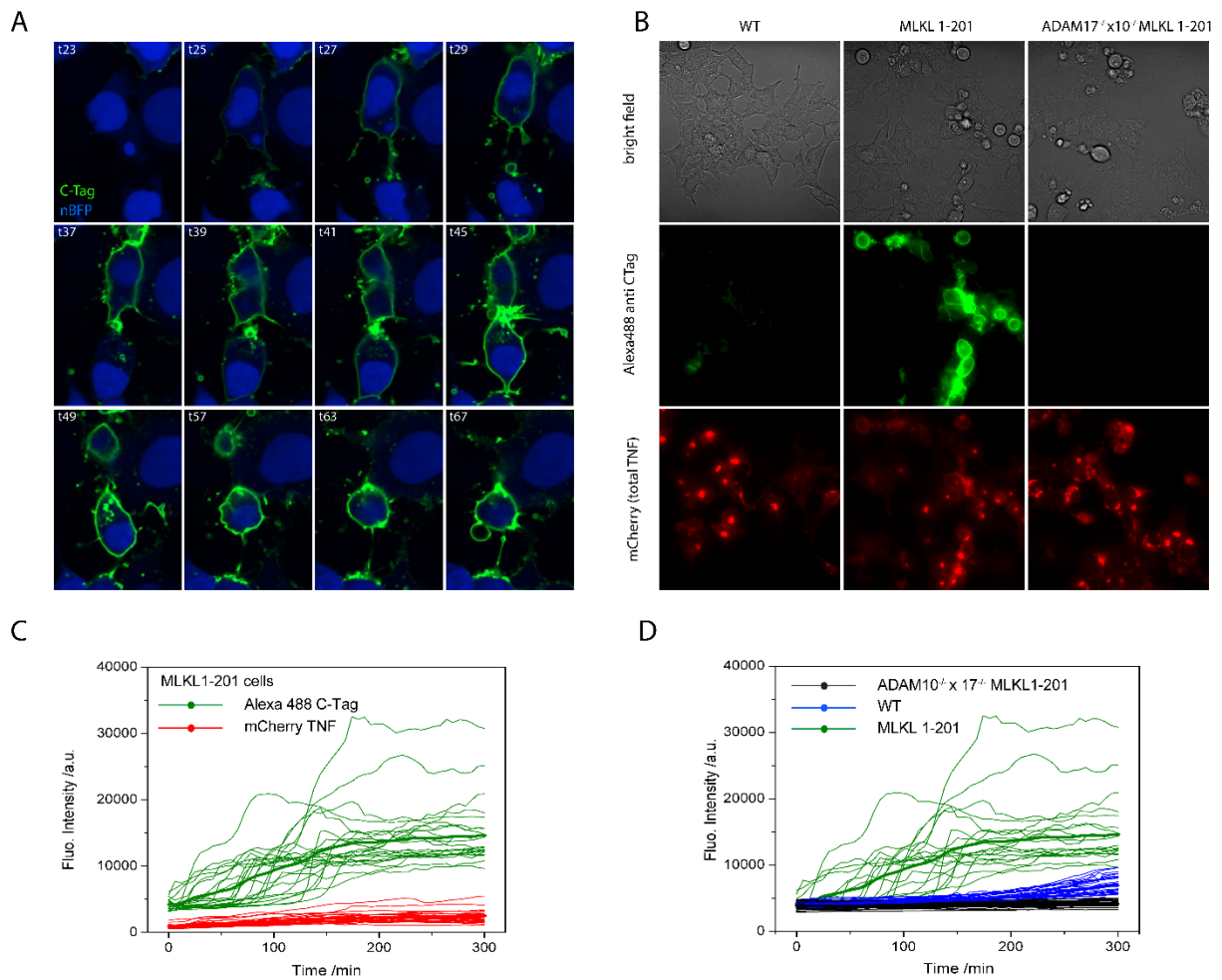
Fig. 4.15 (A) HEK293T MLKL 1-201 were transfected with C-Tag TNF and nBFP and stimulated with 1 ug/ml doxycycline to induce C-Tag TNF expression and necroptosis. 4h30 after, Alexa488 anti-C-Tag nanobody was added to the supernatant and cells were analyzed by spinning disk microscopy with a frame interval of 5 min (frame number is indicated on the top left corner of each image). Overlays of nBFP (in blue) and C-Tag TNF (in green) are shown. Representative cells from a field ow view of two independent experiments with at least three fields of view each. **(B)** Cells of the indicated genotypes were transfected and doxycycline-induced as in (A) and subjected to widefield fluorescent microscopy. Images represent cells 8 h after doxycycline induction. One representative of four acquired fields of view (experiment repeated three independent times). **(C,D)** Cells of the indicated genotypes were transfected, doxycycline-induced as in (A) and analyzed by a widefield fluorescent microscope. Lines in the plots represent the indicated fluorescent signal of individual cells collected from three independent experiments. a.u = arbitrary units.
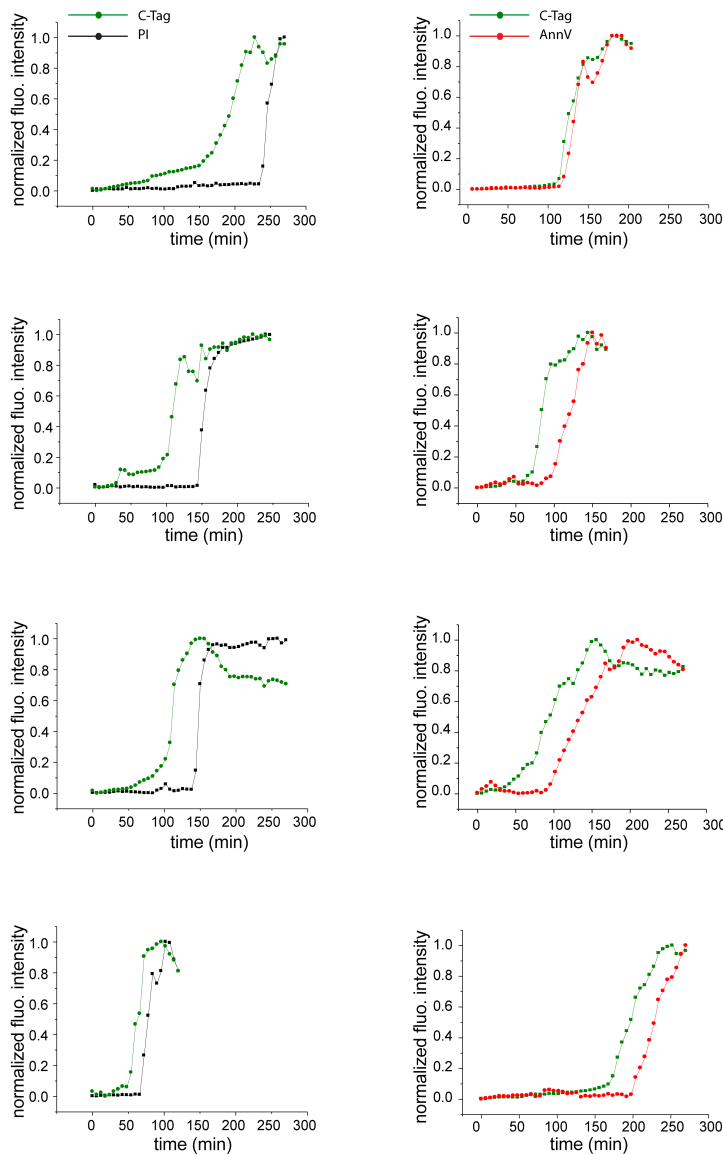
Fig. 4.16 (A) HEK293T MLKL 1-201 cells were treated as in Fig.15 A and subjected to live-cell imaging by widefield microscopy in the presence of Alexa488 anti-C-Tag nanobody + Annexin V or Alexa488 anti-C-Tag nanobody + PI. Graphs depict individual representative cells from three independent experiments of each combination. a.u = arbitrary units. **(B)** Fluorescent signals of Annexin V, PI and Alexa488 anti-C-Tag from experiments performed in (A) were plotted against the time when they reach 50% of the total fluorescence intensity. Each dot represents a cell. Paired t-test was used for statistical analysis. **(C)** Slopes of curves obtained from fluorescence signals of experiments performed in (A) were plotted and compared by paired t-test for statistical significance. Each dot represents a cell.
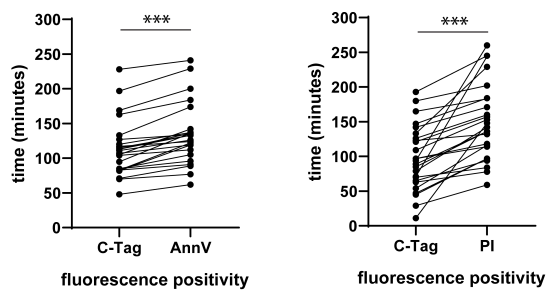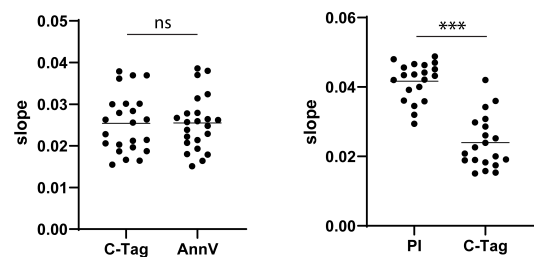
In order to put TNF shedding in relation with established markers of cell death, we repeated the experiment by monitoring over time TNF shedding and positivity for Annexin V or propidium iodide (PI) staining. Doing so, we observed that Annexin V positivity shortly followed C-Tag TNF positivity in necroptotic cells, suggesting that massive phosphatidylserine

exposure does not precede TNF shedding. On the other hand, PI positivity was further delayed compared to both C-Tag positivity and Annexin V positivity (Fig. 4.16A and B). When we compared the slopes of the curves of C-Tag, Annexin V and PI fluorescent signals, which reflect how fast these signal increase over time, we found that PI had a steeper curve than both C-Tag and Annexin V, which showed the same steepness (Fig. 4.16C). This rapid gain in signal in consistent with the notion that PI passively enters the cells when membrane integrity is compromised. In comparison, the slower and kinetically similar gain in C-tag and AnnV positivity suggests that these features depend on an active and possibly the same biological process. In summary, these experiments let us reconstruct the course of events as follows: first, cells express proTNF (mCherry positivity), then MLKL translocation leads to cell membrane modifications that induce a rather fast TNF shedding by ADAM proteases (anti-C-Tag positivity) which shortly precedes massive phosphatidylserine exposure (AnnV positivity); finally, due to dramatic morphological changes typical of necroptotic cells, membrane becomes permeable to PI (PI positivity).

5 Discussion

5.1 An *in vitro* model to study necroptosis-mediated DAMPs/alarmins release and their inflammatory role

Necroptosis, as other forms of regulated necrosis, is morphologically characterized by cell swelling and leakage of cytosolic content. This type of cell death is considered to be inflammatory because of the release of molecules that can act as DAMPs or alarmins (see sections 1.5 and 1.8.2). Although there is a general consensus about release of inflammatory molecules upon necroptotic cell death, few studies have addressed this problem and only some of those identify specific alarmins or DAMPs that drive inflammation in their system (section 1.8.2 and [53,55]). One issue of this research field is to prove a direct relation of causality between molecules released by necroptotic cells and the observed inflammatory phenotype. In this respect, *in vivo* models allow for a better evaluation of the pro-inflammatory phenotype under chosen experimental conditions compared to *in vitro* systems. However, this advantage comes along with some limitations. First of all, it is difficult to employ biochemical tools to identify DAMPs and alarmins *in vivo* and sorting out biological redundancies might be very challenging. Moreover, it is often not possible to establish a direct causality between danger molecules responsible for the observed phenotype and necroptosis: in fact, there is no control on the source of identified inflammatory signals. In addition, *in vivo* studies are carried out in animal models (usually mice) which not always recapitulate human immune responses. Finally, mouse experiments are long to establish and they are ethically concerning, considering the high number of animals needed. *In vitro* systems on the other hand are easier to manipulate and more suitable for the identification of specific danger signals released by necroptotic cells, by means of genetic manipulation and applicability of biochemical assays. In this study we aimed to identify specific necroptotic DAMPs/alarmins and to prove their ability to induce inflammation in bystander cells. For the reasons discussed above, we first focused our attention on the development of a suitable *in vitro* system to address these questions. We made use of the BLaER1 cell line, which can be effectively transdifferentiated into macrophage-like cells and behave similar to primary macrophages [194]. The use of this cell line has mainly two advantages: as myeloid cells they express the proteins necessary for necroptotic cells death, with no need of introducing necroptosis-mediators by overexpression methods. In addition, they express a large set of cytokines and PRRs. This makes them not only able to potentially release a vast set of DAMPs/alarmins upon necroptosis, but also to sense inflammatory molecules as bystander resting cells. Moreover, they are easy to manipulate via CRISPR/Cas9 technology. This allowed us to generate a genetic model of necroptosis and also provided the opportunity to interfere with specific pathways to prove their role in necroptosis-mediated inflammation. First, we generated necroptosis prone BLaER1 cells by deletion of CASP8, a fundamental check point that blocks necroptosis by cleaving its mediators, RIPK1 and RIPK3, which would in turn activate MLKL (see section 1.6 and 1.8.2). By CASP8 deletion, cells are neither able to induce apoptosis, nor able to survive by NF-kB activation upon treatment with ligands such as LPS or

TNF and are therefore committed to necroptosis. In fact, CASP8 deficiency removes the break on RIPK3 activation, unleashing RIPK3-mediated MLKL phosphorylation and necroptosis induction. As control, CASP8$^{-/-}$ x RIPK3$^{-/mut}$ and CASP8$^{-/-}$ x MLKL$^{-/-}$ cells were generated because of their inability to undergo necroptosis given the lack of fundamental mediators of this type of cell death. The ability of CASP8$^{-/-}$ cells to undergo necroptosis was judged by LDH release, an indirect marker of membrane destabilization and damage, and phosphorylation of MLKL, which both occur only in CASP8$^{-/-}$ cells but not in control cells (Fig. 4.1A and B). CASP8$^{-/-}$ and CASP8$^{-/-}$ x RIPK3$^{-/mut}$ or CASP8$^{-/-}$ x MLKL$^{-/-}$ cells were then used as "donor cells" in an *in vitro* system generated to perform supernatant transfer and co-culture experiments on "recipient cells", employed to study the inflammatory response generated by the contact with molecules released by necroptotic cells compared to non-necroptotic cells (Fig. 4.1C). By generating IL-6 deficient donor cells, we could measure this cytokine as readout for the inflammatory response induced in recipient cells upon stimulation with supernatant of necroptotic or control donor cells. In addition, the use of TLR4$^{-/-}$ recipient cells allowed the generation of a system were the stimulus used to induce necroptosis in donor cells (LPS) could not impact on the inflammatory response observed in recipient cells. The comparison of IL-6 secretion by recipient cells upon stimulation with supernatant from necroptotic and control donor cells, allowed us to estimate the magnitude of the inflammatory response directly dependent on necroptosis-associated DAMPs/alarmins, while the effects of LPS-induced inflammatory molecules could be determined by comparison of IL-6 secretion by recipient cells upon stimulation with supernatant of LPS-treated control donor cells. For these reasons, the system we generated had the great advantage of allowing a clear identification of necroptosis-dependent inflammatory responses both in supernatant transfer and co-culture conditions (Fig. 4.2). This greatly facilitated the identification of specific DAMPs/alarmins released by necroptotic cells by further genetic manipulation of donor and recipient cells. Of course, as all experimental models, our *in vitro* system has some limitations that should be considered. First of all, the model is limited to myeloid cells biology and the DAMPs/alarmin released by this type of cells can differ from the ones released by other cell types able to undergo necroptosis (e.g. keratinocytes). In addition, to generate a clean genetic model, we had to employ TLR4$^{-/-}$ recipient cells and IL6$^{-/-}$ donor cells: this precludes the possibility to study the potential roles of TLR4 in DAMPs and alarmins sensing and the effects of IL-6 secretion by donor cells on necroptosis-mediated inflammation. Moreover, the usage of IL-6 as readout for necroptosis-mediated inflammation mainly allows the identification of NF-kB-mediated response in recipient cells, neglecting the potential role of other pathways, such as interferon signaling, in these settings. On the other hand, the *in vitro* system here generated can be easily manipulated to allow the study of other pathways in this context, by changing the stimulus used to induce necroptosis and the cytokine used as readout for inflammation and by generating the respective KOs in recipient and donor cells. Taken together, we generated an *in vitro* model that facilitates research on necroptosis-mediated inflammation.

5.2 TNF as necroptosis-mediated alarmin

Using the described *in vitro* model of donor and recipient cells we were able to clearly prove that necroptotic cells can induce an inflammatory response in resting cells. This finding allowed us to investigate the nature of the inflammatory molecules that provoked NF-kB-dependent IL-6 secretion in recipient cells. To do so, we first analyzed the inflammatory potential of necroptotic supernatant subjected to heat shock to understand whether the DAMP/alarmin was temperature sensitive, which would argue for its proteinaceous nature. Having found that the DAMP/alarmin is heat shock sensitive (Fig. 4.3A), we subjected necroptotic supernatant to size exclusion chromatography, to restrict the range of size of the DAMP/alarmin involved and to confirm it being a protein. For this experiment we utilized THP1 monocytes expressing MLKL 1-201 as donor cells, to easily scale up the production of necroptotic supernatant under FCS-free conditions. With this approach we could confirm that the DAMP/alarmin at least contains a protein component and restrict its size to about 20-70 kDa (Fig. 4.3). Further studies using genetic manipulation in BLaER1 macrophages led us to the discovery that the inflammatory response observable in recipient cells depends on TNF-TNFR1 axis and that ablation of either TNFR1 in recipient cells or TNF in donor cells dramatically reduces the inflammatory capacity of necroptotic supernatant (Fig. 4.5 and 4.6). This finding was surprising for two reasons: first, it demonstrated that necroptosis-mediated inflammation in our system is completely dependent on TNF, without redundant molecules. Second, in our attempt to identify necroptosis-dependent triggers of inflammation, we actually found a molecule that fits the description of an alarmin, rather than a DAMP molecule. In fact, TNF is a master pro-inflammatory cytokine that performs immune-regulatory functions also when secreted by living activated macrophages. Other characterized alarmins include cytokines of the IL-1 family, such as IL-1α and IL-33. These cytokines are constitutively produced by many cell types, reside in the nucleus and are released only upon cell death or stress [201]. Unlike members of the IL-1 family, TNF can also be actively released by living cells and it is produced as a membrane-bound molecule that can exert its functions also in this form via cell-cell contact. This fact also explains why we could observe a less striking difference in terms of IL-6 release in our co-culture system as compared the transfer of supernatant onto recipient cells (Fig. 4.2E): in fact, it is likely that the membrane-bound TNF of non-necroptotic cells also contributed to activate recipient cells. Although TNF can be actively produced by living cells, it can still be defined as a necroptosis-associated alarmin, given the fact that necroptosis greatly promotes its secretion to trigger inflammation. This phenomenon was also observed in primary macrophages where necroptosis induction led to increased TNF secretion compared to control conditions (Fig. 4.12). Contrary to TNF, IL-6 secretion was reduced in primary macrophages upon necroptosis induction, suggesting that dying cells generally secrete less cytokines compared to immune activated living cells, because cell death stops their production, as already suggested [55]. These results hint to the existence of a special role of necroptosis in specifically promoting TNF secretion. Despite its extraordinary role in activating resting cells in our system, TNF has never been described as necroptosis-associated alarmin in previous studies, most probably for the following reasons:

first, TNF is frequently used as a necroptosis-inducing agent in combination with SMAC mimetics and CASP8 inhibitors. In these experimental conditions, TNF acts upstream of necroptosis, and its role as alarmin cannot be addressed. Moreover, in order to observe TNF secretion by necroptotic cells, it is necessary to license its transcription, since it is usually not constitutively produced. We achieved this by inducing necroptosis with LPS, a potent driver of NF-kB activation, but the usage of different necroptosis-inducing stimuli could lead to distinct priming conditions that not necessarily lead to TNF transcription. In addition to what already discussed, there could be cell-specific differences in terms of molecules that may act as DAMPs/alarmins when released. As mentioned above, the use of a myeloid cell line highly responsive to NF-kB-inducing stimuli widened the opportunity to find a NF-kB-dependent alarmin in our study. It is also important to note that it is difficult to distinguish between a real necroptosis-associated alarmin and a pure NF-kB-induced inflammatory molecule, when both signals are involved at the same time. However, with our genetically-defined system we could dissect the role of these two signals. In fact, both necroptosis prone and necroptosis resistant donor cells were LPS-treated, allowing us to control for necroptosis-mediated and NF-kB-dependent inflammatory response in recipient cells. The release of TNF from necroptotic cells can act, similarly to IL-1β or IL-18 released by pyroptotic cells, as an alarm for neighboring cells, which are subsequently activated to better respond to a potential threat. Moreover, TNF can function as upstream signal to amplify necroptosis induction in bystander cells. In case of infections, this could serve to amplify its inflammatory effects and its role in pathogen clearance. As already mentioned, our data demonstrated that TNF was the only necroptosis-mediated alarmin acting in our system, with no other identified DAMP. Classic DAMPs described in past works are HMGB1, heat-shock proteins, ATP, mitochondrial DNA, which do not perform immunological functions in living cells, but can induce inflammation when released upon cell death or stress (see section 1.5). There might be several reasons why we could identify only one alarmin entirely responsible for necroptosis-mediated inflammation in our study. First, it should be taken into account that the role of above-mentioned proteins as DAMPs is highly debated in the literature and could therefore not be relevant in necroptosis-mediated inflammation, at least in our *in vitro* system [53,55]. Second, we studied myeloid cells upon LPS-mediated necroptosis induction, a fact that increased the chances to find alarmins given the abundance of cytokines that these cells produce upon stimulation with a potent NF-kB activator such as LPS. Third, it should be considered that kinetics of necroptosis and DAMPs release could be different *in vitro* and *in vivo* and could vary from cell type to cell type, leading to different sets of molecules released by dying cells that could potentially act as DAMPs. Finally, it cannot be excluded that other NF-kB-induced alarmins or classic DAMPs were released by BLaER1 necroptotic cells and could not be identified within our system. As an example, it is known that necroptotic cells activate NLRP3 inflammasome intrinsically and consequently undergo secondary pyroptosis and secrete IL-1β (see section 1.8.2). Even though IL-1β was more abundantly detected in necroptotic cells also in our study, it had no impact in necroptosis-mediated inflammation, most probably because BLaER1 cells are unresponsive to IL-1β (Fig. 4.4C). As IL-1β, it is

possible that other alarmins/DAMPs could not be sensed by BLaER1 recipient cells and different approaches, such as secretome analysis or RNA sequencing of necroptotic cells, could help with their identification. In summary, we identified mature TNF as a necroptosis-induced alarmin which promotes inflammation in bystander resting cells.

5.3 Mechanism of necroptosis-mediated TNF shedding

After the identification of TNF as unique alarmin released by necroptotic cells able to induce activation of recipient resting cells in our system, we tried to investigate the mechanisms involved in increased TNF secretion upon necroptosis. First, we wanted to assess whether the TNF detectable in the supernatant of necroptotic cells was the matured (shed) form or the TNF membrane precursor. To do so, we analyzed supernatant and lysate of LPS-treated CASP8$^{-/-}$ and CASP8$^{-/-}$ x RIPK3$^{-/mut}$ cells via immunoblot where we could detect increased levels of matured TNF in the supernatant of necroptotic cells compared to CASP8$^{-/-}$ x RIPK3$^{-/mut}$ cells control samples (Fig. 4.7A). To understand whether the increased amount of matured TNF in the supernatant reflected an increased upregulation of proTNF in CASP8$^{-/-}$ compared to CASP8$^{-/-}$ x RIPK3$^{-/mut}$ cells, we also analyzed the proTNF levels in lysates of these cells at different time points. While proTNF levels resulted similar in CASP8$^{-/-}$ and CASP8$^{-/-}$ x RIPK3$^{-/mut}$ cells at early time points (up to 5 h) with a considerable difference in mature TNF detected in the supernatant, at a later time point (8 h) proTNF levels resulted substantially different, with no proTNF detectable in CASP8$^{-/-}$ x RIPK3$^{-/mut}$ cells (Fig. 4.7A and B). These results made us consider that two processes are involved in increased TNF secretion by necroptotic cells: on one hand, post-transcriptional and/or post-translational modifications cause differences in the pool of membrane TNF molecules available for maturation in necroptotic and control cells. For example, it is conceivable that CASP8$^{-/-}$ x RIPK3$^{-/mut}$ cells negatively regulate proTNF production some hours after LPS-mediated NF-kB activation, while CASP8$^{-/-}$ necroptotic cells lose this ability and therefore continue the production of proTNF even if close to death or already dead. The idea that dead cells can still transcribe and translate special targets after loss of membrane integrity has already been addressed in the literature [202]. On the other hand, TNF shedding by membrane metalloproteases is enhanced upon necroptosis. The fact that ADAM proteins can be activated in the context of necroptosis was previously described, even if a specific role of TNF shedding in necroptosis-mediated inflammation was not addressed [203]. Indeed, we observed an involvement of the main TNF sheddase, ADAM17, in necroptosis-mediated TNF shedding in BLaER1 cells (Fig. 4.7D). In addition, this hypothesis was corroborated in a reconstituted model of TNF secretion upon necroptosis in HEK293T cells: in these settings, where TNF production is independent of NF-kB signaling and proTNF levels are comparable in MLKL1-201 expressing cells (necroptotic) and non-necroptotic controls, TNF shedding was strongly increased upon necroptosis and relied on ADAM17 and ADAM10 (Fig. 4.8).
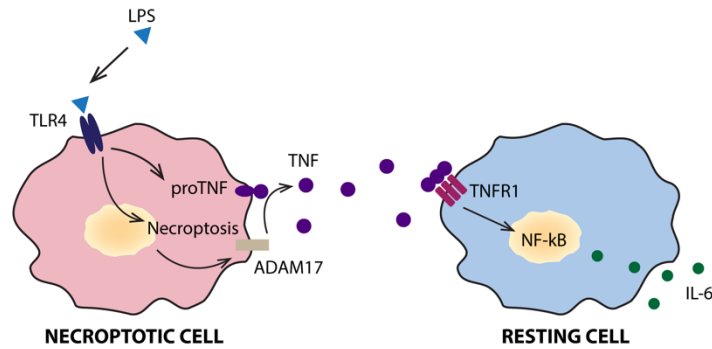
Fig. 5.1 Mechanism of necroptosis-induced inflammation in BLaER1 macrophages: upon LPS stimulation, CASP8^{-/-} cells undergo necroptosis and transcribe proTNF, which is then matured by hyperactivated ADAM17 into its mature form. Soluble TNF then induces NF-kB activation in recipient resting cells via TNFR1.

Further experiments by live-cell imaging using C-Tag TNF as shedding reporter revealed that necroptotic cells secrete TNF with a much faster rate than living cells, despite expressing the same amount of proTNF (Fig. 4.15). While living cells slowly became positive for C-Tag TNF over the period of observation, the C-Tag fluorescent signal of necroptotic cells was more intense and increased relatively rapidly and compared to living cells, until it reached a plateau. In our attempt to understand the mechanism of enhanced TNF shedding upon necroptosis, we focused our attention on ADAM17 biology. The first description of ADAM17 dates back to 1997 [102,103] and since then, research efforts have been concentrated on finding its targets and unravelling how its shedding activity is regulated. Although many different activating and inhibitory mechanisms have been described, at date the regulation of ADAM17 still remains hotly debated (see section 1.7). One of the most recently described activating processes is the interaction of the MPD domain of the enzyme with phosphatidylserine upon phosphatidylserine translocation to the outer leaflet of the cell membrane [109]. This interaction is believed to be mediated by electrostatic attraction of three positively charged amino acids in the MPD domain and the negatively charged head of phosphatidylserine. Since phosphatidylserine exposure massively occurs upon cell death, we investigated whether limiting phosphatidylserine availability for ADAM17 interaction upon necroptosis would impact on TNF shedding. To do so, we induced necroptosis in BLaER1 cells in the presence of Annexin V, which binds to phosphatidylserine competing with its binding to ADAM17. Although Annexin V bound to necroptotic cells, as judged by FACS analysis, it did not impact on TNF shedding, suggesting that ADAM17 interaction with phosphatidylserine is not essential for its activation under investigated conditions (Fig. 4.10). Moreover, when analyzing C-Tag TNF and Annexin V signals in live-cell imaging experiments, C-Tag positivity always preceded Annexin V positivity, even if the two events were strictly correlated in time (Fig. 4.16A and B). However, these data should be cautiously interpreted, since the delay of Annexin V signal could also be due to a lower sensitivity of the technique to this marker compared to C-Tag TNF. Another important mechanism by which ADAMs-mediated shedding is regulated is the mutual position of the enzyme and its target protein. Given the absence of a specific consensus sequence for ADAM-mediated cleavage of target proteins, we reasoned

that the respective position of the enzyme and its substrate is probably the most important player that determines whether the protease will cleave it or not. Since we could not detect translocation of either proTNF or ADAM17 to the cell membrane by live-cell imaging (data not shown), we would argue that perturbation of the cell membrane and its physical changes upon necroptotic cell death could influence the position of ADAM17 and TNF on the cell membrane, favoring their interaction or bringing ADAM17 in an advantageous position to perform its shedding activity. Apart from that, we could rule out that MLKL played a role in inducing shedding activity beyond its function to trigger membrane permeabilization. To this end, an MLKL variant that translocates to the membrane without killing the cells (MLKL D107A/E111A) does not enhance TNF shedding, suggesting that MLKL does not fulfill necroptosis-independent functions which promote ADAM proteases (Fig. 4.11A). To better address the role of morphological changes associated with cell death in ADAMs activation, we induced apoptosis and pyroptosis in BLaER1 macrophages and checked TNF release under these conditions. In both cases, we could not detect increased TNF shedding compared to control conditions, suggesting that necroptosis has a peculiar role in activating ADAM proteases on the cell membrane in BLaER1 cells (Fig. 4.9). These results are in line with previous findings that phosphatidylserine exposure seems not to impact on TNF shedding, since this event occurs both in apoptosis and pyroptosis [198]. However, induction of pyroptosis by overexpression of the N-terminus of Gasdermin D (GSDSM 1-275) or apoptosis in the heterologous HEK293T system revealed increased TNF shedding compared to control conditions both via ELISA analysis and live-cell imaging of C-Tag TNF (data not shown). These results lead to two considerations: on one hand, morphological changes occurring in BLaER1 macrophages upon distinct cell death types could differ from each other and from morphological features of dying HEK293T, leading to cell type and cell death specificity in influencing ADAM proteases activity. On the other hand, it should be considered that the combination of differences in the kinetics of cell death and in the levels of proTNF expression in BLaER1 and HEK293T cells could affect how TNF is processed by ADAM proteins. Contrary to necroptosis, which occurred with similar kinetics in both cell types (at 8 h LDH release was reaching maximal levels in both cases), pyroptosis was much faster in BLaER1 than in HEK293T. This was probably due to the different induction modalities used in the two cell lines: the overexpression of GSDMD 1-275 in HEK293T could in fact lead to similar kinetics observed for necroptosis induced by MLKL 1-201 expression. Altogether, we could show that necroptosis induces TNF maturation from the cell membrane by promoting the shedding activity of ADAM metalloproteases, and that this phenomenon is probably due to membrane perturbation specifically occurring upon this mechanism of cell death. However, further research is needed to clarify the exact mechanism by which necroptosis promotes the activation of ADAM metalloproteases.

5.4 Physiological relevance of necroptosis-induced TNF secretion

As discussed in the introduction (see section 1.6), TNF is a pro-inflammatory cytokine with multiple immunomodulatory functions. It plays a critical role in responses against pathogens and contributes to the regulation of cell death and survival, given its ability to induce different downstream outcomes, namely NF-kB and MAPK and two cell death types (apoptosis and necroptosis) in target cells. However, because of its highly inflammatory properties, it has a deleterious role in septic shock and alterations of its pathway have been implicated in the development of inflammation in both autoinflammatory and autoimmune diseases [92]. For these reasons, anti-TNF therapies have been developed to ameliorate symptoms in the context of the above-mentioned pathological conditions [204]. Anti-TNF drugs, such as infliximab and adalimumab, or anti-TNFR1 agents, such as etanercept, are used for the treatment of autoimmune diseases such as rheumatoid arthritis, psoriasis, but also autoinflammatory diseases as TRAPS (Tumor necrosis factor receptor associated periodic syndrome) and inflammatory bowel diseases, as Chron´s disease. The reason of excessive TNF secretion (and in general of excessive cytokine secretion) in these pathological conditions is described to be the aberrant activation of pathways involved in adaptive (in case of autoimmune diseases) or innate (in case of inflammatory diseases) immune responses. In this regard, it should be considered that cell death, in particular forms of regulated necrosis, is often related to activation of immune pathways. Pyroptosis is induced downstream of inflammasome activation upon recognition of a great variety of PAMPs and DAMPs, and necroptosis can be induced by very classical PAMPs or immune stimuli, such as nucleic acids, LPS and TNF (see section 1.8.2). Therefore, it should not surprise that these forms of cell death can not only have a role in generating a productive response against pathogens, but also be implied in the development or exacerbation of inflammatory pathologies. If a role of pyroptosis in inflammasome-related pathologies can easily be assumed, especially for its importance in the release of a potent inflammatory cytokine as IL-1β, the contribution of necroptosis to the clinical conditions of inflammatory pathologies is still elusive. As discussed in section 1.8.2, there are some evidences both *in vivo* and in tissues from patients with inflammatory diseases such as Chron´s disease, that suggest a role of necroptosis in development or exacerbation of these diseases. However, although the release of DAMPs has been addressed as the main cause of necroptosis-driven inflammation, little is known about the inflammatory signals directly induced downstream of necroptotic cell death. In this study we provide evidences of a connection between two described causes of inflammation, namely TNF release and necroptosis. In particular, we observed that in addition to the common knowledge that TNF is upstream of necroptosis and can induce it by activation of TNFR1, TNF maturation is promoted downstream of necroptosis, in a sort of vicious circle. Similar to proteolytic maturation of IL-1β by Caspase-1 in pyroptotic cells, proTNF is matured to its soluble form by ADAM metalloproteases upon necroptosis. However, IL-1β maturation requires pyroptosis to occur (even if secretion of mature IL-1β by living cells has also been described [205]), while proTNF maturation is substantially increased but not strictly dependent

on necroptosis. Nevertheless, *in vivo* studies are required to assess the inflammatory role of TNF in the context of necroptosis-mediated inflammation. Our preliminary *in vitro* experiments in J774 macrophages and HSCs (Fig. 4.13) not only demonstrate that TNF secretion is increased upon necroptosis also in murine cells, but also provide the basis for a future *in vivo* study on this topic. In particular, taking advantage of the RIPK3-2xFv T2A EGFP construct and of the relatively high efficiency of HSCs transduction, we plan to generate RIPK3-2xFv T2A EGFP expressing HSCs in a WT or TNF KO genetic background to perform bone marrow reconstitution in lethally irradiated WT recipient mice. With this strategy, we will be able to induce necroptosis in the bone marrow of these mice by treatment with the B/B homodimerizer and to monitor the differences in inflammatory outcomes in mice reconstituted with WT or TNF KO necroptosis-prone HSCs. Proving the role of TNF secretion by necroptotic cells in influencing the inflammatory outcome of these mice would provide a rationale for the use of anti-TNF therapies in the context of pathologies where necroptosis has been implicated. In addition, the success of anti-TNF therapy in particular pathologies could be partially explained by a hidden role of unregulated necroptosis in these patients.

5.5 C-Tag TNF as a reporter for ADAM metalloproteases shedding

Because of our finding that necroptosis induces ADAMs-mediated TNF maturation, we focused the rest of our study on understanding the mechanism of activation of these enzymes in necroptotic cells. In particular, we were interested in the relation between TNF shedding, necroptosis-related morphological changes and actual cell death, to understand if TNF secretion occurs in early or late necroptosis, if it is a fast or slow event and if it is likely to be actively regulated. In fact, we thought that focusing our attention on these events rather than already known regulatory mechanisms of ADAM proteins (such as trafficking or phosphorylation) would help us understanding in which terms TNF shedding in necroptotic cells differs from the same event occurring in living cells. To answer these questions, we generated a reporter for ADAM17 and ADAM10-mediated shedding by engineering the TNF sequence with a tag of 4 amino acids, named C-Tag, which immediately precedes the ADAM17 cleavage site (Fig. 4.14A). The modified TNF could be cleaved in an ADAM17 and ADAM10 specific manner in HEK293T cells and shedding efficiency was comparable to what observed for WT TNF in both living and necroptotic cells (Fig. 4.14D). The generation of such a reporter opened the possibility to study the dynamics of TNF shedding by live-cell imaging, a technique that allowed us to observe this specific event in relation to morphological changes of the cells and to other markers of cell death, such as Annexin V and PI positivity. In particular, we could observe that TNF shedding occurs in the early stage of necroptosis in a relatively fast process if compared to TNF maturation in living cells (Fig. 4.15 A-D). Moreover, TNF shedding coincides with the observation of the morphological changes in early necroptosis and precedes both Annexin V positivity, which occurs only few minutes after, and PI positivity, which is a quite late event (Fig. 4.16A and B). In addition, by analyzing the slopes of fluorescent signals of C-Tag, Annexin V and PI, we could observe that the slope of PI fluorescence is steeper than the first two, in line with the fact that is a passive event which occurs within

seconds (Fig. 4.16C). Unlike PI, C-Tag and Annexin V slopes are less steep, probably because they are both active processes which require the activity of enzymes in order to occur. These observations indicate that TNF shedding occurs in the early stage of necroptosis as an active event, which is probably induced by a concomitant biological process, such as alteration of cell membrane dynamics.

Proteolytic cleavage is one of the most frequent post-translational modifications, with about 10% of the membrane proteins being processed by proteases [206]. As such, this process is important in many biological functions and, given its irreversibility, it needs to be tightly regulated. As already discussed above (see section 1.7), ADAM proteases can cleave a vast number of substrates, among which adhesion molecules, cytokines and cytokine receptors, grow factors and others, thereby being implicated in the proper development of different tissues and in the correct function of immune system, nervous system and other organs. The decisive role that they play in activating and inhibiting substrates by proteolytic cleavage also implies them in pathological conditions such as cancer, cardiovascular and inflammatory diseases [206]. Understanding their mode of activation and their regulation is therefore important for multiple human pathologies. At present, the study of the activation of ADAM proteins is mainly based on the end-point analysis of the proteolytic products of their substrates. This is mainly achieved by western blots analysis of ADAMs target proteins to detect their cleaved and precursor forms or by ELISA to quantify the matured form of a substrate in the supernatant upon certain experimental conditions. In addition, alkaline phosphatase (AP) reporters have been described, where the AP is fused to the extracellular domain of a substrate of interest and, upon cleavage by ADAMs, is released in the cell supernatant, where the activity of the enzyme can be detected by addition of colorimetric or fluorogenic AP substrates [207]. Another approach makes use of a fluorogenic peptide as substrate of specific ADAMs: a quencher added to one terminus of the peptide inhibits the fluorescence of a fluorophore added to the other extremity of the peptide, until the peptide is cleaved by the enzyme, leading to a detectable fluorescent signal [208]. This approach detects not only the shedding prone status of the enzyme (described as a status in which the enzyme is not only active, but also in the correct position to cleave its substrates), but any kind of activated form of the enzyme, making it more or less useful depending on specific experimental needs. In the field of Alzheimer´s disease, where the proteolytic cleavage of APP (Amyloid precursor protein) by membrane α- and β-secretases is an essential marker to investigate the events that lead to the formation of amyloid plaques, similar approaches have been exploited. A reporter consisting of the APP protein fused to AP in its extracellular region and a split Gaussia Luciferase in its cytosolic domain consented a combined analysis of matured APP secretion in the supernatant by AP assay and a luciferase assay to detect the interaction between APP and the β-secretase BACE I, where the second split of the Gaussia Luciferase is added: the close proximity of the BACE I and its target APP leads to complementation of the Gaussia Luciferase and to a luminescence signal that can be detected upon addition of a Gaussia Luciferase substrate, also in living cells, consenting a time course analysis of the same sample [209]. FRET-based techniques have also been developed in

combination with fluorescence microscopy to study the interaction between BACE I and APP in living cells [210,211]. However, none of the above-mentioned reporters or techniques allow the real time detection and visualization of shedding of a specific substrate by the respective protease in living cells. Western blotting, ELISA techniques and AP assays are used in end-point experiments which only allow the determination (direct or indirect) of the amount of cleaved product. The complementation assay with the split luciferase enables, in addition, the detection of interactions between the protease and the substrate. The combination of FRET sensors and fluorescence microscopy contribute to the visualization of such interactions, but not to the detection of the shedding process itself. The C-Tag reporter generated in this study has the great advantage of allowing the visualization of the shedding event real-time in living cells. In addition, it allows detection by standard techniques, such as western blots and ELISA, and it can potentially be employed in measuring shedding events by flow cytometry. Another advantage compared to previously discussed reporters is that it requires a minimal genetic manipulation of the system: while AP assays, luciferase assays and FRET methods rely on the generation of fusion proteins for either the substrate or both the substrate and the protease, increasing the risk of interfering with the natural protein functions and interactions, the C-Tag reporter consists of only 4 amino acids to be introduced before the cleavage site in the substrate to be analyzed. For this reason, however, the compatibility of the C-Tag introduction within the cleavage site of the substrate and the processing by the respective protease needs to be verified at first. The C-Tag reporter system can potentially be transferred to any couple of protease and substrate where its introduction does not destroy the cleavage site and where the protease leaves a free C-terminus on its substrate after cleavage. This reporter can be used to study the regulation of ADAM17 and ADAM10 in different contexts by expressing the C-Tag TNF construct in investigated cells and is most probably compatible to other type II transmembrane substrates of these enzymes. Moreover, its employment in the study of BACE I biology, important for new advances in Alzheimer´s disease research, should be investigated: even though APP is not a compatible substrate because it leaves a free N-terminus after cleavage by BACE I, other BACE I substrates, such as the type II transmembrane protein ST6Gal1 [212], could be considered for the generation of a C-Tag reporter for BACE I-mediated shedding. In summary, our work contributed not only to characterize necroptosis-induced inflammation, with the discovery of TNF as alarmin secreted by necroptotic cells, but it also gave a technical contribution to improve the research on ADAM proteases and, potentially, on proteases in general by the generation of the C-Tag reporter for real time studies of proteases-mediated cleavage events.

6. Summary

Necroptosis is a form of regulated necrosis that can be initiated by different receptors, among which death receptors, such as TNFR1 and Fas, and Toll-like receptors TLR3 and TLR4. These pathways lead to downstream activation of the kinase RIPK3 which mediates MLKL phosphorylation, followed by its oligomerization and recruitment to the cell membrane, where it causes mechanical perturbations and, as a consequence, cell disintegration and cytosolic content release. Previous studies suggest that necroptosis is not immunologically silent and that it induces inflammation in resting cells as a result of the secretion of endogenous molecules that trigger inflammation in bystander cells. By definition, these molecules should either be Danger Associated Molecular Patterns (DAMPs) or alarmins. However, very little is known about the identity of such inflammatory molecules and their role in necroptosis-mediated inflammation. Here, we made use of BLaER1 macrophages to establish an *in vitro* system which allows for supernatant transfer and co-culture studies between necroptotic (CASP8$^{-/-}$) or necroptosis-resistant cells (CASP8$^{-/-}$ x RIPK3$^{-/-}$ or CASP8$^{-/-}$ x MLKL$^{-/-}$) and resting cells. These experiments confirmed a pro-inflammatory role of necroptosis, as judged by the ability of necroptotic supernatant to induce IL-6 secretion and NF-kB activation in resting cells. Further experiments involving heath shock and size exclusion chromatography on necroptotic supernatant revealed that the pro-inflammatory molecule responsible for IL-6 secretion in recipient cells has a proteinaceous nature. By systematic deletion of specific immune receptors in recipient cells, we showed that TNFR1 is responsible for downstream IL-6 production. Moreover, we could demonstrate that necroptotic cells secrete more TNF compared to control cells and that the TNF-TNFR1 axis is responsible for necroptosis-mediated inflammation in our system. In addition, studies in BLaER1 and HEK293T cells revealed that necroptosis promotes TNF maturation (shedding) by membrane metalloproteases, namely ADAM17 (in BLaER1 macrophages) and both ADAM17 and ADAM10 in HEK293T cells. Increased TNF shedding was necroptosis-specific and did not occur in pyroptotic or apoptotic BLaER1 macrophages. We performed preliminary experiments in murine hematopoietic stem cells (HSCs) transduced with the necroptosis-inducing construct RIPK3-2xFv and proved that increased TNF secretion also occurs in necroptotic murine cells, thereby allowing future *in vivo* experiments to prove the physiological role of necroptosis-induced TNF shedding. To study the mechanism of increased TNF shedding we generated a reporter that allowed for real time observation of TNF maturation by metalloproteases by live-cell imaging (C-Tag TNF). These experiments showed that TNF shedding occurs with a faster kinetic in necroptotic cells compared to control living cells and that it precedes actual cell death, as judged by morphological changes and Annexin V and PI positivity of investigated cells. Taken together, our work not only describes a novel necroptosis-associated alarmin, which can impact on the treatment of inflammatory pathologies where necroptosis could be involved, but also provides a new tool to study the shedding process by membrane metalloproteases real time in living cells.

7. Bibliography

1. Abbas, A. K., Lichtman, A. H. & Pillai, S. *Cellular and Molecular Immunology - 7th Edition*. (2011).

2. Hoffman, W., Lakkis, F. G. & Chalasani, G. B Cells, Antibodies, and More. *Clin. J. Am. Soc. Nephrol.* **11**, 137–154 (2016).

3. Alcover, A., Alarcón, B. & Di Bartolo, V. Cell Biology of T Cell Receptor Expression and Regulation. *Annu. Rev. Immunol.* **36**, 103–125 (2018).

4. Kumar, B. V., Connors, T. J. & Farber, D. L. Human T Cell Development, Localization, and Function throughout Life. *Immunity* **48**, 202–213 (2018).

5. Banchereau, J. *et al.* Immunobiology of Dendritic Cells. *Annu. Rev. Immunol.* **18**, 767–811 (2000).

6. Doria, A. *et al.* Autoinflammation and autoimmunity: Bridging the divide. *Autoimmun. Rev.* **12**, 22–30 (2012).

7. Brogden, K. A. Antimicrobial peptides: Pore formers or metabolic inhibitors in bacteria? *Nat. Rev. Microbiol.* **3**, 238–250 (2005).

8. Bottazzi, B., Doni, A., Garlanda, C. & Mantovani, A. An Integrated View of Humoral Innate Immunity: Pentraxins as a Paradigm. *Annu. Rev. Immunol.* **28**, 157–183 (2010).

9. Dunkelberger, J. R. & Song, W. C. Complement and its role in innate and adaptive immune responses. *Cell Res.* **20**, 34–50 (2010).

10. Flannagan, R. S., Jaumouillé, V. & Grinstein, S. The Cell Biology of Phagocytosis. *Annu. Rev. Pathol. Mech. Dis.* **7**, 61–98 (2012).

11. Flannagan, R. S., Cosío, G. & Grinstein, S. Antimicrobial mechanisms of phagocytes and bacterial evasion strategies. *Nat. Rev. Microbiol.* **7**, 355–366 (2009).

12. Morizot, A. & Saleh, M. Non-apoptotic functions of cell death effectors in inflammation and innate immunity. *Microbes and Infection* (2012). doi:10.1016/j.micinf.2012.06.005

13. Mandal, A. & Viswanathan, C. Natural killer cells: In health and disease. *Hematol. Oncol. Stem Cell Ther.* **8**, 47–55 (2015).

14. Yan, N. & Chen, Z. J. Intrinsic antiviral immunity. *Nat. Immunol.* **13**, 214–222 (2012).

15. Kawai, T. role of pattern-recognition receptors in innate immunity: U. on toll-like receptors & Akira, S. The role of pattern-recognition receptors in innate immunity: Update on toll-like receptors. *Nat. Immunol.* **11**, 373–384 (2010).

16. Marakalala, M. J. & Ndlovu, H. Signaling C-type lectin receptors in antimycobacterial immunity. *PLoS Pathog.* **13**, 1–8 (2017).

17. KawasakiToll-like receptor signaling pathways, T. & Kawai, T. Toll-like receptor signaling pathways. *Front. Immunol.* **5**, 1–8 (2014).

18. Tobias, P. S. *et al.* Cross-linking of lipopolysaccharide (LPS) to CD14 on THP-1 cells mediated by LPS-binding protein. *J. Immunol.* **150**, 3011–3021 (1993).

19. Song Jiang*, Xinyan Li*, Nicholas J. Hess*, Yue Guan*, and R. I. T. TLR10 is a Negative Regulator of Both MyD88-Dependent and Independent TLR Signaling. *Physiol. Behav.* **176**, 139–148 (2017).

20. Motshwene, P. G. *et al.* An Oligomeric Signaling Platform formed by the toll-like receptor signal transducers MyD88 and IRAK-4. *J. Biol. Chem.* **284**, 25404–25411 (2009).

21. Lin, S.-C., Lo, Y.-C. & Wu, H. Helical assembly in the MyD88–IRAK4–IRAK2 complex in TLR/IL-1R signalling. *Nature* **465**, 885–890 (2010).

22. Liu, T., Zhang, L., Joo, D. & Sun, S. C. NF-κB signaling in inflammation. *Signal Transduct. Target. Ther.* **2**, (2017).

23. Hess, J., Angel, P. & Schorpp-Kistner, M. AP-1 subunits: Quarrel and harmony among siblings. *J. Cell Sci.* **117**, 5965–5973 (2004).

24. Cusson-Hermance, N., Khurana, S., Lee, T. H., Fitzgerald, K. A. & Kelliher, M. A. Rip1 mediates the trif-dependent Toll-like receptor 3- and 4-induced NF-κB activation but does not contribute to interferon regulatory factor 3 activation. *J. Biol. Chem.* **280**, 36560–36566 (2005).

25. Uematsu, S. & Akira, S. Toll-like receptors and type I Interferons. *J. Biol. Chem.* **282**, 15319–15324 (2007).

26. Loo, Y. M. & Gale, M. Immune Signaling by RIG-I-like Receptors. *Immunity* **34**, 680–692 (2011).

27. Ablasser, A. *et al.* CGAS produces a 2'-5'-linked cyclic dinucleotide second messenger that activates STING. *Nature* **498**, 380–384 (2013).

28. Hornung, V., Hartmann, R., Ablasser, A. & Hopfner, K. P. OAS proteins and cGAS: Unifying concepts in sensing and responding to cytosolic nucleic acids. *Nat. Rev. Immunol.* **14**, 521–528 (2014).

29. Unterholzner, L. *et al.* IFI16 is an innate immune sensor for intracellular DNA. *Nat. Immunol.* **11**, 997–1004 (2010).

30. Hornung, V. *et al.* AIM2 recognizes cytosolic dsDNA and forms a caspase-1 activating inflammasome with ASC. **458**, 514–518 (2009).

31. Kim, Y. K., Shin, J. S. & Nahm, M. H. NOD-like receptors in infection, immunity, and diseases. *Yonsei Med. J.* **57**, 5–14 (2016).

32. Dinarello, C. A. Overview of the IL-1 family in innate inflammation and acquired immunity. *Immunol. Rev.* **281**, 8–27 (2018).

33. Maelfait, J. *et al.* Stimulation of Toll-like receptor 3 and 4 induces interleukin-1β maturation by caspase-8. *J. Exp. Med.* **205**, 1967–1973 (2008).

34. Murakami, M. *et al.* IL-6-induced homodimerization of gp130 and associated activation of a tyrosine kinase. *Science (80-.).* **260**, 1808–1810 (1993).

35. Tanaka, T., Narazaki, M. & Kishimoto, T. IL-6 in Inflammation, Immunity, and Disease.

6, 1–16 (2014).

36. Tsai, M. H., Pai, L. M. & Lee, C. K. Fine-tuning of type I interferon response by STAT3. *Front. Immunol.* **10**, 1–10 (2019).

37. Shouval, D. S. *et al.* Interleukin 10 Receptor Signaling. 177–210 (2014). doi:10.1016/b978-0-12-800267-4.00005-5

38. Vénéreau, E., Ceriotti, C. & Bianchi, M. E. DAMPs from cell death to new life. *Front. Immunol.* **6**, 1–11 (2015).

39. Matzinger, P. TOLERANCE , DANGER , DANGER , AND AND THE THE EXTENDED FAMILY. *Annu. Rev.lmmunol* **12**, 991–1045 (1994).

40. Land, W. Allograft injury mediated by reactive oxygen species: From conserved proteins of drosophila to acute and chronic rejection of human transplants. Part III: Interaction of (oxidative) stress-induced heat shock proteins with toll-like receptor-bearing cells . *Transplant. Rev.* **17**, 67–86 (2003).

41. Pradeu, T. & Cooper, E. L. The danger theory: 20 years later. *Front. Immunol.* **3**, 1–9 (2012).

42. Rajamuthiah, R. & Mylonakis, E. Effector triggered immunity activation of innate immunity in metazoans by bacterial effectors. *Virulence* **5**, 697–702 (2014).

43. Miller, Y. I. *et al.* Oxidation-specific epitopes are danger-associated molecular patterns recognized by pattern recognition receptors of innate immunity. *Circ. Res.* **108**, 235–248 (2011).

44. Itagaki, K. & Hauser, C. J. Circulating Mitochondrial DAMPs Cause Inflammatory Responses to Injury. *Nature* **464**, 104–107 (2010).

45. Kono, H. & Rock, K. L. How dying cells alert the immune system to danger. *Nat. Rev. Immunol.* **8**, 279–289 (2008).

46. Scaffidi, P., Misteli, T. & Bianchi, M. E. Release of chromatin protein HMGB1 by necrotic cells triggers inflammation (Nature (2002) 418 (191-195)). *Nature* **418**, (2002).

47. Park, J. S. *et al.* Involvement of Toll-like Receptors 2 and 4 in Cellular Activation by High Mobility Group Box 1 Protein. *J. Biol. Chem.* **279**, 7370–7377 (2004).

48. Mariathasan, S. *et al.* Cryopyrin activates the inflammasome in response to toxins and ATP. *Nature* **440**, 228–232 (2006).

49. Vabulas, R. M. *et al.* Endocytosed HSP60s Use Toll-like Receptor 2 (TLR2) and TLR4 to Activate the Toll/Interleukin-1 Receptor Signaling Pathway in Innate Immune Cells. *J. Biol. Chem.* **276**, 31332–31339 (2001).

50. Shi Du Yan, Xi Chen, Jin Fu, Ming Chen, Huaijie Zhu, Alex Roher*, Timothy Slatteryt, Lei Zhaot, Mariko Nagashimat, John Morsert, Antonio Migheli:j:, Peter Nawroth§, D. S. & A. M. S. RAGE and amyloid-P peptide neurotoxicity in Alzheimer's disease. **382**, (1996).

51. Duewell, P. *et al.* NLRP3 inflammasomes are required for atherogenesis and activated by cholesterol crystals. *Nature* **464**, 1357–1361 (2010).

52. Hofmann, M. A. *et al.* RAGE Mediates a Novel Proinflammatory Axis: A Central Cell Surface Receptor for S100/Calgranulin Polypeptides. *Cell* **97**, 889–901 (1999).

53. Kaczmarek, A., Vandenabeele, P. & Krysko, D. V. Necroptosis: The Release of Damage-Associated Molecular Patterns and Its Physiological Relevance. *Immunity* **38**, 209–223 (2013).

54. Martinon, F., Pétrilli, V., Mayor, A., Tardivel, A. & Tschopp, J. Gout-associated uric acid crystals activate the NALP3 inflammasome. *Nature* **440**, 237–241 (2006).

55. Pasparakis, M. & Vandenabeele, P. Necroptosis and its role in inflammation. *Nature* **517**, 311–320 (2015).

56. Rock, Kenneth L; Kono, H. The Inflammatory Response to Cell Death. *Annu. Rev. Pathol. Dis.* **3**, 67–97 (2008).

57. Roh, J. S. & Sohn, D. H. Damage-associated molecular patterns in inflammatory diseases. *Immune Netw.* **18**, 1–14 (2018).

58. Kokkola, R. *et al.* Successful treatment of collagen-induced arthritis in mice and rats by targeting extracellular high mobility group box chromosomal protein 1 activity. *Arthritis Rheum.* **48**, 2052–2058 (2003).

59. Hendriks, L. E. L. & Dingemans, A. M. C. Heat shock protein antagonists in early stage clinical trials for NSCLC. *Expert Opin. Investig. Drugs* **26**, 541–550 (2017).

60. Aggarwal, B. B., Gupta, S. C. & Kim, J. H. Historical perspectives on tumor necrosis factor and its superfamily: 25 years later, a golden journey. *Blood* **119**, 651–665 (2012).

61. Šedý, J., Bekiaris, V. & Ware, C. F. Tumor necrosis factor superfamily in innate immunity and inflammation. *Cold Spring Harb. Perspect. Biol.* **7**, (2015).

62. Ward-Kavanagh, L. K., Lin, W. W., Šedý, J. R. & Ware, C. F. The TNF Receptor Superfamily in Co-stimulating and Co-inhibitory Responses. *Immunity* **44**, 1005–1019 (2016).

63. Schneider, K., Potter, K. G. & Ware, C. F. Lymphotoxin and LIGHT signaling pathways and target genes. *Immunol. Rev.* **202**, 49–66 (2004).

64. Upadhyay, V. & Fu, Y. X. Lymphotoxin signalling in immune homeostasis and the control of microorganisms. *Nat. Rev. Immunol.* **13**, 270–279 (2013).

65. Grivennikov, S. I. *et al.* Distinct and nonredundant in vivo functions of TNF produced by T cells and macrophages/neutrophils: Protective and deleterious effects. *Immunity* **22**, 93–104 (2005).

66. Holbrook, J., Lara-Reyna, S., Jarosz-Griffiths, H. & McDermott, M. Tumour necrosis factor signalling in health and disease. *F1000Research* **8**, 1–12 (2019).

67. Marino, M. W. *et al.* Characterization of tumor necrosis factor-deficient mice. *Proc. Natl. Acad. Sci. U. S. A.* **94**, 8093–8098 (1997).

68. Jeong, D.-G., Seo, J.-H., Heo, S.-H., Choi, Y.-K. & Jeong, E.-S. Tumor necrosis factor-alpha deficiency impairs host defense against Streptococcus pneumoniae . *Lab. Anim. Res.* **31**, 78 (2015).

69.	Carpentier, I., Coornaert, B. & Beyaert, R. Function and Regulation of Tumor Necrosis Factor Receptor Type 2. *Curr. Med. Chem.* **11**, 2205–2212 (2004).

70.	Marsters, S. A., Frutkin, A. D., Simpson, N. J., Fendly, B. M. & Ashkenazi, A. Identification of cysteine-rich domains of the type 1 tumor necrosis factor receptor involved in ligand binding. *J. Biol. Chem.* **267**, 5747–5750 (1992).

71.	Hsu, H., Xiong, J. & Goeddel, D. V. The TNF receptor 1-associated protein TRADD signals cell death and NF-κB activation. *Cell* **81**, 495–504 (1995).

72.	Haas, T. L. *et al.* Recruitment of the Linear Ubiquitin Chain Assembly Complex Stabilizes the TNF-R1 Signaling Complex and Is Required for TNF-Mediated Gene Induction. *Mol. Cell* **36**, 831–844 (2009).

73.	Varfolomeev, E. *et al.* c-IAP1 and c-IAP2 are critical mediators of tumor necrosis factor α (TNFα)-induced NF-κB activation. *J. Biol. Chem.* **283**, 24295–24299 (2008).

74.	Tada, K. *et al.* Critical Roles of TRAF2 and TRAF5 in Tumor Necrosis Factor-induced NF-κB Activation and Protection from Cell Death. *J. Biol. Chem.* **276**, 36530–36534 (2001).

75.	Kanayama, A. *et al.* TAB2 and TAB3 activate the NF-κB pathway through binding to polyubiquitin chains. *Mol. Cell* **15**, 535–548 (2004).

76.	Wang, C. *et al.* TAK1 is a ubiquitin-dependent kinase of MKK and IKK. *Nature* **412**, 346–351 (2001).

77.	Ea, C. K., Deng, L., Xia, Z. P., Pineda, G. & Chen, Z. J. Activation of IKK by TNFα Requires Site-Specific Ubiquitination of RIP1 and Polyubiquitin Binding by NEMO. *Mol. Cell* **22**, 245–257 (2006).

78.	Beg, A. A. & Baltimore, D. An Essential Role for NF-κB in Preventing TNF-α-Induced Cell Death. **274**, 782–785 (1996).

79.	Tsuchiya, Y., Nakabayashi, O. & Nakano, H. FLIP the switch: Regulation of apoptosis and necroptosis by cFLIP. *Int. J. Mol. Sci.* **16**, 30321–30341 (2015).

80.	Kovalenko, A. *et al.* The tumour suppressor CYLD negatively regulates NF-kB signalling by deubiquitination. *Nature* 801–805 (2003). doi:10.1038/nature01811.1.

81.	Brenner, D., Blaser, H. & Mak, T. W. Regulation of tumour necrosis factor signalling: Live or let die. *Nat. Rev. Immunol.* **15**, 362–374 (2015).

82.	Chan, F. K.-M., Luz, N. F. & Moriwaki, K. Programmed Necrosis in the Cross Talk of Cell Death and Inflammation. *Annu. Rev. Immunol.* 1–28 (2014). doi:10.1146/annurev-immunol-032414-112248

83.	Rothe, M., Sarma, V., Dixit, V. M. & Goeddel, D. V. TRAF2-mediated activation of NF-κB by TNF receptor 2 and CD40. *Science (80-.).* **269**, 1424–1427 (1995).

84.	Rauert, H. *et al.* Membrane Tumor Necrosis Factor (TNF) induces p100 processing via TNF receptor-2 (TNFR2). *J. Biol. Chem.* **285**, 7394–7404 (2010).

85.	Eissner, G. *et al.* Reverse Signaling Through Transmembrane TNF Confers Resistance to Lipopolysaccharide in Human Monocytes and Macrophages. *J. Immunol.* **164**, 6193–

6198 (2000).

86. Eissner, G., Kolch, W. & Scheurich, P. Ligands working as receptors: Reverse signaling by members of the TNF superfamily enhance the plasticity of the immune system. *Cytokine Growth Factor Rev.* **15**, 353–366 (2004).

87. Friedmann, E. *et al.* SPPL2a and SPPL2b promote intramembrane proteolysis of TNFα in activated dendritic cells to trigger IL-12 production. *Nat. Cell Biol.* **8**, 843–848 (2006).

88. Fluhrer, R. *et al.* A γ-secretase-like intramembrane cleavage of TNFα by the GxGD aspartyl protease SPPL2b. *Nat. Cell Biol.* **8**, 894–896 (2006).

89. Harashima, S. *et al.* Outside-to-Inside Signal Through the Membrane TNF-α Induces E-Selectin (CD62E) Expression on Activated Human CD4 + T Cells . *J. Immunol.* **166**, 130–136 (2001).

90. Carswell, E. A. *et al.* An endotoxin induced serum factor that cuases necrosis of tumors. *Proc. Natl. Acad. Sci. U. S. A.* **72**, 3666–3670 (1975).

91. Monaco, C., Nanchahal, J., Taylor, P. & Feldmann, M. Anti-TNF therapy: Past, present and future. *Int. Immunol.* **27**, 55–62 (2015).

92. Aggarwal, B. B., Gupta, S. C. & Kim, J. H. Historical perspectives on tumor necrosis factor and its superfamily : 25 years later , a golden journey. *Blood* **119**, 651–666 (2012).

93. Wolfsberg, T. G., Primakoff, P., Myles, D. G. & White, J. M. ADAM, a novel family of membrane proteins containing A Disintegrin And Metalloprotease domain: Multipotential functions in cell-cell and cell- matrix interactions. *J. Cell Biol.* **131**, 275–278 (1995).

94. Huxley-Jones, J. *et al.* The evolution of the vertebrate metzincins; Insights from Ciona intestinalis and Danio rerio. *BMC Evol. Biol.* **7**, 1–20 (2007).

95. Edwards, D. R., Handsley, M. M. & Pennington, C. J. The ADAM metalloproteinases. *Mol. Aspects Med.* **29**, 258–289 (2009).

96. Grötzinger, J., Lorenzen, I. & Düsterhöft, S. Molecular insights into the multilayered regulation of ADAM17: The role of the extracellular region. *Biochim. Biophys. Acta - Mol. Cell Res.* **1864**, 2088–2095 (2017).

97. Maskos, K. *et al.* Crystal structure of the catalytic domain of human tumor necrosis factor-α-converting enzyme. *Proc. Natl. Acad. Sci. U. S. A.* **95**, 3408–3412 (1998).

98. Düsterhöft, S. *et al.* Membrane-proximal domain of a disintegrin and metalloprotease-17 represents the putative molecular switch of its shedding activity operated by protein-disulfide isomerase. *J. Am. Chem. Soc.* **135**, 5776–5781 (2013).

99. Düsterhöft, S. *et al.* Extracellular Juxtamembrane Segment of ADAM17 Interacts with Membranes and Is Essential for Its Shedding Activity. *Biochemistry* **54**, 5791–5801 (2015).

100. Lambrecht, B. N., Vanderkerken, M. & Hammad, H. The emerging role of ADAM metalloproteinases in immunity. *Nat. Rev. Immunol.* **18**, 745–758 (2018).

101. Heng, T. S. P., Painter, M. W. & The Immunological genome project consortium. The Immunological Genome Project : networks of gene expression in immune cells. **9**, 1091–1094 (2008).

102. Black, R. A. *et al.* A metalloproteinase disintegrin that releases tumour-necrosis factor-Ø from cells. *Nature* **385**, 729–733 (1997).

103. Moss, M. L. *et al.* Cloning of a disintegrin metalloproteinase that processes precursor tumour-necrosis factor-α. *Nature* **386**, 738 (1997).

104. Wisniewska, M. *et al.* Structural Determinants of the ADAM Inhibition by TIMP-3: Crystal Structure of the TACE-N-TIMP-3 Complex. *J. Mol. Biol.* **381**, 1307–1319 (2008).

105. Elena Dıaz-Rodrıguez, Juan Carlos Montero, Azucena Esparıs-Ogando, Laura Yuste, and A. P. Extracellular Signal-regulated Kinase Phosphorylates Tumor Necrosis Factor a-converting Enzyme at Threonine 735: A Potential Role in Regulated Shedding. *Mol. Biol. Cell* **13**, 2170–2179 (2002).

106. Schwarz, J. *et al.* Polo-like kinase 2, a novel ADAM17 signaling component, regulates tumor necrosis factor α ectodomain shedding. *J. Biol. Chem.* **289**, 3080–3093 (2014).

107. Gooz, P. *et al.* A disintegrin and metalloenzyme (ADAM) 17 activation is regulated by α5β1 integrin in kidney mesangial cells. *PLoS One* **7**, 1–9 (2012).

108. Tellier, E. *et al.* The shedding activity of ADAM17 is sequestered in lipid rafts. *Exp. Cell Res.* **312**, 3969–3980 (2006).

109. Sommer, A. *et al.* Phosphatidylserine exposure is required for ADAM17 sheddase function. *Nat. Commun.* **7**, (2016).

110. Mcilwain, D. R. *et al.* iRhom2 Regulation of TACE Controls TNF-Mediated Protection Against Listeria and Responses to LPS. *Science (80-.).* **335**, 229–232 (2012).

111. Adrain, C., Zettl, M., Christova, Y., Taylor, N. & Freeman, M. Tumor necrosis factor signaling requires iRhom2 to promote trafficking and activation of TACE. *Science (80-.).* **335**, 225–228 (2012).

112. Cavadas, M. *et al.* Phosphorylation of iRhom2 Controls Stimulated Proteolytic Shedding by the Metalloprotease ADAM17/TACE. *Cell Rep.* **21**, 745–757 (2017).

113. Oikonomidi, I. *et al.* ITap, a novel irhom interactor, controls TNF secretion by policing the stability of iRhom/TACE. *Elife* **7**, 1–35 (2018).

114. Künzel, U. *et al.* FRMD8 promotes inflammatory and growth factor signalling by stabilising the iRhom/ADAM17 sheddase complex. *Elife* **7**, 1–33 (2018).

115. D'Arcy, M. S. Cell death: a review of the major forms of apoptosis, necrosis and autophagy. *Cell Biol. Int.* **43**, 582–592 (2019).

116. Lockshin, R. A. & Williams, C. M. Programmed cell death-II. Endocrine potentiation of the breakdown of the intersegmental muscles of silkmoths. *J. Insect Physiol.* **10**, 643–649 (1964).

117. Kerr, J. F. ., Wyllie, S. & Currie, A. . Apoptosis: A basic biological phenomenon with wide-

ranging implications in human disease. *Br. J. Cancer* **26**, (1972).

118. Tait, S. W. G., Ichim, G. & Green, D. R. Die another way - non-apoptotic mechanisms of cell death. *J. Cell Sci.* **127**, 2135–2144 (2014).

119. Elmore, S. Apoptosis: A Review of Programmed Cell Death. *Toxicol Pathol.* **35**, 495–516 (2007).

120. Szondy, Z., Sarang, Z., Kiss, B., Garabuczi, É. & Köröskényi, K. Anti-inflammatory mechanisms triggered by apoptotic cells during their clearance. *Front. Immunol.* **8**, (2017).

121. Man, S. M., Karki, R. & Kanneganti, T. Molecular mechanisms and functions of pyroptosis, inflammatory caspases and inflammasomes in infectious diseases. **277**, 61–75 (2017).

122. Monack, D. M., Raupach, B., Hromockyj, A. E. & Falkow, S. Salmonella typhimurium invasion induces apoptosis in infected macrophages (bacterial invasion/programmed cell death/cytotoxicity). *Proc Natl Acad Sci U S A.* **93**, 9833–9838 (1996).

123. Hilbi, H. *et al.* Shigella-induced apoptosis is dependent on caspase-1 which binds to IpaB. *J. Biol. Chem.* **273**, 32895–32900 (1998).

124. Cookson, B. T. & Brennan, M. A. Pro-inflammatory programmed cell death [2]. *Trends Microbiol.* **9**, 113–114 (2001).

125. Lamkanfi, M. & Dixit, V. M. Mechanisms and functions of inflammasomes. *Cell* **157**, 1013–1022 (2014).

126. Fernandes-Alnemri, T., Yu, J. W., Datta, P., Wu, J. & Alnemri, E. S. AIM2 activates the inflammasome and cell death in response to cytoplasmic DNA. *Nature* **458**, 509–513 (2009).

127. Zhao, Y. & Shao, F. The NAIP-NLRC4 inflammasome in innate immune detection of bacterial flagellin and type III secretion apparatus. *Immunol. Rev.* **265**, 85–102 (2015).

128. Sandstrom, A. *et al.* Functional degradation: A mechanism of NLRP1 inflammasome activation by diverse pathogen enzymes. *Science (80-.).* **364**, (2019).

129. Swanson, K. V., Deng, M. & Ting, J. P. Y. The NLRP3 inflammasome: molecular activation and regulation to therapeutics. *Nat. Rev. Immunol.* **19**, (2019).

130. He, W. *et al.* Gasdermin D is an executor of pyroptosis and required for interleukin-1β secretion. *Cell Res.* **25**, 1285–1298 (2015).

131. Kayagaki, N. *et al.* Caspase-11 cleaves gasdermin D for non-canonical inflammasome signalling. *Nature* **526**, 666–671 (2015).

132. Shi, J. *et al.* Cleavage of GSDMD by inflammatory caspases determines pyroptotic cell death. *Nature* **526**, 660–665 (2015).

133. Rühl, S. & Broz, P. GSDMD membrane pore formation constitutes the mechanism of pyroptotic cell death. *EMBO J.* **35**, e201694696-13 (2016).

134. Ding, J. & Shao, F. SnapShot: The Noncanonical Inflammasome. *Cell* **168**, 544-544.e1

(2017).

135. Broderick, L., De Nardo, D., Franklin, B. S., Hoffman, H. M. & Latz, E. The Inflammasomes and Autoinflammatory Syndromes. *Annu. Rev. Pathol. Mech. Dis.* **10**, 395–424 (2015).

136. Halle, A. *et al.* The NALP3 inflammasome is involved in the innate immune response to amyloid-β. *Nat. Immunol.* **9**, 857–865 (2008).

137. Degterev, A. *et al.* Chemical inhibitor of nonapoptotic cell death with therapeutic potential for ischemic brain injury. *Nat. Chem. Biol.* **1**, 112–119 (2005).

138. N., H. *et al.* Fas triggers an alternative, caspase-8-independent cell death pathway using the kinase RIP as effector molecule. *Nat. Immunol.* **1**, 489–495 (2000).

139. Vercammen, D. *et al.* Dual signaling of the Fas receptor: Initiation of both apoptotic and necrotic cell death pathways. *J. Exp. Med.* **188**, 919–930 (1998).

140. Sakade, N. RIP3, an Energy Metabolism Regulator That Switches TNF-Induced Cell Death from Apoptosis to Necrosis. *Science (80-.).* **325**, 332–336 (2009).

141. Laster, S. M., Wood, J. G. & Gooding, L. R. Tumor necrosis factor can induce both apoptic and necrotic forms of cell lysis. *J. Immunol.* **141**, 2629 LP – 2634 (1988).

142. He, S., Liang, Y., Shao, F. & Wang, X. Toll-like receptors activate programmed necrosis in macrophages through a receptor-interacting kinase-3-mediated pathway. *Proc. Natl. Acad. Sci. U. S. A.* **108**, 20054–20059 (2011).

143. Kaiser, W. J. *et al.* Toll-like receptor 3-mediated necrosis via TRIF, RIP3, and MLKL. *J. Biol. Chem.* **288**, 31268–31279 (2013).

144. McComb, S. *et al.* Type-I interferon signaling through ISGF3 complex is required for sustained Rip3 activation and necroptosis in macrophages. *Proc. Natl. Acad. Sci.* **111**, E3206 LP-E3213 (2014).

145. Thapa, R. J. *et al.* NF-κB inhibition by bortezomib permits IFN-γ-activated RIP1 kinase-dependent necrosis in renal cell carcinoma. *Mol. Cancer Ther.* **12**, 1568–1578 (2013).

146. Ch'en, I. L., Tsau, J. S., Molkentin, J. D., Komatsu, M. & Hedrick, S. M. Mechanisms of necroptosis in T cells. *J. Exp. Med.* **208**, 633 LP – 641 (2011).

147. Tenev, T. *et al.* The Ripoptosome, a Signaling Platform that Assembles in Response to Genotoxic Stress and Loss of IAPs. *Mol. Cell* **43**, 432–448 (2011).

148. Sun, L. *et al.* Mixed lineage kinase domain-like protein mediates necrosis signaling downstream of RIP3 kinase. *Cell* **148**, 213–227 (2012).

149. Rebsamen, M. *et al.* DAI/ZBP1 recruits RIP1 and RIP3 through RIP homotypic interaction motifs to activate NF-kappaB. *EMBO Rep.* **10**, 916–922 (2009).

150. Upton, J. W., Kaiser, W. J. & Mocarski, E. S. DAI/ZBP1/DLM-1 complexes with RIP3 to mediate virus-induced programmed necrosis that is targeted by murine cytomegalovirus vIRA. *Cell Host Microbe* **11**, 290–297 (2012).

151. Li, J. *et al.* The RIP1/RIP3 Necrosome Forms a Functional Amyloid Signaling Complex

Required for Programmed Necrosis. *Cell* **150**, 339–350 (2012).

152. Arne , K. H. *et al.* Analysis of the N-terminal region of human MLKL, as well as two distinct MLKL isoforms, reveals new insights into necroptotic cell death. *Biosci. Rep.* **36**, e00291–e00291 (2016).

153. Chen, X. *et al.* Translocation of mixed lineage kinase domain-like protein to plasma membrane leads to necrotic cell death. *Cell Res.* **24**, 105–121 (2014).

154. Cai, Z. *et al.* Plasma membrane translocation of trimerized MLKL protein is required for TNF-induced necroptosis. *Nat. Cell Biol.* **16**, 55–65 (2014).

155. Tanzer, M. C. *et al.* Evolutionary divergence of the necroptosis effector MLKL. *Cell Death Differ.* **23**, 1185–1197 (2016).

156. Wang, H. *et al.* Mixed Lineage Kinase Domain-like Protein MLKL Causes Necrotic Membrane Disruption upon Phosphorylation by RIP3. *Mol. Cell* **54**, 133–146 (2014).

157. Dondelinger, Y. *et al.* MLKL Compromises Plasma Membrane Integrity by Binding to Phosphatidylinositol Phosphates. *Cell Rep.* **7**, 971–981 (2014).

158. Petrie, E. J. *et al.* Conformational switching of the pseudokinase domain promotes human MLKL tetramerization and cell death by necroptosis. *Nat. Commun.* **9**, (2018).

159. Huang, D. *et al.* The MLKL Channel in Necroptosis Is an Octamer Formed by Tetramers in a Dyadic Process. *Mol. Cell. Biol.* **37**, 1–17 (2017).

160. Oberst, A. *et al.* Catalytic activity of the caspase-8-FLIP(L) complex inhibits RIPK3-dependent necrosis. *Nature* **471**, 363–367 (2011).

161. Kaiser, W. J. *et al.* RIP3 mediates the embryonic lethality of caspase-8-deficient mice. *Nature* **471**, 368–372 (2011).

162. Varfolomeev, E. E. *et al.* Targeted Disruption of the Mouse Caspase 8 Gene Ablates Cell Death Induction by the TNF Receptors, Fas/Apo1, and DR3 and Is Lethal Prenatally. *Immunity* **9**, 267–276 (1998).

163. Upton, J. W., Kaiser, W. J. & Mocarski, E. S. Virus inhibition of RIP3-dependent necrosis. *Cell Host Microbe* **7**, 302–313 (2010).

164. Cho, Y. *et al.* Phosphorylation-Driven Assembly of the RIP1-RIP3 Complex Regulates Programmed Necrosis and Virus-Induced Inflammation. *Cell* **137**, 1112–1123 (2009).

165. McCormick, A. L., Skaletskaya, A., Barry, P. A., Mocarski, E. S. & Goldmacher, V. S. Differential function and expression of the viral inhibitor of caspase 8-induced apoptosis (vICA) and the viral mitochondria-localized inhibitor of apoptosis (vMIA) cell death suppressors conserved in primate and rodent cytomegaloviruses. *Virology* **316**, 221–233 (2003).

166. Bertin, J. *et al.* Death effector domain-containing herpesvirus and poxvirus proteins inhibit both Fas- and TNFR1-induced apoptosis. *Proc. Natl. Acad. Sci. U. S. A.* **94**, 1172–1176 (1997).

167. Thome, M. *et al.* Viral FLICE-inhibitory proteins (FLIPs) prevent apoptosis induced by

death receptors. *Nature* **386**, 517–521 (1997).

168. Petrie, E. J. *et al.* Viral MLKL Homologs Subvert Necroptotic Cell Death by Sequestering Cellular RIPK3. *Cell Rep.* **28**, 3309-3319.e5 (2019).

169. Conos, S. A. *et al.* Active MLKL triggers the NLRP3 inflammasome in a cell-intrinsic manner. *Proc. Natl. Acad. Sci. U. S. A.* **114**, E961–E969 (2017).

170. Gutierrez, K. D. *et al.* MLKL Activation Triggers NLRP3-Mediated Processing and Release of IL-1β Independently of Gasdermin-D. *J. Immunol.* **198**, 2156–2164 (2017).

171. Welz, P.-S. *et al.* FADD prevents RIP3-mediated epithelial cell necrosis and chronic intestinal inflammation. *Nature* **477**, 330–334 (2011).

172. Bonnet, M. C. *et al.* The Adaptor Protein FADD Protects Epidermal Keratinocytes from Necroptosis In Vivo and Prevents Skin Inflammation. *Immunity* **35**, 572–582 (2011).

173. Wu, J. *et al.* Mlkl knockout mice demonstrate the indispensable role of Mlkl in necroptosis. *Cell Res.* **23**, 994–1006 (2013).

174. Pavlosky, A. *et al.* RIPK3-mediated necroptosis regulates cardiac allograft rejection. *Am. J. Transplant.* **14**, 1778–1790 (2014).

175. Lau, A. *et al.* RIPK3-mediated necroptosis promotes donor kidney inflammatory injury and reduces allograft survival. *Am. J. Transplant.* **13**, 2805–2818 (2013).

176. Linkermann, A. *et al.* Two independent pathways of regulated necrosis mediate ischemia-reperfusion injury. *Proc. Natl. Acad. Sci. U. S. A.* **110**, 12024–12029 (2013).

177. Günther, C. *et al.* Caspase-8 regulates TNF-α-induced epithelial necroptosis and terminal ileitis. *Nature* **477**, 335–339 (2011).

178. Saito, N. *et al.* An annexin A1-FPR1 interaction contributes to necroptosis of keratinocytes in severe cutaneous adverse drug reactions. *Sci. Transl. Med.* **6**, 245ra95 (2014).

179. Gautheron, J. *et al.* A positive feedback loop between RIP3 and JNK controls non-alcoholic steatohepatitis. *EMBO Mol. Med.* **6**, 1062–74 (2014).

180. Roychowdhury, S., Mcmullen, M. R., Pisano, S. G., Liu, X. & Nagy, L. E. Absence of receptor interacting protein kinase 3 prevents ethanol-induced liver injury. *Hepatology* **57**, 1773–1783 (2013).

181. Dhuriya, Y. K. & Sharma, D. Necroptosis: A regulated inflammatory mode of cell death. *J. Neuroinflammation* **15**, 1–9 (2018).

182. Ofengeim, D. *et al.* Activation of necroptosis in multiple sclerosis. *Cell Rep.* **10**, 1836–1849 (2015).

183. Cvetanovic, M. & Ucker, D. S. Innate immune discrimination of apoptotic cells: repression of proinflammatory macrophage transcription is coupled directly to specific recognition. *J. Immunol.* **172**, 880–889 (2004).

184. Miles, K. *et al.* Dying and necrotic neutrophils are anti-inflammatory secondary to the release of alpha-defensins. *J. Immunol.* **183**, 2122–2132 (2009).

185. El Mezayen, R. *et al.* Endogenous signals released from necrotic cells augment inflammatory responses to bacterial endotoxin. *Immunol. Lett.* **111**, 36–44 (2007).

186. Moriwaki, K. *et al.* The Necroptosis Adaptor RIPK3 Promotes Injury-Induced Cytokine Expression and Tissue Repair. *Immunity* **41**, 567–578 (2014).

187. Orozco, S. & Oberst, A. RIPK3 in cell death and inflammation: The Good, the Bad, and the Ugly. *Immunol. Rev.* **277**, 102–112 (2017).

188. Najjar, M. *et al.* RIPK1 and RIPK3 Kinases Promote Cell-Death-Independent Inflammation by Toll-like Receptor 4. *Immunity* 1–14 (2016). doi:10.1016/j.immuni.2016.06.007

189. Greulich, W. *et al.* TLR8 Is a Sensor of RNase T2 Degradation Products. *Cell* **179**, 1264-1275.e13 (2019).

190. Schmidt, T., Schmid-Burgk, J. L. & Hornung, V. Synthesis of an arrayed sgRNA library targeting the human genome. *Sci. Rep.* **5**, 14987 (2015).

191. Doench, J. G. & Root, D. . Optimized sgRNA design to maximize activity and minimize off-target effects of CRISPR-Cas9 Synthesis of an arrayed sgRNA library targeting the human genome. *Nat. Biotechnol.* **34**, 184–191 (2016).

192. Labun, K. *et al.* CHOPCHOP v3: expanding the CRISPR web toolbox beyond genome editing. *Nucleic Acids Res.* **47**, W171–W174 (2019).

193. Schmid-Burgk, J. L. *et al.* OutKnocker: A web tool for rapid and simple genotyping of designer nuclease edited cell lines. *Genome Res.* **24**, 1719–1723 (2014).

194. Rapino, F. *et al.* C/EBP?? Induces Highly Efficient Macrophage Transdifferentiation of B Lymphoma and Leukemia Cell Lines and Impairs Their Tumorigenicity. *Cell Rep.* **3**, 1153–1163 (2013).

195. Lepock, J. R. Protein Denaturation During Heat Shock. in *Thermobiology* (eds. Bittar, E. E. & Willis, J. S. B. T.-A. in M. and C. B.) **19**, 223–259 (Elsevier, 1997).

196. Coll, R. C. *et al.* A small-molecule inhibitor of the NLRP3 inflammasome for the treatment of inflammatory diseases. *Nat. Med.* **21**, 248–257 (2015).

197. Mülberg, J. *et al.* The soluble interleukin-6 receptor is generated by shedding. *Eur. J. Immunol.* **23**, 473–480 (1993).

198. Nagata, S., Suzuki, J., Segawa, K. & Fujii, T. Exposure of phosphatidylserine on the cell surface. *Cell Death Differ.* **23**, 952–961 (2016).

199. Yatim, N. *et al.* RIPK1 and NF- B signaling in dying cells determines cross-priming of CD8+ T cells. *Science (80-.).* **350**, 328–34 (2015).

200. Tucher, J. *et al.* LC-MS based cleavage site profiling of the proteases ADAM10 and ADAM17 using proteome-derived peptide libraries. *J. Proteome Res.* **13**, 2205–2214 (2014).

201. Bertheloot, D. & Latz, E. HMGB1, IL-1α, IL-33 and S100 proteins: Dual-function alarmins. *Cell. Mol. Immunol.* **14**, 43–64 (2017).

202. Orozco, S. L. *et al.* RIPK3 Activation Leads to Cytokine Synthesis that Continues after Loss of Cell Membrane Integrity. *Cell Rep.* **28**, 2275-2287.e5 (2019).

203. Cai, Z. *et al.* Activation of cell-surface proteases promotes necroptosis, inflammation and cell migration. *Cell Res.* **26**, 886–900 (2016).

204. Chatzantoni, K. & Mouzaki, A. Anti-TNF-a Antibody Therapies in Autoimmune Diseases. *Curr. Top. Med. Chem.* **6**, 1707–1714 (2006).

205. Gaidt, M. M. *et al.* Human Monocytes Engage an Alternative Inflammasome Pathway. *Immunity* 1–14 (2016). doi:10.1016/j.immuni.2016.01.012

206. Zunke, F. & Rose-John, S. The shedding protease ADAM17: Physiology and pathophysiology. *Biochimica et Biophysica Acta - Molecular Cell Research* **1864**, 2059–2070 (2017).

207. Lichtenthaler, S. F. *et al.* The cell adhesion protein P-selectin glycoprotein ligand-1 is a substrate for the aspartyl protease BACE1. *J. Biol. Chem.* **278**, 48713–48719 (2003).

208. Moss, M. L. & Rasmussen, F. H. Fluorescent substrates for the proteinases ADAM17, ADAM10, ADAM8, and ADAM12 useful for high-throughput inhibitor screening. *Anal. Biochem.* **366**, 144–148 (2007).

209. Merezhko, M. *et al.* Multiplex assay for live-cell monitoring of cellular fates of amyloid-β precursor protein (APP). *PLoS One* **9**, (2014).

210. Kinoshita, A. *et al.* Demonstration by FRET of BACE interaction with the amyloid precursor protein at the cell surface and in early endosomes. *J. Cell Sci.* **116**, 3339–3346 (2003).

211. Thomas, A. V., Berezovska, O., Hyman, B. T. & von Arnim, C. A. F. Visualizing interaction of proteins relevant to Alzheimer´s disease in intact cells. *Bone* **44**, 299–303 (2008).

212. Kitazume, S. *et al.* Characterization of α2,6-sialyltransferase cleavage by Alzheimer's β-secretase (BACE1). *J. Biol. Chem.* **278**, 14865–14871 (2003).

8. List of abbreviations

ADAM	A Disintegrin and Metalloproteinase
AIM2	Absent in melanoma 2
AP	alkaline phosphatase
APOBEC3	Apolipoprotein B mRNA Editing Catalytic Polypeptide-like 3
APP	Amyloid precursor protein
BMDMs	Bone marrow derived macrophages
CANDIS	Conserved Adam seventeen Dynamic Interaction Sequence
CAPS	cryopyrin-associated periodic syndromes
CD	cluster of differentiation
cFLIP$_L$	FLICE-like inhibitory protein long
cGAMP	cyclic GMP-AMP
cGAS	cyclic GMP AMP synthase
cIAP	cellular inhibition of apoptosis protein
CLRs	C-type lectin receptors
CMV	cytomegalovirus
CTG	Cell titer-glo
CYLD	cylindromatosis enzyme
DCs	Dendritic cells
DNA	Deoxyribonucleic acid
dNTPs	deoxynucleoside triphosphates
ELISA	Enzyme-linked Immunosorbent Assay
ER	Endoplasmic reticulum
ETI	Effector-triggered immunity
FACS	Fluorescence-activated cell sorting
FADD	Fas associated death domain
FCS	Fetal cow serum
FRET	Fluorescence Resonance Energy Transfer
FRMD8	FERM Domain Containing 8
GSDMD	gasdermin D
HMGB1	high mobility group box 1
HSCs	Hematopoietic stem cells
HSPs	Heat shock proteins
IFN	interferon
IkB	inhibitor of nuclear factor B
IKK	IkB kinase complex
IL	interleukin
iNOS	inducible nitric oxide synthase
IRAK	IL-1 receptor-activated protein kinase
IRF	interferon regulatory factor
JAK	Janus kinase
LDH	Lactate Dehydrogenase
LGP2	laboratory of genetics and physiology 2
LPS	lipopolysaccharide
LRRs	leucin reach repeats

LT	lymphotoxin
LUBAC	linear ubiquitin chain assembly complex
M-CSF	macrophage colony-stimulating factor
MACS	Magnetic-activated cell sorting
MAL	MyD88 adaptor like protein
MAPK	mitogen-activated protein kinase
MAVS	mithocondrial antiviral signaling protein
MD2	myeloid differentiation factor 2
MDA5	melanoma differentiation-associated protein 5
MHC	major histocompatibility complex
MLKL	mixed lineage kinase domain-like protein
MPD	membrane proximal domain
Myd88	myeloid differentiation primary response gene 88
NADPH	nicotinamide adenine dinucleotide phosphate
NAIP	NLR Family Apoptosis Inhibitory Protein
NF-kB	nuclear factor kappa-light-chain-enhancer of activated B cells
NIK	NF-κB inducing kinase
NLCR	NLR family CARD domain-containing protein 4
NLRP	NOD-, LRR- and pyrin domain-containing protein
NLRs	NOD like receptors
OAS	2'-5'-oligoadenylate synthase
PAMPs	pathogen associated molecular patterns
PBMCs	peripheral blood mononuclear cells
PCR	Polymerase chain reaction
PI	Propidium iodide
PLK2	Polo-like kinase 2
PMA	phorbol 12-myristate 13-acetate
PRR	pathogen recognition receptors
RAGE	Receptor for advanced glycation end products
RHBDF	rhomboid 5 homolog 1 or rhomboid family member
RHIM	RIP homotypic interaction motif
RIG-I	retinoic-acid inducible gene I
RIPK	Receptor-interacting serine/threonine-protein kinase
RLRs	RIG-I like receptors
RNA	Ribonucleic acid
RNaseL	Ribonuclease L
ROS	reactive oxygen species
SAMHD1	SAM domain and HD domain-containing protein 1
SOCS3	Suppressor of cytokine signaling 3
SPPL2	Signal peptide peptidase-like
STAT	signal transducers and activators of transcription
STING	stimulator of interferon genes
TAB	TAK1 binding protein
TACE	TNFα converting enzyme
TAK1	transforming growth factor b activated protein kinase 1

TBK1	TANK-binding kinase1
TCR	T-cell receptor
TGF-β	transforming factor-beta
TIMP3	tissue inhibitor of metalloproteinase
TIR	Toll/Interleuchin-1 (domain)
TLRs	Toll-like receptors
TNF	Tumor necrosis factor
TNFR	TNF receptor
TNFRSF	TNF receptor superfamily
TNFSL	tumor necrosis factor superfamily of ligands
TRADD	Tumor necrosis factor receptor type 1-associated death domain
TRAF	tumor necrosis factor receptor associated factor
TRAM	Trif related adaptor molecule
TRAPS	Tumor necrosis factor receptor associated periodic syndrome
TRIF	TIR-domain containing adaptor protein inducing IFNβ
ZBP1	Z-DNA-binding protein 1

9. Acknowledgments

First, I would like to thank Veit Hornung for his close supervision and support throughout my all PhD time. He always had an open door to discuss results and problems and always found the time for me when I needed. He was also always there to have fun with us during our lab skiing trips, hiking tours and get-togethers.

A big thank you to all my colleagues, from past and present: you filled these 4 years with very happy moments, which I will always remember. The working atmosphere was always great and you were always there to motivate me and make me laugh. Some of you are now friends for life.

Thanks to Moritz Gaidt for bringing ideas to push the project forward.

Thanks to Dr. Jung for his great work in analyzing live-cell imaging data.

Thanks to Larissa and Andi for the technical support. You make our lives so much easier!

Thanks to the students who helped me with the experiments. In particular, I would like to mention Yannick and Maggie, who shared months of lab work with me. Some of the results presented in this thesis were possible also because of their precious help.

Finally, I want to thank Manuel. You are not only my better half, but also the best scientist I know. Thanks for all the work-related discussions we had and for helping with the spinning disk microscopy. But, especially, thanks for our every-day life together. You helped me surviving the moments of stress and you shared my happiness when I had some progresses. You incredibly contributed to this thesis with your every-day love.